Department of Electrical and Computer Engineering
School of Engineering
University of Cyprus

Performance Assessment of Different Grid-Connected PV Technologies Utilising Real Outdoor Measurements

George Makrides

A thesis submitted for the degree of
Doctor of Philosophy
April 2012

APPROVAL PAGE FOR THESIS DISSERTATION

SUBMITTED IN FULFILMENT OF REQUIREMENTS FOR DEGREE OF DOCTOR OF PHILOSOPHY AT UNIVERSITY OF CYPRUS BY:

George Makrides
Candidate

TITLE: **Performance Assessment of Different Grid-Connected PV Technologies Utilising Real Outdoor Measurements**

APPROVED:

Prof. Charalambos Charalambous	
Committee Chairperson	Signature
Dr George E. Georghiou	
Research Supervisor	Signature
Prof. Wilfried Van Sark	
Committee Member	Signature
Dr George Mitsis	
Committee Member	Signature
Dr Andreas Kyprianou	
Committee Member	Signature
Dr Andreas Stavrou	
Committee Member	Signature

DATE: April 27, 2012

Abstract

Over the past years, photovoltaics (PV) have shown rapid development and a wide variety of new technologies from different manufacturers have emerged. For each PV module type, manufacturers provide typical rated performance parameter information which includes, amongst others, the maximum power point (MPP) power, efficiency and temperature coefficients, all at standard test conditions (STC) of solar irradiance 1000 W/m^2, air mass (AM) of 1.5 and cell temperature of 25 °C. As this combination of environmental conditions rarely occurs outdoors, manufacturer data-sheet information is not sufficient to accurately estimate PV operation under different climatic conditions. For this reason, outdoor PV performance monitoring and evaluations are necessary.

The motivation behind this work and hence its contribution was to evaluate the outdoor performance of different grid-connected PV technologies under the same climatic conditions, from acquired outdoor data both in Nicosia, Cyprus and Stuttgart, Germany. The information extracted from the investigations carried out in this work assists in developing our understanding of how different PV technologies perform according to the operating conditions they are exposed to during their lifetime. In particular, the performance analysis evaluations of the different technologies in both locations are important for the scientific community as these may assist the selection of PV technologies based on the climatic conditions and as a function of location. The performance evaluations undertaken in this research, which include energy yield monitoring, seasonal behaviour, estimation of produced energy, effects of temperature and performance loss, provide novel results particularly useful to the academic community and investors, which seek to optimise the output and deployment of PV systems. Most importantly, all the results obtained from this outdoor study are the only proof of the real operation and of the various performance issues of each PV technology, once installed in the field.

Firstly, an advanced research infrastructure was set up at the University of Cyprus (UCY), Nicosia, Cyprus in May 2006, which includes amongst others, twelve grid-connected PV systems of different technologies. The different grid-connected PV systems installed range from mono-crystalline silicon (mono-c-Si) and multi-crystalline silicon (multi-c-Si), Heterojunction with Intrinsic Thin layer (HIT), Edge defined Film-fed Growth (EFG), Multi-crystalline Advanced Industrial cells (MAIN) to amorphous silicon (a-Si), cadmium telluride (CdTe), copper-indium-gallium-diselenide (CIGS) and other PV technologies. Each system has a nominal capacity of approximately 1 kW_p and is equipped with the same type of inverter installed in close proximity behind each respective system (SMA SB 1100, SMA Technology AG, Niestetal, Germany). The infrastructure also includes a data-acquisition and monitoring platform for both meteorological and PV system measurements. More specifically, the platform comprises of a number of sensors connected to a central data-logging system that stores data at a resolution of one second and accumulation steps of fifteen-minute averages. The data were stored since the beginning of June 2006 and were used in the performance evaluation investigations. The same technologies and infrastructure were also installed at the Institut für Photovoltaik (*ipv*) of the University of Stuttgart, Stuttgart, Germany to primarily facilitate the performance evaluations and comparisons at the two different climatic conditions. The test-sites in both Cyprus and Germany are the first of their kind, enabling performance investigations and comparisons of different grid-connected PV systems at different climatic conditions.

Based on the measured annual DC energy yield of the different grid-connected PV systems in Cyprus, the estimation errors of four models (namely: the single-point efficiency; single-point efficiency with temperature correction; the Photovoltaic for Utility-Scale Applications (PVUSA); and the one-diode model) were initially compared against the outdoor measurements. The different models showed wide estimation variations, demonstrating a strong dependence between model performance and the different technologies. The combined uncertainties associated with the estimated energy yield as a function of the input parameters for the single-point efficiency, single-point efficiency with temperature correction and the PVUSA models were also evaluated. The estimation and comparison of the energy yield of different models for the installed PV

technologies provides useful information about which model is more suitable for each technology.

Accordingly, the seasonal performance exhibited by each technology in Cyprus was analysed from the monthly DC energy yield and monthly average DC performance ratio (PR) time series, constructed from acquired outdoor measurements over a four-year period. Additionally, a seasonal performance investigation on the monthly average AC PR over a three-year period was performed for the systems, in both locations, to identify performance differences in the warm conditions of Nicosia, Cyprus and the moderate climate of Stuttgart, Germany. The seasonal behaviour of the installed PV technologies in Cyprus was further investigated using the classical series decomposition (CSD) technique. This technique was used to better understand the behaviour of the different technologies, as the extracted seasonality was used to obtain a repeatable set of twelve monthly seasonal values (the seasonal indices) for each PV technology. The results obtained from the seasonal performance assessments of the different technologies in both Nicosia and Stuttgart reveal the behaviour patterns that assist in the better understanding of the seasonal effects and optimum deployment of each technology.

After analysing the seasonal performance behaviour, a more detailed investigation into the effect of temperature on the performance of the systems installed in Cyprus was carried out by first evaluating the temperature coefficients based on an outdoor and data-evaluation procedure for the extraction of the MPP power temperature coefficients, γ. The outdoor temperature coefficient analysis demonstrated that the installed thin-film technologies have lower MPP power temperature coefficients compared to the crystalline-silicon (c-Si) technologies - hence, a better temperature behaviour. Subsequently, the thermal effects were further investigated, by evaluating the performance losses due to the temperature effect on the annual energy yield of each technology. This was accomplished using measurements of module temperature and the manufacturer provided γ. The same methodology was also applied using the outdoor evaluated γ for comparison.

Additionally, temperature effects on the seasonal performance of the different technologies were evident on the monthly average PR, particularly for the c-Si

technologies. For the a-Si technologies, a performance increase from spring until early autumn was observed and was attributed to thermal annealing. This effect became more evident by filtering DC MPP power measurements at high irradiance (greater than 800 W/m^2) and restricting the values at geometric air mass (AM) in the range $1 \leq$ geometric AM ≤ 1.5. The extracted DC MPP power was corrected for irradiance and temperature at STC over a period of two years. Accordingly, the effect of thermal annealing was further investigated by extracting DC MPP power measurements at geometric AM in the range $1.4 \leq$ geometric AM ≤ 1.6, in order to minimise the spectral influences on the performance of a-Si technologies. An increase in power for all the a-Si technologies was apparent during the warm summer season and was recorded over the period of March until September for both years.

Subsequently, the annual performance loss rates were obtained for the systems in Cyprus, using the statistical techniques of linear regression and CSD, applied on the monthly average DC PR time series between June 2006 and June 2011 (i.e. a period of five years). Information of the performance loss rates is a crucial issue in the deployment and performance evaluation of PV technologies and is particularly interesting to investors and manufacturers. The average annual performance loss rate of the mono-c-Si and multi-c-Si systems using linear regression was -0.64 and -0.62 %/year, respectively, over this period. On the other hand, the average annual performance loss rate of the thin-film systems was -1.78 %/year. The results obtained using CSD were slightly higher for the mono-c-Si and multi-c-Si systems which exhibited average annual performance losses of -1.04 and -1.10 %/year, respectively, while this was -1.81 %/year for the thin-film systems. The obtained results clearly show that deviations in the performance loss rates arise because of the selection of the technique applied and must be considered for these studies under field conditions. Furthermore, the annual performance loss rates were re-evaluated at shorter measurement time periods, by using the same statistical techniques in order to determine whether the performance loss rates can be evaluated in shorter time periods. The three- and four-year period annual performance loss rates were compared to the longer-term performance loss rates of the five-year investigation and the obtained results demonstrated that although the choice of the analysis technique affects the results, the performance loss trends exhibited the same pattern for most technologies.

Finally, the systems will remain grid-connected for more years, in order to accurately judge whether the resulting performance loss rates represent the real degradation rates and also to identify which technique obtained accurately the degradation rate and at which duration. Moreover, the existing infrastructure can be further utilised as a platform for testing other emerging PV technologies at the cell, module and system level.

Abstract

Ραγδαία εξέλιξη έχει σημειωθεί τα τελευταία χρόνια στον τομέα των Φωτοβολταϊκών (ΦΒ) και ως εκ τούτου έχει δημιουργηθεί ένα ευρύ φάσμα τεχνολογιών από διάφορους κατασκευαστές. Για κάθε ΦΒ πλαίσιο οι κατασκευαστές παρέχουν σε πρότυπες τυπικές συνθήκες ηλιακής ακτινοβολίας 1000 W/m^2, μάζα αέρος (ΜΑ) 1.5 και θερμοκρασία κυττάρου 25 °C, πληροφορίες αναφορικά με τις παραμέτρους απόδοσης όπως την ισχύ στο μέγιστο σημείο, την απόδοση και τους συντελεστές θερμοκρασίας. Καθώς αυτή η σύνθεση περιβαλλοντικών συνθηκών σπάνια παρατηρείται σε εξωτερικούς χώρους, οι πληροφορίες που δίνονται στα εγχειρίδια των κατασκευαστών δεν είναι επαρκείς ως προς την ακριβή πρόβλεψη της λειτουργίας των ΦΒ κάτω από διαφορετικές κλιματολογικές συνθήκες. Ως εκ τούτου, η παρακολούθηση και αξιολόγηση ΦΒ τεχνολογιών σε εξωτερικούς χώρους κρίνεται ιδιαίτερα σημαντική.

Ο κύριος στόχος και η συνεισφορά αυτής της διατριβής είναι η αξιολόγηση της απόδοσης διαφόρων ΦΒ τεχνολογιών, συνδεδεμένων στο δίκτυο, από τη συνεχή επιτήρηση των πιο σημαντικών λειτουργικών τους παραμέτρων στις κλιματολογικές συνθήκες της Λευκωσίας (Κύπρος) και της Στουτγάρδης (Γερμανία). Οι πληροφορίες που θα αντληθούν από τα περισυλλεγμένα δεδομένα και την εκτενή ανάλυση έχουν ως στόχο την ανάπτυξη της υφιστάμενης γνώσης ως προς τη λειτουργία των ΦΒ τεχνολογιών κάτω από πραγματικές συνθήκες. Συγκεκριμένα, η αξιολόγηση της απόδοσης των διαφόρων ΦΒ τεχνολογιών στις δύο περιοχές είναι πολύ σημαντική για την επιστημονική κοινότητα καθώς τα αποτελέσματα βοηθούν στην επιλογή της βέλτιστης ΦΒ τεχνολογίας ανά περιοχή. Η αξιολόγηση που διεξήχθη σε αυτή την έρευνα, που συμπεριλαμβάνει καταγραφή της απόδοσης και παραγωγής ενέργειας, επιρροή της θερμοκρασίας στην απόδοση των συστημάτων και υποβάθμιση, παρέχει καινοτόμα αποτελέσματα σημαντικά στην ακαδημαϊκή κοινότητα και στους επενδυτές που αποσκοπούν να αναπτύξουν την παραγωγή ενέργειας και την εγκατάσταση ΦΒ.

Κυριότερα, όλα τα αποτελέσματα αυτής της έρευνας αποτελούν την μοναδική απόδειξη της πραγματικής λειτουργίας των ΦΒ τεχνολογιών κάτω από πραγματικές συνθήκες εγκατάστασης.

Αρχικά, η ερευνητική υποδομή που περιλαμβάνει μεταξύ άλλων 12 ΦΒ συστήματα διαφόρων τύπων, διασυνδεδεμένων στο δίκτυο παροχής ηλεκτρισμού, αναπτύχθηκε στο Πανεπιστήμιο Κύπρου (ΠΚ), στην Λευκωσία τον Μάιο 2006. Τα εν λόγω ΦΒ συστήματα περιλαμβάνουν τεχνολογίες μονο-κρυσταλλικού, πολυ-κρυσταλλικού, άμορφου πυριτίου, CdTe, CIGS και άλλες. Το κάθε σύστημα είναι ονομαστικής ισχύος 1 kW_p και είναι διασυνδεδεμένο με ίδιου τύπου μετατροπέα εγκατεστημένο σε κοντινή απόσταση από το ΦΒ σύστημα (SMA SB 1100, SMA Technology AG, Niestral, Germany). Η υποδομή πλαισιώνεται από διαγνωστικό εξοπλισμό για τις μετρήσεις των λειτουργικών και μετεωρολογικών παραμέτρων. Συγκεκριμένα, η πλατφόρμα αποτελείται από αρκετούς αισθητήρες που συνδέονται με κεντρικό σύστημα καταγραφής και αποθήκευσης δεδομένων με ανάλυση ενός δευτερολέπτου και μέσου όρου συσσώρευσης δεκαπέντε λεπτών. Τα δεδομένα περισυλλέγονται από τον Ιούνιο 2006 και έχουν χρησιμοποιηθεί στην ανάλυση της απόδοσης των συστημάτων. Επίσης, τα ίδια συστήματα έχουν εγκατασταθεί και στο Institut für Photovoltaik (*ipv*) του Πανεπιστημίου της Στουτγάρδης με πρωταρχικό στόχο την ανάλυση και την σύγκριση της απόδοσης των συστημάτων στις διαφορετικές κλιματολογικές συνθήκες. Οι ερευνητικές υποδομές τόσο στην Κύπρο όσο και στην Γερμανία είναι από τις πρώτες που έχουν δημιουργηθεί στον τομέα τους για την διεξαγωγή ερευνητικών δραστηριοτήτων σε ΦΒ τεχνολογίες, κάτω από διαφορετικές κλιματολογικές συνθήκες.

Με βάση την μετρημένη DC παραγόμενη ενέργεια από τα διαφορετικά ΦΒ συστήματα στην Κύπρο, έχουν διεξαχθεί συγκρίσεις μεταξύ των πραγματικών δεδομένων και των αποτελεσμάτων τεσσάρων μοντέλων. Συγκεκριμένα, τα μοντέλα που εξετάστηκαν ήταν το μοντέλο μοναδικού-σημείου απόδοσης, μοναδικού-σημείου απόδοσης με διόρθωση θερμοκρασίας, το PVUSA και το μοντέλο μιας-διόδου. Τα εν λόγω μοντέλα ανέδειξαν ένα ευρύ φάσμα σφαλμάτων ως προς την ικανότητα να υπολογίσουν την ενέργεια, υποδεικνύοντας παράλληλα την άμεση σχέση ανάμεσα στην απόδοσή τους και τις διαφορετικές ΦΒ τεχνολογίες. Η αβεβαιότητα της υπολογιζόμενης παραγόμενης ενέργειας σε συνάρτηση με τις παραμέτρους εισόδου για το κάθε μοντέλο είχαν επίσης

αξιολογηθεί. Ο υπολογισμός της ενέργειας και η σύγκριση των αποτελεσμάτων των διαφόρων μοντέλων για τις εγκατεστημένες ΦΒ τεχνολογίες, παρέχουν σημαντικές πληροφορίες για την επιλογή του καταλληλότερου μοντέλου για κάθε τύπο ΦΒ τεχνολογίας.

Επιπλέον, η εποχιακή απόδοση της κάθε τεχνολογίας στην Κύπρου αναλύθηκε από τις χρονο-σειρές της μηνιαίας DC παραγωγής ενέργειας και αποδοτικότητας (PR) που δημιουργήθηκαν από τις μετρήσεις κατά την διάρκεια των τεσσάρων χρόνων αξιολόγησης. Επιπρόσθετα, η εποχιακή απόδοση εξετάστηκε και αναφορικά με την μηνιαία χρονο-σειρά AC αποδοτικότητας για την περίοδο τριών χρόνων για τα εγκατεστημένα συστήματα στις δυο περιοχές, ώστε να διαπιστωθούν οι διαφορές στην απόδοση μεταξύ του ζεστού κλίματος στην Λευκωσία και του αίθριου κλίματος στην Στουτγάρδη. Η εποχιακή απόδοση των συστημάτων στην Κύπρο αναλύθηκε περαιτέρω χρησιμοποιώντας την τεχνική κλασσικής αποσύνθεσης χρονο-σειράς (CSD). Αυτή η τεχνική χρησιμοποιήθηκε για να προβληθεί καθαρά η συμπεριφορά των εγκατεστημένων τεχνολογιών. Παράλληλα, η εξαγόμενη εποχικότητα χρησιμοποιήθηκε για την άντληση μιας επαναλαμβανόμενης σειράς από 12 μηνιαίους εποχιακούς δείκτες για κάθε τεχνολογία. Τα αποτελέσματα της εποχιακής απόδοσης στην Λευκωσία και Στουτγάρδη αποκαλύπτουν πληροφορίες απόδοσης που είναι χρήσιμες για την κατανόηση των εποχιακών διαφορών παραγωγής ενεργείας της κάθε ΦΒ τεχνολογίας.

Αφού αναλύθηκε η εποχιακή απόδοση, διεξήχθη μια εκτενέστερη διερεύνηση για την επιρροή της θερμοκρασίας στην απόδοση των συστημάτων στην Κύπρο. Πρωτίστως όμως αξιολογήθηκαν οι συντελεστές θεοκρασίας χρησιμοποιώντας μεθοδολογία βασισμένη σε τεχνική εξωτερικού χώρου και αξιολόγηση μετρήσεων για να εξαχθούν οι συντελεστές θερμοκρασίας μέγιστης ισχύος, γ. Τα αποτελέσματα από την μεθοδολογία εξωτερικού χώρου έδειξαν πως οι τεχνολογίες λεπτής επίστρωσης είχαν χαμηλότερους συντελεστές θερμοκρασίας μέγιστης ισχύος και ως εκ τούτου καλύτερη θερμική συμπεριφορά, σε σχέση με τις τεχνολογίες κρυσταλλικού πυριτίου. Μεταγενέστερα, διερευνήθηκαν οι επιπτώσεις της θερμοκρασίας στην απόδοση των ΦΒ τεχνολογιών με την αξιολόγηση των απωλειών στην ετήσια παράγωγη ενεργείας λόγω της θερμοκρασίας για κάθε τεχνολογία, χρησιμοποιώντας μετρήσεις της θερμοκρασίας πλαισίων και τους συντελεστές θερμοκρασίας γ όπως δίνονται από τους κατασκευαστές. Η ίδια

μεθοδολογία διεξήχθη ξανά αλλά χρησιμοποιώντας τους συντελεστές θερμοκρασίας γ που εξήχθηκαν από την μεθοδολογία εξωτερικού χώρου.

Ακολούθως, οι επιπτώσεις της θερμοκρασίας στην εποχιακή απόδοση των τεχνολογιών ήταν εμφανή από την μηνιαία χρονο-σειρά αποδοτικότητας και πιο συγκεκριμένα από τις τεχνολογίες κρυσταλλικού πυριτίου. Αναφορικά με τις τεχνολογίες άμορφου πυριτίου παρατηρήθηκε αύξηση στην απόδοσή τους από την άνοιξη μέχρι και τις αρχές του φθινοπώρου λόγω της θερμικής ανόπτησης. Αυτό το φαινόμενο έγινε πιο εμφανές φιλτράροντας μετρήσεις DC μέγιστης ισχύος σε υψηλή ηλιακή ακτινοβολία (μεγαλύτερη από 800 W/m^2) και περιορίζοντας τα αποτελέσματα στο φάσμα γεωμετρικής μάζας αέρος $1 \leq$ γεωμετρική $MA \leq 1.5$. Οι μετρήσεις της μεγίστης ισχύος που εξήχθηκαν, διορθώθηκαν κατόπιν ως προς την ακτινοβολία και θερμοκρασία στις σταθερές τυπικές συνθήκες για περίοδο δύο χρόνων. Επιπρόσθετα, το φαινόμενα της θερμικής ανόπτησης διερευνήθηκε εκτενέστερα εξάγοντας μετρήσεις DC μέγιστης ισχύος στο φάσμα γεωμετρικής μάζας αέρος $1.4 \leq$ γεωμετρική $MA \leq 1.6$ ούτως ώστε να ελαχιστοποιηθεί η επιρροή φάσματος στην απόδοση των τεχνολογιών άμορφου πυριτίου. Αύξηση στην ισχύ και για τις δύο τεχνολογίες άμορφου πυριτίου ήταν εμφανής κατά την διάρκεια της ζεστής καλοκαιρινής περιόδου και συγκεκριμένα από τον Μάρτιο μέχρι τον Σεπτέμβριο και για τα δύο χρόνια.

Μετέπειτα, ο ρυθμός υποβάθμισης διερευνήθηκε χρησιμοποιώντας τις στατιστικές τεχνικές της γραμμικής οπισθοδρόμησης και κλασικής αποσύνθεσης χρονο-σειράς στην χρονο-σειρά της μηνιαίας DC αποδοτικότητας για τα συστήματα στην Κύπρο κατά την περίοδο Ιούνιου 2006 - Ιούνιου 2011 (πέντε χρόνια). Ο ρυθμός υποβάθμισης είναι ένα από τα πιο σημαντικά θέματα που επηρεάζουν την απόδοση καθώς και την εφαρμογή ΦΒ τεχνολογιών, ενώ παράλληλα είναι πολύ ενδιαφέρων για τους επενδυτές και κατασκευαστές ΦΒ πλαισίων. Ο μέσος όρος της ετήσιας υποβάθμισης για τις τεχνολογίες μονο-κρυσταλλικού και πολυ-κρυσταλλικού πυριτίου χρησιμοποιώντας την τεχνική γραμμικής οπισθοδρόμησης ήταν -0.64 και -0.62 %/έτος αντίστοιχα για αυτήν την περίοδο. Από την άλλη, ο μέσος όρος υποβάθμισης για τα συστήματα λεπτής επίστρωσης ήταν -1.78 %/έτος. Τα αποτελέσματα που εξήχθησαν χρησιμοποιώντας την τεχνική κλασικής αποσύνθεσης χρονο-σειράς ήταν σχετικά ψηλότερα για τις τεχνολογίες μονο-κρυσταλλικού και πολύ-κρυσταλλικού πυριτίου αφού ήταν -1.04 και -1.10 %/έτος

αντίστοιχα, ενώ για τα συστήματα λεπτής επίστρωσης ήταν -1.81 %/έτος. Τα αποτελέσματα υποδεικνύουν ότι οι διαφορές στην υποβάθμιση προκύπτουν από την τεχνική που χρησιμοποιείται. Επιπλέον, η ετήσια υποβάθμιση για κάθε σύστημα επαναξιολογήθηκε σε μικρότερες χρονικές περιόδους χρησιμοποιώντας τις ίδιες στατιστικές τεχνικές. Η σύγκριση τον αποτελεσμάτων υποβάθμισης των τριών και τεσσάρων ετών με την μακρόχρονη των πέντε ετών, έδειξαν ότι ενώ η επιλογή της τεχνικής ανάλυσης επηρεάζει τα αποτελέσματα, η τάση της υποβάθμισης εκθέτει το ίδιο πρότυπο για τις πλείστες τεχνολογίες.

Ολοκληρώνοντας, αξίζει να σημειωθεί ότι τα συστήματα θα παραμείνουν συνδεδεμένα στο δίκτυο για ακόμα μερικά χρόνια ώστε να εξακριβωθεί κατά πόσο τα αντλούμενα αποτελέσματα ρυθμού υποβάθμισης αντιπροσωπεύουν τον πραγματικό ρυθμό υποβάθμισης ώστε να βρεθεί ποια τεχνική και σε πιο χρονικό περιθώριο έδωσε τα πιο ακριβή αποτελέσματα. Παράλληλα, οι υποδομή μπορεί να χρησιμοποιηθεί εκτενέστερα ως πλατφόρμα για αξιολόγηση καινούργιων ΦΒ τεχνολογιών στο επίπεδο κυττάρων, πλαισίων και συστημάτων.

Acknowledgements

First and foremost, I would like to express my sincere gratitude to my supervisor Dr. George E. Georghiou, for his valuable guidance and many encouragements during this project. Working with him has been both pleasant and very fruitful for my personal and professional development.

Special thanks to my colleagues and friends at the University of Cyprus and particularly those in the PV Technology group, for their helpfulness, useful discussions and encouragement at all times.

I am also deeply grateful to Dr. Jürgen H. Werner and Dr. Markus Schubert, for their vision, continuous support and encouragement throughout the years. Above all I would like to thank Dr. Bastian Zinsser, for both his assistance and friendship.

I also gratefully acknowledge the contributions of the German Federal Ministry for the Environment, Nature Conservation and Nuclear Safety (BMU), which supported this work under contract No. 0327553. In addition, I would like to thank the companies Atersa, First Solar GmbH, Phönix Sonnenstrom AG, Q-cells AG, Schott Solar GmbH, SMA Technologies AG, SolarWorld AG, Solon AG and Würth Solar GmbH & Co.KG, for their support. The financial support of the Cyprus Research Promotion Foundation is also greatly appreciated.

Finally, I would like to thank my wife and family that have been next to me with their love and support all the time.

I would like to dedicate this thesis to my loving wife, parents and brothers

Contents

List of Figures

List of Tables

Nomenclature

Abbreviations

AC	Alternating current
ACF	Autocorrelation function
Al	Aluminium
AM	Air mass
AOI	Angle of incidence
APE	Absolute percentage error
AR	Autoregressive
ARIMA	Autoregressive integrated moving average
a-Si	Amorphous silicon
a-Si/μc-Si	Amorphous silicon/micro-crystalline silicon
a-Si:H	Hydrogenated amorphous silicon
BOS	Balance-of-system
CdTe	Cadmium telluride
CIGS	Copper-indium-gallium-diselenide Cu(In,Ga)Se2
CIS	Copper-indium-selenide
CSD	Classical series decomposition
c-Si	Crystalline silicon
DC	Direct current
DNI	Direct normal irradiance
EFG	Edge defined film-fed growth
EVA	Ethylene vinyl acetate
FF	Fill factor
Ga	Gallium

GUC	German University Cairo
HIT	Heterojunction with intrinsic thin layer
ipv	Institut für Photovoltaik
MA	Moving average
MAIN	Multi-crystalline advanced industrial cells
Mo	Molybdenum
Mono-c-Si	Mono-crystalline silicon
MPP	Maximum power point
MPPT	Maximum power point tracking
Multi-c-Si	Multi-crystalline silicon
Na	Sodium
NOCT	Nominal operating cell temperature
PACF	Partial autocorrelation function
PECVD	Plasma enhanced chemical vapour deposition
POA	Plane-of-array
PR	Performance ratio
PSH	Peak sun hours
PTC	PVUSA test conditions
PV	Photovoltaics
PVUSA	Photovoltaic for Utility-Scale Applications
RMSE	Root mean squared error
RSS	Root-sum-squares
Si	Silicon
SnO_2	Tin Oxide
STC	Standard test conditions
SWE	Staebler-Wronski effect
UCY	University of Cyprus
UV	Ultra-violet
WMO	World Meteorological Organisation
ZnO	Zinc Oxide
µc-Si	microcrystalline silicon

Mathematical

A	Solar cell/module area (m^2)
C_{ph}	Photocurrent density coefficient (V^{-1})
C_s	Shockley saturation diode parameter ($Acm^{-2}K^{-3}$)
C_t	Light generated current density temperature coefficient ($V^{-1}K^{-1}$)
E_{AC}	Energy yield AC (kWh)
$E_{AC(Normalised)}$	Energy yield AC normalised to STC manufacturer power (kWh/kW_p)
E_{DC}	Energy yield DC (kWh)
$E_{DC(Normalised)}$	Energy yield DC normalised to STC manufacturer power (kWh/kW_p)
E_g	Band-gap energy (eV)
E_{real}	Real energy yield (kWh)
E_{STC}	Energy yield at STC (kWh)
G	Global irradiance (W/m^2)
G_{POA}	Global irradiance in the plane-of-array (W/m^2)
G_{STC}	Global irradiance at STC (W/m^2)
H	Global irradiation (kWh/m^2)
I	Current (A)
I_0	Diode saturation current (A)
I_{MPP}	Maximum power point current (A)
I_{ph}	Photocurrent (A)
I_{SC}	Short-circuit current (A)
$I_{SC\ STC}$	Short-circuit current at STC (A)
J	Current density (A/m^2)
K	Boltzmann's constant (eV/K)
l	Lag
m	Moving average half-width
n	Diode ideality factor
P_{DC}	Power DC (W)
P_{MPP}	Maximum power point power (W)
PR	Performance ratio (%)
PR_{AC}	Performance ratio AC (%)

PR_{DC}	Performance ratio DC (%)
$PR_{peak\text{-}peak}$	PR peak-to-peak (%)
P_{STC}	Nameplate STC manufacturer power (W_p)
q	Electric charge (C)
R^2	Coefficient of determination
r_k	Autocorrelation coefficient
R_{series}	Series resistance (Ω)
R_{shunt}	Shunt resistance (Ω)
S_t	Seasonality at time *t*
$S_{t(normalised)}$	Normalised seasonality
T	Temperature (K)
t	Time
T_{amb}	Ambient temperature (K)
T_{module}	Module temperature (K)
T_{STC}	Module temperature at STC (K)
T_t	Trend at time *t*
u_C	Combined uncertainty
V	Voltage (V)
V_{MPP}	Maximum power point voltage (V)
V_{OC}	Open circuit voltage (V)
$V_{OC\ STC}$	Open circuit voltage at STC (V)
WD	Wind direction (°)
WS	Wind speed (m/s)
Y_f	Final energy yield (kWh/kW_p)
α	Short-circuit current temperature coefficient (%/K)
β	Open-circuit voltage temperature coefficient (%/K)
γ	Maximum power point power temperature coefficient (%/K)
η	Efficiency (%)
η_{STC}	Efficiency at STC (%)
η_T	Temperature deviation factor (%)
κ	Moving average order

σ	Standard deviation

Chapter 1

Introduction

1.1 Motivation

Amongst the various renewable energy sources, photovoltaic (PV) technologies that convert sunlight directly to electricity have been gaining ground and popularity, especially in countries with high solar irradiation. Over the past years, PV has shown rapid development and a wide variety of new technologies from different manufacturers have emerged. For each PV module type, manufacturers provide typical rated performance parameter information, which includes, amongst others, the maximum power point (MPP) power, efficiency and temperature coefficients, all at standard test conditions (STC) of global irradiance 1000 W/m^2, air mass (AM) of 1.5 and cell temperature of 25 °C. As this combination of environmental conditions rarely occurs outdoors, manufacturer data-sheet information is not sufficient to accurately estimate PV operation under different climatic conditions and, therefore, outdoor PV performance evaluations and side-by-side comparisons of different technologies are necessary and important.

Apart from the requirement for more outdoor performance evaluations, there has also been a pressing need to further develop our understanding of how different PV technologies perform under the operating conditions they are exposed to during their lifetime, and to improve the energy yield estimation, by employing different modelling approaches. When undertaking modelling investigations, it is also essential to identify the

strengths and weaknesses of each approach and to further highlight the main reasons why the results deviate from the measured values.

In addition, seasonal performance investigations of grid-connected PV systems can provide useful information about the losses affecting each PV technology, revealing additional behaviour patterns that can be correlated and explained in terms of the environmental conditions.

In particular, in warm climates, thermal loss is probably the most important performance loss factor. As the systems in this study were exposed to warm environmental conditions (indicative of the climate in Cyprus) it became important to investigate the thermal effects on the performance of each technology. With respect to amorphous-silicon (a-Si) technologies, the thermal effects can further enhance the performance, through a process known as thermal annealing.

Another major issue in the deployment and performance evaluation of PV technologies is degradation or progressive performance loss. This is an important topic in the performance assessment of PV technologies, especially for the new ones, such as thin-film due to the lack of field data related to the performance evolution over time.

In this work the abovementioned research topics were investigated in order to contribute to our knowledge in the field of outdoor PV performance evaluation. More specifically, the infrastructure at the University of Cyprus (UCY), Nicosia, Cyprus was first set up for the continuous monitoring and evaluation of the operational parameters of different PV systems, installed side-by-side under the same climatic conditions. The various grid-connected PV systems installed have a nominal capacity of approximately 1 kW_p and range from mono-crystalline silicon (mono-c-Si) and multi-crystalline silicon (multi-c-Si), Heterojunction with Intrinsic Thin layer (HIT), Edge defined Film-fed Growth (EFG), Multi-crystalline Advanced Industrial cells (MAIN) to amorphous silicon (a-Si), cadmium telluride (CdTe), copper-indium-gallium-diselenide (CIGS) and other PV technologies. The same PV technologies were also installed at the Institut für Photovoltaik (*ipv*) of the University of Stuttgart, Stuttgart, Germany. Both test-sites have been operating since June 2006 and the locations selected cover the climatic exposure to the warm conditions of Nicosia, typical of the Mediterranean region, and also the moderate conditions of Stuttgart, typical of central Europe. The accuracy of different

widely used models was first investigated and compared against the measured energy yield of each installed technology at the testing facility in Cyprus. Accordingly, a seasonal performance investigation was carried out and the performance patterns exhibited by each technology in both Cyprus and Germany were analysed and compared. The most important performance loss factor for the technologies installed in Cyprus was the temperature, which was further investigated and quantified. Conversely, for the a-Si technologies a concurrent investigation was performed to quantify the performance increase due to the exposure of these modules to prolonged periods of high temperatures.

Finally, the performance loss rate of each system was obtained by employing the statistical techniques of linear regression and classical series decomposition (CSD) over a five-year period. The performance loss rates were re-evaluated by applying both techniques on the three- and four-year time series of each technology. It became obvious from the results that deviations in the performance loss rates arise both due to the selection of the technique applied and the duration of the time series. Furthermore, the annual performance loss rates were re-evaluated at shorter measurement time periods, by using the same statistical techniques in order to determine whether the performance loss rates can be evaluated in shorter time periods. The three- and four-year period annual performance loss rates were compared to the longer-term performance loss rates of the five-year investigation and the obtained results demonstrated that although the choice of analysis technique affects the results, the performance loss trends exhibited the same pattern for most technologies.

1.2 Research objectives

The main research objectives of this work are summarised as follows:

- To evaluate the outdoor performance of different grid-connected PV technologies under the same climatic conditions from acquired outdoor data, both in Nicosia, Cyprus and Stuttgart, Germany
- To estimate and compare the energy yield of different models, acquiring information about which model is more suitable for each technology

- To analyse the seasonal behaviour exhibited by the systems installed and to provide information about the performance fluctuations present during any given year
- To compare the performance behaviour of the technologies installed in Nicosia, Cyprus and Stuttgart, Germany
- To study the thermal effects on the performance of the installed PV systems which are particularly important in warm climates
- To evaluate the effect and magnitude of thermal annealing on a-Si technologies
- To provide information of the annual performance loss rates of the installed PV technologies, by applying statistical analysis
- To evaluate the effect of the technique applied and the duration of the time series on the annual performance loss rates

1.3 Aim of the thesis

The aim of this thesis was to evaluate the performance of twelve latest PV technologies installed under the same climatic conditions. The outdoor performance evaluations provide useful information that enhances the knowledge of the scientific community, in the fields of energy yield modelling, seasonal behaviour, thermal effects and annealing and performance loss rates of PV technologies. In addition, the knowledge acquired from the field testing, is important to enhance the understanding of the underlying loss processes and to optimise PV integration.

Finally, the information compiled through these investigations can be further applied to improve the selection of PV technology according to the climatic conditions of the location and, consequently, to increase the performance and hence the energy production.

1.4 Novelty of the research

The research undertaken in this thesis was an attempt to evaluate the performance of twelve latest PV technologies installed under the same climatic conditions. It is the first

time that twelve different grid-connected PV systems were continuously monitored for a number of years, in order to establish their outdoor behaviour, and to obtain real PV operating and climatic data. More specifically, the same infrastructure installed in Cyprus was also replicated in two other locations for the scope of investigating the performance of different PV technologies under different climatic conditions. The three selected locations include the *ipv* University of Stuttgart, Germany, the UCY, Nicosia, Cyprus and the German University in Cairo (GUC), Cairo, Egypt. This was also the first time that the PV potential was evaluated as a function of the location (in Cyprus), to establish the limitations and capabilities of each technology.

The performance of each PV technology was also assessed against known used models and for each technology the strengths and weaknesses of each approach were identified.

In particular, the seasonal performance investigation performed for each PV technology provides useful information about their behaviour and is an essential requirement for the successful and optimum deployment at a particular location. The results of the seasonality comparison of both the systems in Nicosia and Stuttgart demonstrated that each technology provided different performance variations throughout a year at each location.

As a consequence of the seasonal performance evaluation, the thermal effects on the systems were also investigated and useful information of this effect on the performance of the different technologies was extracted. In addition, the thermal annealing effect was also explored for the a-Si technologies and the magnitude of this effect was quantified for the warm climate of Cyprus.

Finally, useful information was obtained for the degradation or performance loss rate of each PV technology, using the linear statistical techniques of linear regression and CSD. The field of degradation is very important as, in the fast evolving industry of PV, there is a pressing need to determine the degradation rates accurately, in order to minimise investment risk - especially for emerging technologies such as thin-film.

1.5 Literature review

1.5.1 Modelling approaches

With the advent of new PV technologies there has been a pressing need to improve the energy yield estimation through the development of various simulation tools [1–7]. Different mathematical, empirical and electrical models for estimating the performance and output of PV technologies have been developed and are presented in the literature [8–14]. Over the years, there has been a concerted effort to improve these models, in order to provide more accurate estimations [15–20].

In general, previous analyses of the different existing models focused on their estimation accuracy or estimation errors and on their complexity. The accuracy of each model mainly depends on the input parameters and can also be affected by the associated uncertainties of the parameters used. The input data for each model is either provided from manufacturer data-sheets or collected from sensors installed on-site, that measure meteorological and PV operational parameters. Typical parameters include the global irradiance in the plane-of-array (POA), G_{POA}, wind direction, *WD*, wind speed, *WS*, as well as ambient temperature, T_{amb}, and module temperature, T_{module}. The electrical parameters include the MPP current, I_{MPP}, MPP voltage, V_{MPP}, AC power, P_{AC}, DC power, P_{DC}, AC energy yield, E_{AC} and DC energy yield, E_{DC}. All these parameters include measurement uncertainties which propagate through the model and affect the results.

A fundamental mathematical model used to estimate the power produced by a PV system is the single-point efficiency model [21], which requires only the global irradiance in the POA, G_{POA}, the area of the PV array, *A*, and the efficiency at STC, η_{STC}. The simplicity of this model's input parameters is compromised by the fact that it cannot sufficiently account for the deviations in efficiency associated with the different PV technologies and the climatic conditions of the place of operation [22]. In order to optimise the estimation accuracy, more elaborate models including up to thirty different parameters have been developed, in an attempt to fully model PV performance and account for factors such as temperature, angle of incidence (AOI), spectrum, mismatches, cable losses as well as others [23].

An improvement to the single-point efficiency model, particularly for PV technologies operating in warm climates, is to consider a deviation factor, in order to account for the effect of increased temperature on the power production. The effect of temperature has been extensively studied in the past and all studies in the literature agree that the performance of crystalline silicon (c-Si) PV is reduced with increasing temperatures [24–26].

A different modelling approach exists through electrical models that describe the PV characteristics in terms of an equivalent electrical circuit. The most established and widely used electrical model is the one-diode model [27], which requires knowledge or determination of the different electrical parameters of the PV technology. In its simplest form, the one-diode model comprises of a current source in parallel to a diode [28]. Improvements to the electrical circuit are made possible with the inclusion of a series and shunt resistance [29–31]. Unfortunately, this model does not take into account the initial stabilisation, seasonal effects [23] and the current-voltage dependence, which for amorphous silicon technologies must be considered [32]. The diffusion length in a-Si is a thousand times smaller compared to c-Si and for this reason a-Si cells are designed to establish a high field region in the intrinsic layer (i-layer) to sweep photo-carriers to the contacts before they recombine [33]. In particular, the photocurrent in a-Si p-i-n technologies depends almost entirely on field-aided drift rather than diffusion of minority carriers which is the case for c-Si p-n technologies. The electric field in the i-layer is strongly dependent on the voltage bias across the device, which makes the photocurrent collection dependent on the operating bias of the cell [33]. Modifications and improvements to the equivalent one-diode model have already been presented, especially for amorphous, microcrystalline silicon (μc-Si) and CdTe technologies [7]. In the case of hydrogenated amorphous silicon (a-Si:H) cells and modules, improvements became obvious with the addition of a new term to account for recombination losses in the i-layer of the device [34].

Another approach to estimate energy yield and power output was to establish empirical models that are restricted to simple algebraic methods, and which could also be associated with meteorological data [35–38]. Algebraic methods that compromise simplicity and accuracy are usually preferred in PV system engineering while second

order effects such as spectral effects and low irradiance performance are usually not considered or left to more complicated models [39]. A widely known empirical model is the Photovoltaic for Utility-Scale Applications (PVUSA) model, which establishes the relationships between the PV output and measurement data of global irradiance in the POA, ambient temperature and wind speed [40].

1.5.2 Seasonal performance

An essential requirement in the deployment of the different existing and emerging PV technologies is an understanding of the performance exhibited by each technology, once installed outdoors. Information about the outdoor behaviour and variations exhibited is necessary because the outdoor PV electrical characteristics differ throughout the year from the reference STC characteristics described in manufacturer data-sheets.

In particular, various studies performed in the past based on the performance parameters of the energy yield and performance ratio (PR), clearly demonstrated that both c-Si and thin-film PV technologies exhibited strong seasonality and performance variations, which are repeatable over the years [41–48]. More specifically, c-Si technologies exhibit seasonal performance behaviour which is mainly affected by environmental conditions, such as global irradiance, ambient temperature and spectrum, and follow a seasonal pattern throughout the year, with slight variations due to the varying meteorological conditions from year to year [49–51].

Similarly, the performance of thin-film technologies such as a-Si, CIGS and CdTe is also affected by the seasonal variations of irradiance, temperature and spectrum; although in the case of a-Si and CdTe the temperature dependence is weaker in comparison to c-Si technologies [43]. Furthermore, the spectral effects are more pronounced for the a-Si technologies, as compared to CdTe (which is less sensitive to spectral changes) and c-Si and CIGS (which are the least affected) [52].

Previous studies on a-Si have also reported seasonal characteristics, with peak performance occurring during summer and not during winter [53–55]. This behaviour was explained partly as being due to seasonal annealing of the initial stage Staebler-Wronski effect (SWE) and also due to spectral effects [44]. The source of thermal

annealing and, in particular, whether the seasonal patterns observed in the performance of a-Si technologies were due to high temperatures, or the more favourable spectrum in the summer, has also been considered extensively in the literature [53], [56].

In this respect, seasonal behaviour investigations are important because certain characteristics that assist in the better understanding of the seasonal effects and optimum deployment of each technology are revealed.

1.5.3 Thermal effects

The performance of PV systems is directly related to environmental conditions, such as global irradiance, ambient temperature and spectrum, while other factors, such as degradation and progressive failure mechanisms also affect the long-term performance [57–60]. For PV technologies operating in warm climates, the increased module temperature is a very important performance loss factor and all past studies agree that the performance of c-Si PV is reduced with temperature increase [61–63]. Regarding a-Si technologies, numerous studies have further shown that high module operating temperatures actually improve the performance of stabilised a-Si modules due to thermal annealing [23], [64], [65]. This effect describes the process of a-Si modules recovering some or all of their initial performance, as a consequence of prolonged exposure to high temperatures [56], [66], [67].

The dependence of the electrical characteristics of PV on the operating temperature is provided by the temperature coefficients [25]. Another important thermal parameter that describes the temperature of a PV module is the nominal operating cell temperature (NOCT), which is provided by PV manufacturers as an indication of how module temperature is affected by the solar irradiation, ambient temperature and thermal properties of the PV material. Temperature coefficients of PV devices are usually evaluated using indoor laboratory techniques. A commonly used methodology is to illuminate a PV cell or module that is placed on a temperature controlled structure. Accordingly, the *I-V* curves of the device are acquired over a range of different cell temperatures, but at controlled STC irradiance and air mass. The rate of change of either

the voltage, current or power with temperature is then calculated and provides the value of the temperature coefficients [25].

In addition, a useful technique to obtain the temperature coefficients under real operating conditions is to employ outdoor field test measurements. In outdoor investigations, the PV devices are first shaded to lower the temperature close to ambient conditions and as soon as the device is uncovered and left to increase in temperature, several *I-V* curves are acquired at different temperatures [25], [61], [68], [69]. As in indoor investigations, the rate of change of the investigated parameter against temperature provides the temperature coefficient. Both techniques are used by manufacturers and professionals within the field. Previous studies have shown that the power of c-Si PV modules decreases by approximately -0.45 %/K [61], [70]. On the other hand, thin-film technologies of CdTe and CIGS show lower power temperature coefficients compared to c-Si technologies and, in the case of CdTe modules, the measured temperature coefficient is around -0.25 %/K [71]. In addition, a-Si shows the lowest power temperature coefficient of approximately -0.20 %/K [72], while numerous studies have further shown that high module operating temperatures improve the performance of stabilised a-Si modules, due to thermal annealing [23], [53], [64]. The thermal behaviour of a-Si suggests that a unique temperature coefficient, as in the case of other PV technologies, cannot characterise completely the temperature behaviour of this technology [73]. In general, the output power and performance of CdTe and a-Si modules is less temperature sensitive than CIS and c-Si technologies. Table 1.1 summarises the MPP power temperature coefficients, γP_{MPP}, of commercial PV technologies.

Table 1.1. Typical MPP power temperature coefficients for different PV technologies.

Technology	**Approximate MPP power temperature coefficient, γP_{MPP} (%/K)**
Mono-c-Si	-0.40
Multi-c-Si	-0.45
a-Si	-0.20
a-Si/μc-Si	-0.26
CIGS	-0.36
CdTe	-0.25

1.5.4 PV degradation

The performance of PV modules varies according to climatic conditions and gradually deteriorates through the years [74–78]. The most important issue in long-term performance assessments especially for emerging technologies is degradation, which is the outcome of a power or performance loss progression; dependent on a number of factors such as degradation at the cell, module or even system level. In almost all cases, the main environmental factors related to known degradation mechanisms include temperature, humidity, water ingress and ultra-violet (UV) intensity. All these factors impose significant stress, over the lifetime of a PV device and, as a result, detailed understanding of the relation between external factors, stability issues and module degradation is necessary. In general, degradation mechanisms describe the effects from both physical mechanisms and chemical reactions and can occur at PV cell, module and system levels.

1.5.4.1 Degradation mechanisms

The degradation mechanisms at the cell level include gradual performance loss due to ageing of the material and loss of adhesion of the contacts or corrosion, which is usually the result of water vapor ingress. Other degradation mechanisms include metal mitigation through the p-n junction and antireflection coating deterioration. All the above-mentioned degradation mechanisms have been identified from previous experience on c-Si technologies [75], [78], [79].

In the case of a-Si cells, an important degradation mechanism occurs when this technology is first exposed to sunlight, as the power stabilizes at a level that is approximately 70 - 80 % of the initial power. This degradation mechanism is known as the Staebler-Wronski effect [80] and is attributed to recombination-induced breaking of weak Si-Si bonds by optically excited carriers after thermalisation, producing defects that decrease carrier lifetime [81].

Other degradation mechanisms have also been observed for thin-film technologies of CdTe and CIGS at the cell level. For CdTe technologies, the effects of cell degradation can vary with the properties of the cell and also with the applied stress factors. More

specifically, as the p-type CdTe cannot be ohmically contacted with a metal, most devices use copper to dope the CdTe surface before contacting [82], [83]. Copper inclusion may cause dramatic changes in the electrical properties of the CdTe thin-film [83]. As copper is very mobile it can diffuse along grain boundaries of the CdTe cell and result in a recombination centre situated close to the p-n junction. Very low levels of copper reduce the conductivity of CdTe and it is possible that the diffusion of copper can transform the back contact to non-ohmic. Another effect associated with CdTe degradation is due to the applied voltage, either arising from the cell or the external voltage, which, as a result of the electric field, can force copper ions towards the front contact. It was previously found that open-circuit conditions affected cell degradation during accelerated ageing for different CdTe cell types [84]. In addition, impurity diffusion and changes in doping profiles may affect device stability [85], but the industry has resolved this problem by using special alloys.

CIGS has a flexible structure that enhances its tolerance to chemical changes and, because of this, it has been previously argued that copper atoms do not pose stability problems for CIGS cells [86]. Damp heat tests performed on unencapsulated CIGS cells have indicated that humidity degrades cell performance and is more obvious as V_{OC} and fill factor (FF) degradation, due to the increased concentration of deep acceptor states in the CIGS absorber [87]. Other important factors include donor-type defects [88] and the influence of Ga-content on cell stability [89].

Table 1.2 summarises the main thin-film failure modes and failure mechanisms [90].

At the module level, degradation occurs due to failure mechanisms of the cell, as well as, due to degradation of the packaging materials, interconnects, cell cracking, manufacturing defects, bypass diode failures, encapsulant failures and delamination [27], [91], [92].

At the system level, degradation includes all cell and module degradation mechanisms and is further caused by module interconnects and inverter degradation.

Table 1.2. Thin-film failure modes and failure mechanisms [90].

Failure modes	Effect on *I-V* curve	Possible failure mechanisms
1. Cell degradation		
a. Main junction: increased recombination	Loss in fill factor, *I*sc, and *V*oc	Diffusion of dopants and impurities. Electromigration
b. Back barrier; loss of ohmic contact CdTe	Roll-over, cross-over of dark and light *I-V*, higher R_{series}	Diffusion of dopants and impurities. Corrosion, oxidation, electromigration
c. Shunting	R_{shunt} decreases	Diffusion of metals, impurities, etc.
d. Series; ZnO,Al	R_{series} increases	Corrosion, diffusion
e. De-adhesion SnO_2 from soda-lime glass	*I*sc decreases and R_{series} increases	Na ion migration to SnO_2/glass interface
f. De-adhesion of back metal contact	*I*sc decreases	Lamination stresses
2. Module degradation		
Interconnect degradation		
a. Interconnect resistance; ZnO:Al/Mo or Mo, Al interconnect	R_{series} increases	Corrosion, electromigration
b. Shunting	R_{shunt} decreases	Corrosion, electromigration
Busbar degradation	R_{series} increases or open circuit	Corrosion, electromigration
Solder joint	R_{series} increases or open circuit	Fatigue, coarsening
Encapsulation failure		
a. Delamination	Loss in fill-factor, *I*sc, and possible open circuit	Surface contamination, UV degradation, hydrolysis of silane/glass bond, thermal expansion mismatch
b. Loss of seal		
c. Glass breakage		

1.5.4.2 Degradation rates

Indoor degradation investigations are mainly performed at the module level, as the interconnection and addition of other materials to form a modular structure increases stability issues. In particular, accelerated ageing tests performed indoors and under controlled conditions can provide information about different degradation mechanisms. Degradation investigations using indoor methodologies are based on the acquisition of *I-V* curves and power at STC. The electrical characteristics of PV modules are initially measured at STC, with the modules then exposed either outdoors or indoors through accelerated procedures [49], [93], [94]. For each investigated PV cell or module, the electrical characteristics are regularly acquired using the solar simulator, while the current, voltage or power differences from the initial value provide indications of the degradation rates at successive time periods.

In addition, many groups have performed outdoor monitoring of individual PV modules, through the acquisition and comparison of *I–V* curves, as the modules are exposed to real outdoor conditions [68], [94], [95]. Another method by which to investigate degradation outdoors has been based on power and energy yield measurements of PV systems subjected to actual operating conditions. A common approach has been to first establish time series, usually on a monthly basis, of either the PR or the maximum power normalised to PVUSA Test Conditions (PTC) of solar irradiance 1000 W/m^2, air temperature of 20 °C and wind speed of 1 m/s. Time series analysis, such as linear regression, CSD and Autoregressive Integrated Moving Average (ARIMA), is then used to obtain the trend and hence the degradation rate [94], [96]. Outdoor field tests are very important in exploring the degradation mechanisms under real conditions. These mechanisms cannot otherwise be revealed from indoor stability tests. The outcomes of such outdoor investigations can provide useful feedback to improve the stability, and enhance the understanding of the different technology dependent degradation mechanisms, while they can also be used as tools for the adaptation of accelerated ageing tests, so as to suit the degradation mechanisms for each technology.

For both indoor and outdoor evaluations a variety of degradation rates have been reported and a survey of the results of degradation studies is given below. A recent study has shown that, on average, the historically reported degradation rates of different PV technologies was 0.7 %/year, while the reported median was 0.5 %/year [97]. More specifically, investigations performed on outdoor exposed mono-c-Si and multi-c-Si PV modules, showed performance losses of approximately 0.7 %/year [94]. Results of field tests have generally shown stable performance for CdTe devices [98–100], although field results are limited for modules utilizing new cell structures [101]. Previous studies performed on thin-film copper-indium-selenide (CIS) modules, showed that after outdoor exposure the efficiency was found to decrease [102] and to exhibit either moderate, in the range of 2 - 4 %/year, to negligible or less than 1 %/year degradation rates, due to increases in the series resistance in some of the modules [103].

Evaluations based on monthly PR and PVUSA values revealed degradation rates, for the PR investigation, of 1.5 %/year for a-Si, 1.2 %/year for CdTe and 0.9 %/year for

mono-c-Si [104]. The results were slightly different for the PVUSA investigation, which showed a degradation rate of 1.1 %/year for the a-Si, 1.4%/year for the CdTe and 1.3 %/year for the mono-c-Si [104]. Based on linear fits applied to the PVUSA power rating curves over the six-year time period for a thin-film a-Si system, degradation rates of 0.98 %/year at the DC side and 1.09 %/year at the AC side of the system were obtained, while the same investigation on PR data-sets indicated a similar degradation rate of 1.13 %/year at the AC side [41].

Additionally, in a recent long-term performance assessment of a-Si tandem cell technologies in Germany, it was demonstrated that an initial two-year stabilisation phase occurred, then followed by a stable phase with a minor power decrease of maximum 0.2 %/year [105]. In another study, it was reported that thin-film modules showed somewhat higher than 1 %/year degradation rates [76]. On the other hand, an important consideration in relation to thin-film degradation rate investigations was found to be the date of installation of the modules, as it appeared that CdTe and CIGS modules manufactured after 2000 exhibited improved stability relative to older designs [97].

1.6 Outline of the thesis

The thesis is divided and organised into eight chapters. Specifically, chapter 1 is the introduction and includes the motivation, literature review and research objectives of the proposed thesis.

A general overview of the different existing PV technologies is presented in chapter 2. In addition, a description of the operation and basic theory of PV technology is also given in this chapter.

In chapter 3, a detailed overview of the testing infrastructure used to investigate the outdoor performance is provided. This chapter also introduces all the instrumentation and the overall uncertainties which are associated with the investigations.

Based on the measured energy yield results, chapter 4 presents the investigation undertaken to assess the performance of four different modelling approaches. Furthermore, the uncertainty evaluation of each model is demonstrated.

In chapter 5, the seasonal performance exhibited by each technology is analysed based on the constructed monthly energy yield and PR time series. The seasonal behaviour results obtained by using time series decomposition are also presented in this chapter.

After analyzing the seasonal performance behaviour, a more detailed analysis of the thermal effects is provided in chapter 6. In this chapter, the methodology used to evaluate the temperature coefficients of each PV system is first described and the effect of temperature on the annual energy yield of each technology is also presented, followed by a study on thermal annealing for the a-Si technologies.

The approach that was followed to calculate the annual performance losses of the different PV technologies and the comparison of the results obtained by different statistical techniques and duration periods are summarised in chapter 7.

Finally, in the last chapter, chapter 8, the conclusions and future work are presented.

Chapter 2

Basic theory

2.1 Introduction

The objective of this chapter is to provide an overview of the different existing PV technologies, ranging from c-Si to thin-film. Particular focus is given on the physical properties and manufacturing progress exhibited throughout the years for each technology. In addition, a detailed description of the operation of grid-connected PV systems is provided. More specifically, this includes an outline of the main operational parts and electrical characteristics of grid-connected PV systems.

Finally, the requirement for outdoor performance evaluations and the different approaches used to describe outdoor performance are also considered in this chapter.

2.2 Overview of PV technologies

A wide range of PV technologies now exists that include mono-c-Si, multi-c-Si, thin-film of a-Si, micromorph (microcrystalline/amorphous silicon), CdTe, CIGS and other emerging PV technologies. Each technology is mainly described and classified according to the material used, manufacturing procedure, efficiency and cost.

Amongst the various existing PV technologies, c-Si is the most developed and well understood, due to mainly its use in the integrated circuit industry. In addition, silicon is at present the most abundant material found in the earth's crust and its physical properties

are well defined and studied. C-Si dominates the PV technology market with a share of approximately 80 % today [106]. The type of c-Si technology depends on the wafer production and includes mono-c-Si, multi-c-Si, ribbon and sheet-defined film growth (ribbon/sheet c-Si).

The main characteristic of mono-c-Si is its ordered crystalline structure with all the atoms in a continuous crystalline lattice. Mono-c-Si technologies are highly efficient but are, at the same time, the most expensive amongst the existing flat-plate PV technologies, mainly because of their relatively costly manufacturing processes. Over the past years, manufacturing improvements in c-Si PV technology have focused on the decrease of wafer thickness (from 400 μm to 200 μm) and, in parallel, the increase in area (from 100 cm^2 to 240 cm^2). The most important limitation of this technology is the cost of the silicon feedstock, which renders the material cost relatively high, particularly as the silicon substrate must have a thickness of approximately 200 μm in order to allow the incident light to be absorbed over a wide range of wavelengths. Despite the high material cost, this technology has remained competitive due to several manufacturing improvements, such as enhancements in wire cutting techniques (that have reduced the wafer thickness) and also the production of kerf-less wafers. Recently, Sunpower announced an efficiency of 24.2 % for a large 155 cm^2 silicon cell fabricated on an n-type Czochralski grown wafer [107].

The fact that mono-c-Si modules are produced with relatively expensive manufacturing techniques initiated a series of efforts for the reduction of the manufacturing cost. Such a cost improvement was accomplished with the production of multi-c-Si PV, which can be produced by simpler and cheaper manufacturing processes. Multi-c-Si PV cell wafers consist of small grains of mono-c-Si and are made in a number of manufacturing processes. The substrate thickness is approximately 160 μm, while attempts are being made to lower the thickness even more. In general, multi-c-Si PV cells are cheaper compared to mono-c-Si as they are produced through a less elaborate manufacturing process, at the expense of slightly lower efficiencies. The lower efficiency is attributed to recombination at the grain boundaries within the multi-c-Si structure. Nonetheless, multi-c-Si currently has the largest PV market share.

Ribbon silicon is another type of multi-c-Si technology, produced from multi-c-Si strips suitable for the photovoltaic industry. In the manufacturing process of this technology, high temperature-resistant wires are pulled through molten silicon to form a ribbon which is subsequently cut and processed in the usual manner, to produce PV cells. An advantage of this technology is that the production costs are lower than other c-Si technologies, while the efficiency and quality of the cells remain the same as other multi-c-Si technologies (but lower than mono-c-Si).

The main incentive for the development of thin-film technologies has been their cheap production cost compared to the c-Si counterparts. Over the past years, thin-film technologies have shown very encouraging development as the global production capacity had reached around 3.5 GW in 2010 and is expected to reach between 6 - 8.5 GW in 2012 [108]. Amongst the many thin-film technologies, some of the most promising are CdTe, a-Si, micromorph tandem cells (a-Si/μc-Si) and CIGS. The rapid growth and importance of thin-film PV is further highlighted by the fact that the world's first PV manufacturer to exceed the 1 GW/year production rate and hence to capture 13 % of the global market was First Solar, a manufacturer of thin-film CdTe modules, in 2009 [109]. Specifically, CdTe has grown from a 2 % market share in 2005 to 13 % in 2010 [106].

A-Si has been on the PV market longer than other thin-film technologies, allowing researchers and manufacturers to understand several aspects of its behaviour. This technology was first commercialised in the early 1980s and since then has increased gradually in efficiency. The manufacturing of a-Si technologies is dominated by deposition processes, such as plasma enhanced chemical vapour deposition (PECVD). Thus, large area, flexible and cheap substrates, such as stainless steel and thin foil polymer, can be used in the manufacturing process [110]. In comparison to mono-c-Si, a-Si PV cells have no crystalline order leading to dangling bonds, which have a severe impact on the material properties and behaviour. Another important material limitation arises from the fact that this technology suffers from light-induced degradation, the Staebler–Wronski effect, which explains the initial performance decrease when a-Si modules are first exposed to light [80]. In general, this effect has been minimised by employing double or triple-junction devices and developing micromorph tandem cells,

which is a hybrid technology of c-Si and a-Si. An important advantage of a-Si is the high absorption coefficient, which is approximately 10 times higher than c-Si, resulting in much thinner cells.

Table 2.1 summarises the key characteristics of typical commercial PV modules.

Table 2.1. Typical commercial PV module characteristics.

Technology	Material thickness (μm)	Area (m^2)	Efficiency (%)	Area for 1 kW_p system (m^2)
Mono-c-Si	200	1.4-1.7 (typical)	14-20	~7
Multi-c-Si	160	1.4-1.7 (typical) 2.5 (up to)	11-15	~8
a-Si	1	~1.5	4-8	~15
a-Si/μc-Si	2	~1.4	7-9	~12
CdTe	~1-3	~0.6-1	10-11	~10
CIGS	~2	~0.6-1	7-12	~10

2.3 Grid-connected PV systems

Grid-connected PV systems are connected to the public electricity grid, which is assumed to be available permanently. A grid-connected inverter converts the DC output of the PV array to 230 V or 400 V 50 Hz AC for direct connection to the grid supply.

These systems offer the advantage that all the energy generated by the PV system is consumed by the grid. Furthermore, the export of all PV electricity is allowed, which is important if a premium price is paid for this energy. However, the disadvantage of this system is the need of grid presence for the inverter to function.

Grid-connected PV systems consist of the PV modules, the inverter and balance-of-system (BOS) components, which include mounting materials for the modules, wire, lighting protectors, circuit breakers and grounding connections.

2.4 Standard Test Conditions (STC) performance

In general, PV manufacturers provide information about the electrical characteristics of modules at STC. Specifically, such information includes the open-circuit voltage, V_{OC}, short-circuit current, I_{SC}, MPP voltage, V_{MPP}, current I_{MPP}, power, P_{MPP}, efficiency, η, and temperature coefficients. Such data given by PV manufacturers are only valid under certain conditions, including global irradiance of 1000 W/m^2, AM 1.5 and cell

temperature of 25 °C. In an installed system, the rated power at STC is called nameplate power or installed Watt-peak, W_p. Performance data can also be obtained when values are quoted for the NOCT, which denotes the temperature measured at nominal operating conditions of irradiance 800 W/m^2, AM 1.5, ambient temperature 20 °C, wind speed 1m/s and an open back-side mounting.

In practice, the operating conditions are most often different to the STC and, thus, the performance of a module significantly varies from the one expected from the manufacturers' data-sheet. More specifically, STC uses a spectrum that is typically present during spring and autumn, an operating temperature that might be achieved in winter and irradiance typical of summer days. These conditions obviously favour the performance of a module and, thus, any real performance will almost always be less than expected. However, performance indicators have to be calculated at STC so as to have a meaningful comparison.

2.5 Performance parameters

The main outdoor evaluated PV performance parameters include the energy yield, the outdoor efficiency and performance ratio. More specifically, the most important parameter for grid-connected PV systems is the energy yield, which is closely associated with cost evaluations.

In particular, the payback of a PV system and the level of investment are associated with the energy production and the feed-in-tariff scheme in place. The normalised PV system energy yield, Y_f, is defined as the total energy produced by a PV system during a period with the DC energy yield, E_{DC}, further normalised to the nameplate manufacturer DC power at STC, P_{STC}, to allow for comparison between the different installed PV technologies [104]. The final normalised energy yield, Y_f, is given by:

$$Y_f = \frac{E_{DC}}{P_{STC}} \tag{2.1}$$

Furthermore, important performance aspects are obtained by the evaluation of the outdoor efficiency, η, and PR, for each of the PV technologies installed. The efficiency is given by:

$$\eta = \frac{E_{\mathrm{DC}}}{H \times A} \tag{2.2}$$

where H is the global irradiation and A is the area of the PV array.

The PR is calculated from the above parameters and used as a useful way of quantifying the overall effect of losses due to PV module temperature, spectrum, module mismatch, as well as other losses, such as optical reflection, soiling and downtime failures. The DC PR, PR_{DC}, is defined as the ratio between the real DC energy production, E_{real}, and the DC energy the PV array would produce, if it had no losses at STC, E_{STC}, [111]. It is given by:

$$PR = \frac{E_{\mathrm{real}}}{E_{\mathrm{STC}}} = \frac{E_{\mathrm{DC}}}{H \times A \times \eta_{\mathrm{STC}}} \tag{2.3}$$

where η_{STC} is the PV module efficiency at STC.

The main application area of PV technologies is in grid-connected PV systems. As the information provided by manufacturers is not adequate to describe their outdoor performance, and especially its evolution over time, it is important to undertake outdoor evaluations. The infrastructure necessary to acquire such knowledge is presented in the next chapter.

Chapter 3

Infrastructure implementation

3.1 Introduction

In order to evaluate the outdoor performance of different PV technologies installed side-by-side under the same climatic conditions, an advanced research infrastructure was set up and is described in detail in this chapter. The purpose of the installed infrastructure, which comprised of twelve grid-connected PV systems, of nominal power 1 kW_p each, was to evaluate the PV performance and potential in Cyprus, while also providing the opportunity for direct comparisons under the same climatic conditions. The same infrastructure installed in Cyprus was replicated in two other locations, for the scope of investigating the performance of different PV technologies under different climatic conditions. The three selected locations are the Institut für Photovoltaik, University of Stuttgart, Germany, the University of Cyprus, Nicosia, Cyprus and the German University in Cairo, Cairo, Egypt. For the purpose of this thesis, performance results from the test sites in Cyprus and Germany are presented as the systems in Egypt were not operational during the evaluation period.

Furthermore, the infrastructure includes a data-acquisition and monitoring platform for both meteorological and PV system measurements, which are subsequently stored in a central database. More specifically, the platform comprises of meteorological and electrical sensors connected to a central data-logging system. This system stores data at a

resolution of one-second and accumulation steps of fifteen-minute averages, which were used in the performance evaluation investigations.

Finally, the main sources of uncertainty in the outdoor PV performance evaluations, due to the instrumentation and methodology, were also thoroughly investigated.

3.2 Outdoor PV test facility

The outdoor PV test facility in Cyprus was commissioned in May 2006 and includes, amongst others, twelve grid-connected PV systems of different technologies. The fixed-plane PV systems installed range from mono-c-Si and multi-c-Si, HIT, EFG, MAIN to a-Si, CdTe, CIGS, to other PV technologies [61], [111]. Each system has a nominal capacity of approximately 1 kW_p and is equipped with the same type of inverter installed behind each respective system in close proximity (SMA SB 1100, SMA Technology AG, Niestetal, Germany). The same inverters are used in order to exclude the influence of different maximum power point tracking (MPPT) methods to the DC yield. The inverters are also oversized, to ensure that the systems are always working at their maximum power point [111]. The systems are installed in two arrays, as shown in Figure 3.1.

Figure 3.1. Outdoor PV testing facility at the University of Cyprus, Nicosia, Cyprus.

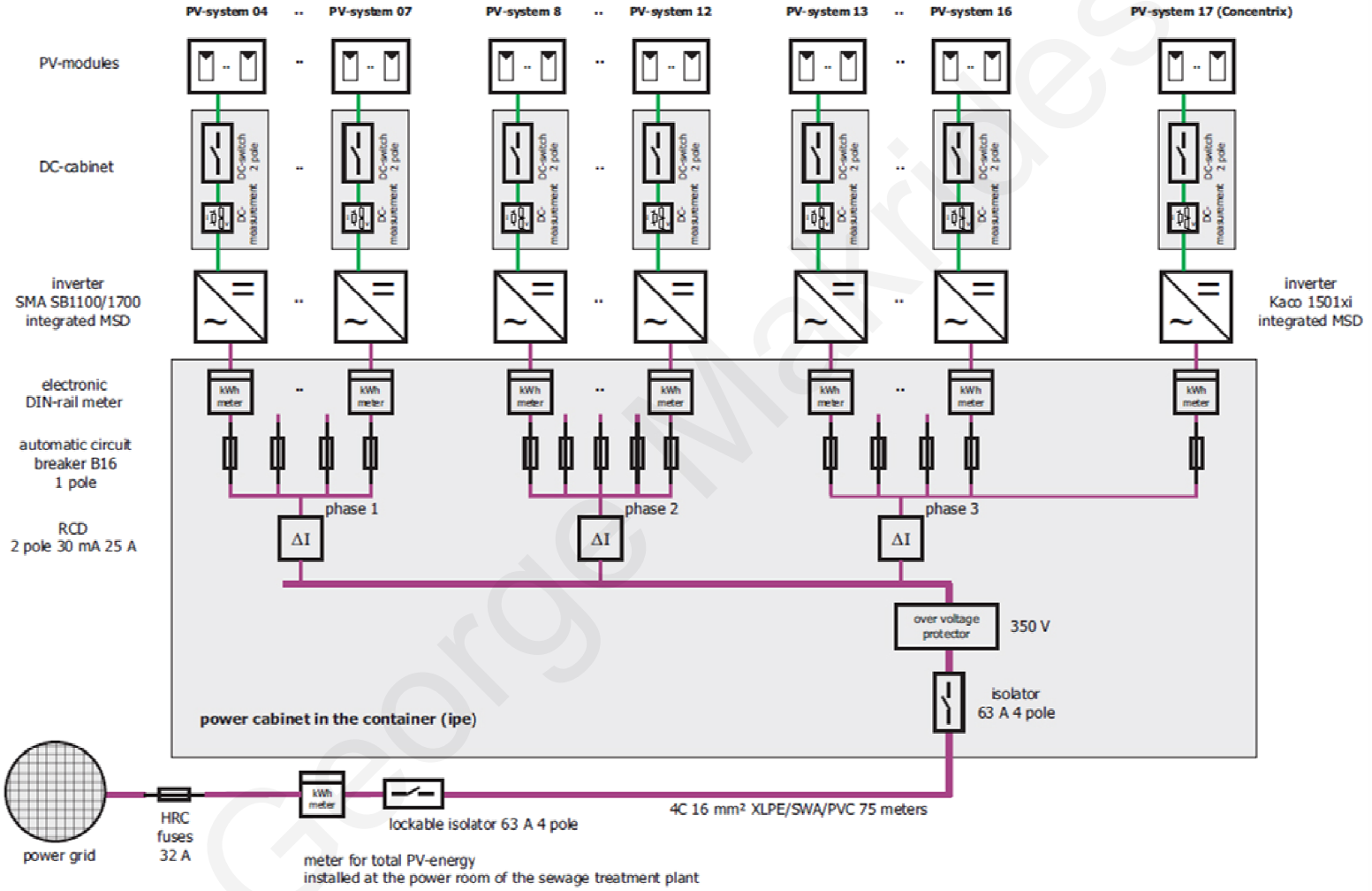

Figure 3.2. Electricity grid connection of the PV systems.

The electricity grid connection of the installed systems is shown in Figure 3.2.

The fixed plane PV systems are installed at the optimum annual energy yield angle for Cyprus of 27.5˚ and are ground-mounted on frames in an array configuration, with most modules placed in series. Table 3.1 gives a brief summary of the installed systems [112].

Table 3.1. Installed PV technologies.

Manufacturer	Technology	Series modules	Parallel modules	System power (kW_p)
Mono-crystalline silicon				
Atersa	mono-c-Si	6	1	1.020
BP Solar	mono-c-Si (Saturn cell)	6	1	1.110
Sanyo	mono-c-Si (HIT cell)	5	1	1.025
Suntechnics	mono-c-Si (back-contact cell)	5	1	1.000
Multi-crystalline silicon				
Schott Solar	multi-c-Si (MAIN cell)	6	1	1.020
Schott Solar	multi-c-Si (EFG)	4	1	1.000
SolarWorld	multi-c-Si	6	1	0.990
Solon	multi-c-Si	7	1	1.540
Thin-film				
Mitsubishi Heavy Industries (MHI)	a-Si (single cell)	2	5	1.000
Schott Solar	a-Si (tandem cell)	6	5	0.960
First Solar	CdTe	3	6	1.080
Würth Solar	CIGS	6	2	0.900

Table 3.2 provides detailed information of each technology, including efficiency, open-circuit voltage and others. All the inverters have a maximum efficiency of 93 %.

Table 3.2. Detailed information of installed PV modules.

Manufacturer	Module type	η_{STC} (%)	V_{oc} (V)	I_{sc} (A)	I_{MPP} (A)	V_{MPP} (V)	P_{MPP} (W)	A (m^2)
Mono-crystalline silicon								
Atersa	A-170M 24V	12.9	44.0	5.10	4.75	35.8	170	1.32
BP Solar	BP7185S	14.8	44.8	5.50	5.10	36.5	185	1.25
Sanyo	HIP-205NHE1	16.4	50.3	5.54	5.05	40.7	205	1.25
Suntechnics	STM 200 FW	16.1	47.8	5.40	5.00	40.0	200	1.24
Multi-crystalline silicon								
Schott Solar	ASE-165-GT-FT/MC	13.0	44.0	5.25	4.71	36	170	1.31
Schott Solar	ASE-260-DG-FT	11.7	70.9	4.91	4.55	57.1	250	2.14
SolarWorld	SW165 poly	12.7	43.9	5.10	4.60	35.5	165	1.30
Solon	P220/6+	13.4	36.5	8.25	7.62	28.9	220	1.64
Thin-film								
MHI	MA100T2	6.4	141.0	1.17	0.93	108	100	1.57
Schott Solar	ASIOPAK-30-SG	5.4	49.0	1.13	0.89	36	32.2	0.60
First Solar	FS60	8.3	90.0	1.14	0.94	64	60	0.72
Würth Solar	WS 11007/75	10.3	45.5	2.50	2.22	36	75	0.73

The infrastructure developed in Cyprus was also replicated in Germany at the *ipv*, University of Stuttgart, and shown in Figure 3.3. The fixed plane PV systems are installed at the optimum annual energy yield angle for Germany of 33˚.

Figure 3.3. Outdoor PV testing facility at the *ipv*, University of Stuttgart, Germany.

3.3 Data measurement infrastructure

The monitoring of the PV systems started at the beginning of June 2006. Both meteorological and PV system measurements are being acquired and stored through an advanced measurement platform. The platform comprises of meteorological and electrical sensors, connected to a central data-logging system that stores data at a resolution of one-second and accumulation steps of fifteen-minute averages. Figure 3.4 shows the installed data-logging equipment.

Figure 3.4. Installed data-logging and storage equipment.

The monitored meteorological parameters include the global irradiance in the POA, wind direction and speed, as well as ambient and module temperature. The electrical parameters measured include DC current and voltage, DC and AC power at MPP, as obtained at each PV system output. All the installed sensors and data-logging devices are listed in Table 3.3.

Table 3.3. Data acquisition equipment and sensors.

Parameter	Manufacturer	Model
Data acquisition	Delphin	Topmessage
Ambient temperature	Theodor Friedrich	2030
Module temperature	Heraeus	PT 100
Global irradiance	Kipp Zonen	CM 21-CV 2
Direct normal irradiance (DNI)	Kipp Zonen	CH 1
DC voltage	Custom made	Potential divider
DC current	Custom made	Shunt resistor
DC power	Delphin	Topmessage
AC energy	NZR	AAD1D5F
Wind speed	Theodor Friedrich	4034
Wind direction	Theodor Friedrich	4122

3.4 Measurement uncertainties

The main sources of uncertainty in the outdoor PV performance evaluations, due to the instrumentation were also investigated. The global irradiance was measured using a thermopile pyranometer in the spectral range of 310-2800 nm and with a ±2 % expected daily uncertainty. In practice, as the expected daily uncertainty of the pyranometer is based on a particular daily profile of irradiance, solar path and ambient temperature variations of a particular location, the application of the sensor in other climatic conditions renders the uncertainty of the pyranometer a function of many variables such as directional errors in zenith and azimuth directions, cosine response, temperature sensitivity and level of irradiance. For a secondary standard instrument, the expected maximum errors are ±2 % for the daily total error, described by the World Meteorological Organisation (WMO), because some response variations cancel out each other if the integration period is long. To further reduce the remaining errors, the conversion of voltage to irradiance, obtained from the calibration sheet of the instrument, is specified and can be important as a bias. For the pyranometer installed in the POA and used in this investigation, the initial calibration value was 11.84 $\mu V/Wm^{-2}$. After four years, the new calibration sensitivity value was 11.86 $\mu V/Wm^{-2}$, yielding an absolute percentage error (APE) of -0.17 % over four years. In addition, the response time of this pyranometer is 5 s (for 95 % response), which is longer than the PV module response time and the one-second data-logging interval. This introduces an additional uncertainty contribution in the measurements that has not been considered in this investigation. Furthermore, the pyranometer was also ventilated and heated, to avoid incorrect measurements caused by dew and snow.

Ambient temperature measurements were accurately recorded with an uncertainty of ±0.15 °C at 25 °C, while PT100 (class B) sensors installed on the back plate of each module provided a measurement with an uncertainty of ±0.425 °C at 25 °C. Module temperature measurements suffer from additional variations due to mounting, heat transfer and temperature variations, which provide additional uncertainties. Previous temperature investigations, based on infrared images taken of the installed PV modules, clearly showed that the temperature distribution in a module is uniform; apart from areas

around the junction box and the main bus-bar interconnection point, which tend to be at a higher temperature, as expected (around 2-3 °C higher) [61].

Parameters including MPP voltage and current were obtained using an *I-V* sensor board and were then connected to the data-logger's analogue channels. The DC voltage was measured by down scaling the PV voltage using a potential divider with two resistors of 0.1 % tolerance each. Accordingly, the DC current was measured using a shunt resistor of 0.1 % tolerance. Both the DC voltage and current resistor tolerances were calibrated by using a high accuracy multi-meter (Keithley 197). The methodology followed was to evaluate the uncertainty differences between the measurement values at the data-logger input and the values measured by the multi-meter, at different current and voltage levels. For each current and voltage level, different calibration factors were calculated and used to increase the measurement accuracy of the acquired measurements.

Subsequently, the evaluated uncertainties at the different levels were applied to the current and voltage fifteen-minute data-points acquired over a one year period (June 2007 - June 2008) to calculate the total uncertainty of the DC energy yield. Before calibration, the PV technologies showed an annual average measurement DC energy yield uncertainty of 0.2 %. After calibration, the annual average measurement DC energy yield uncertainty was much lower (0.04 %) and, was therefore, assumed insignificant. In addition, it must be mentioned that the Keithley 197 used to calibrate the *I-V* cards, was associated with a ±0.015 % uncertainty in the DC voltage range of 20 - 1000 V and with a ±0.75 % uncertainty in the current range of over 2 A and up to 10 A. As almost the entire energy yield in Cyprus is produced at voltage level over 20 V and at high currents over 2 A, a ±0.765 % uncertainty for the annual DC energy yield was assumed.

Additionally, the annual AC energy yield was primarily associated with a metering measurement uncertainty of ±1 % and an additional ±1 % uncertainty that accounts for differences caused by the inverters (efficiency and maximum power point tracking accuracy) [113]. As in the case of the normalised annual DC energy yield, the uncertainty of the AC energy yield increased when normalised to the nominal STC power [114].

Table 3.4 shows the maximum uncertainty of each sensor, acquired from the manufacturer data-sheets and calibration files.

Table 3.4. Installed data-acquisition equipment, sensors and their uncertainties.

Parameter	Manufacturer	Maximum uncertainty
Data measurement	Delphin	±0.01 % of measuring range
Temperature ambient	Theodor Friedrich	$\text{Value}=0.1+\frac{0.005\cdot(C)}{3}$ where C is the measured value ±0.6 % (0.15 °C at 25 °C)
Temperature module	Heraeus	$\text{Value}=0.3+0.005\cdot(C)$ where C is the measured value ±1.7 % (0.425 °C at 25 °C)
Global irradiance	Kipp Zonen	±2 % expected daily uncertainty, ±20 W/m^2 for 1000 W/m^2
Global irradiance	Mencke & Tegtmeyer	±5 % (compared to calibration device)
Wind speed	Theodor Friedrich	±0.3 ms^{-1} at v<10 ms^{-1}
Wind direction	Theodor Friedrich	±2.5 °
AC energy	NRZ	±1 % (measurement uncertainty of AC metering)
DC voltage	Self designed	Potential divider (resistors ±0.1 % tolerance)
DC current	Self designed	Shunt resistor of ±0.1 % tolerance

Furthermore, Table 3.5 shows the uncertainties calculated for the annual AC and DC energy yield measurements.

Table 3.5. Annual AC and DC energy yield measurement uncertainties.

Parameter	Uncertainty	Description
Annual AC energy yield	±2 %	±1 % metering measurement uncertainty and additional ±1 % to account for uncertainties caused by the inverter
Annual DC energy yield	±0.765 %	±0.015 % in the DC voltage range of 20-1000 V and ±0.75 % in the current range of over 2 A and up to 10 A. Calibration measurement uncertainty is insignificant

It must also be noted that the measured annual DC energy yield for each PV technology presented in this work was normalised to the nominal STC power, P_{STC}, given by manufacturer data-sheets, with an assumed power tolerance of ±5 %. Both measured and estimated normalised annual DC energy yield (kWh/kW$_p$) results are also affected by this uncertainty. As the uncertainty investigations are performed at the PV system level, with a multiple number of modules, an important consideration at this point is to also assume that the power tolerance and efficiency uncertainty of each PV system may be lower than ±5 %, as the mean value of a random sample of modules will tend to the nameplate rating if a symmetrical distribution is assumed.

The infrastructure in Cyprus, comprising the different grid-connected PV technologies, the installed sensors and the data-acquisition system, was necessary for the acquisition of data, subsequently used in the analysis of the energy yield modelling, seasonal performance, thermal effects and performance loss rate investigations.

Additionally, data obtained from the systems installed in Germany were also used to compare the performance exhibited at the two locations.

Chapter 4

Energy yield estimation

4.1 Introduction

In this chapter, the estimation of the annual DC energy yield of four models for different grid-connected PV technologies is analysed. The models investigated are the single-point efficiency, single-point efficiency with temperature correction based on manufacturer MPP power temperature coefficients, the PVUSA and the one-diode model.

For each model, the error was found by comparing the estimated energy yield with the outdoor measurements over the four-year evaluation period, June 2006 to June 2010. Furthermore, the degree of accuracy of each model was evaluated by the statistical test of the root mean square error (RMSE), which is a representative indicator of the quality of the model and its ability to describe the real behaviour of each system. More specifically, the RMSE of the monthly average residuals between the measured and each model estimated fifteen-minute average power data-points were evaluated on a monthly basis over a one-year period.

Additionally, the combined uncertainty associated with the estimated annual DC energy yield for the single-point efficiency, the single-point efficiency with temperature correction and PVUSA models was also evaluated, from the uncertainties of each model's input parameters. All the model input parameter uncertainties were obtained from data-sheet specifications provided by the manufacturers. The combined uncertainty of the DC energy yield estimation for each model was calculated using uncertainty propagation techniques.

4.2 Methodology

Initially, the energy yield at the DC side of the installed PV systems was estimated by using the four different modelling approaches. The estimations were then compared against the outdoor measured annual DC energy yield. More details on the different models employed are given below.

4.2.1 Single-point efficiency model

The first and simplest model used was the single-point efficiency model, which estimated the power output of a PV system based on the global irradiance in the POA, STC efficiency and the area of the PV array. All the model parameters were provided from manufacturer data-sheets and the power was obtained from the following equation [21]:

$$P_{\mathrm{DC}} = \eta_{\mathrm{STC}} \cdot A \cdot G_{\mathrm{POA}} \tag{4.1}$$

where P_{DC} is the DC power output, η_{STC} the STC efficiency of the PV module, A the PV array area and G_{POA} is the global irradiance in the POA. The estimated power output was then integrated for all data-sets, over the period of one year, to provide the annual DC energy yield.

4.2.2 Single-point efficiency with temperature correction model

The single-point efficiency model was enhanced with the incorporation of temperature correction, in order to account for thermal losses, which are particularly important for systems installed outdoors in locations with high temperatures (such as Cyprus). The temperature correction parameter, η_{T}, accounts for the thermal losses using the manufacturers' MPP power temperature coefficient, γ, and the difference of module temperature, T_{module}, with respect to the STC module temperature, T_{STC}, at 25 °C. The following equations were used to calculate the power produced [2]:

$$P_{\mathrm{DC}} = \eta_{\mathrm{T}} \cdot \eta_{\mathrm{STC}} \cdot A \cdot G_{\mathrm{POA}} \tag{4.2}$$

$$\eta_{\mathrm{T}} = \begin{cases} 1 + \gamma \cdot (T_{\mathrm{module}} - T_{\mathrm{STC}}), & T_{\mathrm{module}} > 25\ ^{\circ}C \\ 1, & T_{\mathrm{module}} \leq 25\ ^{\circ}\mathrm{C} \end{cases} \quad (4.3)$$

Thermal gains that would be observed if the temperature correction parameter η_{T} was not set to 1, for module temperatures below and equal to 25 °C, were not accounted for in this investigation. At module temperatures ≤ 25 °C this model operated exactly as the single-point efficiency model with no associated power losses or gains. Nonetheless, only a few data-points fall in this range (at temperatures ≤ 25 °C) hence even if the power gain was considered for these data-points, the energy yield gain would still be insignificant as most of the energy production in Cyprus occurred at module temperatures over 25 °C

In the end, each estimated power data-set was summed up over the period of one year, to provide the DC annual energy yield estimation.

4.2.3 Photovoltaic for Utility-Scale Applications (PVUSA) model

The PVUSA model uses a simple regression to rate PV systems at the PVUSA Test Conditions, which are defined as 1000 W/m^2 POA irradiance, 20 $^{\circ}$C ambient temperature, and 1 m/s wind speed, based on outdoor measured data of irradiance at the POA, ambient temperature, wind speed and power [38]. The outdoor measured data over the period June 2007 - June 2008 was used to find the best-fit for the PVUSA rating, according to the equation below [38]:

$$P_{\mathrm{DC}} = G_{\mathrm{POA}} \cdot (a + b\, G_{\mathrm{POA}} + c\, T_{\mathrm{amb}} + d\, WS) \quad (4.4)$$

where P_{DC} is the DC power output, G_{POA} the total irradiance in the POA, T_{amb} the ambient temperature, *WS* the wind speed, and *a*, *b*, *c* and *d* are regression coefficients. The resulting equation and regression coefficients were then used to estimate PV performance, given the global irradiance in the POA, ambient temperature and wind speed measurements. Finally, the estimated power data-sets were again integrated over one year, to provide a value for the annual DC energy yield for each technology.

4.2.4 One-diode model

For the one-diode model five parameters that are not directly available from manufacturer data-sheets, were required: the photocurrent, I_{ph}, diode saturation current, I_0, diode ideality factor, n, series and shunt resistance, R_{series} and R_{shunt}. These parameters were computed through the INSEL simulation software, using manufacturer data-sheet information [8], [32]. More specifically, this software is capable of calculating the photocurrent density, C_{ph}, the coefficient of light generated current density, C_t, the Shockley saturation diode parameter, C_s, the series resistance R_{series}, and the shunt resistance R_{shunt}, which are used by the one-diode model, by two different methods. In the first method, the parameters are obtained by the software by using a fitting procedure to one or more experimentally measured *I-V* curves [32]. In the second method, which was employed in this investigation, the software was used to calculate the one-diode model parameters using algebraic analysis, purely based on the data-sheet parameters of module manufacturers [32].

More specifically, the parameters of C_{ph}, C_t, C_s, R_{series} and R_{shunt} were calculated from the nominal power at MPP, P_{MPP}, the short-circuit current I_{sc} and its temperature coefficient α, the open-circuit voltage V_{oc} and its temperature coefficient β and a set of equations that also consider parameters such as the open-circuit voltage V_{oc} at current density, J, equal to zero, the MPP voltage and current, the derivative of voltage with respect to temperature at the open circuit voltage and finally the derivative of power with respect to voltage at the MPP voltage.

The current produced by the one-diode model for a solar cell is given as [27]:

$$I = I_{ph} - I_0 \cdot \left(e^{\frac{q(V + I\,R_{series})}{n\,k\,T}} - 1 \right) - \frac{V + I\,R_{series}}{R_{shunt}} \tag{4.5}$$

where I, is the current output, V, the voltage, k, Boltzmann's constant, T, the temperature and q is the electric charge. The photocurrent density is obtained from the following equation:

$$J_{ph} = \left(C_{ph} + C_t\,T\right) \cdot G \tag{4.6}$$

where J_{ph}, is the photocurrent density, C_{ph}, the coefficient of light generated current density, C_t, the temperature coefficient of light generated current density, T, the temperature and G is the global irradiance. Subsequently, the diode saturation current density, J_0, is given by:

$$J_0 = C_s \cdot T^3 e^{\frac{-E_g}{nkT}} \quad (4.7)$$

where C_s, is the Shockley saturation diode parameter and E_g is the band-gap energy of the material.

The MPP current and voltage data-sets were then calculated and used to estimate the DC MPP power data-sets, which were then integrated over the one-year period, to provide the annual DC energy yield for each system.

4.2.5 Annual energy yield model uncertainty

The combined uncertainties of the single-point efficiency, single-point efficiency with temperature correction and PVUSA models associated with the output annual DC energy yield estimation were also investigated. The data-sheet power tolerance and the module efficiency uncertainty for all installed PV technologies were taken to be ±5 %. All the model input uncertainties associated with the data-sheet specifications are listed in detail in Table 4.1.

Table 4.1. Model input parameter uncertainties.

Parameter	Measurement	Maximum uncertainty
MPP power	Datasheet general tolerance value of P_{MPP}	±5 %
Efficiency	Datasheet general tolerance value of η_{STC}	±5 %
Power temperature coefficient	Datasheet general tolerance value of γ	γ ±0.05 %/K

4.2.5.1 Single-point efficiency model annual energy yield uncertainty

The combined uncertainty of the DC energy yield estimation for the single-point efficiency model was calculated using uncertainty propagation techniques [115]. In this case, the combined uncertainty associated with the value for a single estimated power data-point, was found by summing up the percentage relative errors when multiplication of the input

parameters occurred. More specifically, this is shown in the following equation by considering the input parameters of the model, such as the STC efficiency of the PV module (uncertainty of ±5 %) and the global irradiance in the POA (uncertainty of ±2 %):

$$E_{\mathrm{DC}} = \sum_{i=0}^{year} \eta_{\mathrm{STC}} \cdot A \cdot G_{\mathrm{POAi}} \tag{4.8}$$

where *i*, is the index of summation of the 15-minute data-sets over a period of a year.

For this model, since the uncertainties are given as percentage relative errors, the ±7 % combined uncertainty found for each estimated DC power data-point applies also to the annual DC energy yield value.

4.2.5.2 Single-point efficiency with temperature correction model annual energy yield uncertainty

Similarly, the combined uncertainty associated with the annual DC energy yield estimated value for the single-point efficieny with temperature correction model was also investigated. In this case, considering equation 4.9 and its expanded form shown in equation 4.10, where η_{T} is the temperature correction parameter as in equation 4.3, the uncertainty in each input parameter propagates through the sensitivity coefficients, which are the partial derivatives of each uncertainty parameter [115].

$$P_{\mathrm{DC}} = \eta_{\mathrm{T}}\, \eta_{\mathrm{STC}}\, A\, G_{\mathrm{POA}} \tag{4.9}$$

$$P_{\mathrm{DC}} = \eta_{\mathrm{STC}}\, A\, G_{\mathrm{POA}} + \gamma\, T_{\mathrm{module}}\, \eta_{\mathrm{STC}}\, A\, G_{\mathrm{POA}} - \gamma\, T_{\mathrm{STC}}\, \eta_{\mathrm{STC}}\, A\, G_{\mathrm{POA}} \tag{4.10}$$

The sensitivity coefficients, with respect to the parametric uncertainties of η_{STC}, G_{POA}, γ_{PMPP} and T_{module}, were evaluated and used to obtain the combined uncertainty, u_{C}.

The combined uncertainty of a single estimated DC power data-point based on the absolute uncertainties and sensitivity coefficients for the single-point efficiency with temperature correction model, was obtained by combining the individual standard uncertainties using the law of propagation uncertainties and the root-sum-squares (RSS) of all uncertainty components [115]:

$$u_{\mathrm{C}} = \sqrt{\left[\left(\frac{\partial P_{DC}}{\partial \eta_{\mathrm{STC}}} u_{\eta_{\mathrm{STC}}}\right)^2 + \left(\frac{\partial P_{DC}}{\partial \gamma} u_{\gamma}\right)^2 + \left(\frac{\partial P_{DC}}{\partial T_{\mathrm{module}}} u_{T_{\mathrm{Module}}}\right)^2 + \left(\frac{\partial P_{DC}}{\partial G_{\mathrm{POA}}} u_{G_{\mathrm{POA}}}\right)^2\right]} \quad (4.11)$$

The combined uncertainty associated with the annual DC energy yield was evaluated by integrating all calculated uncertainties of each power data-point over a year for each PV technology.

4.2.5.3 PVUSA model annual energy yield uncertainty

Finally, the combined uncertainty associated with the estimated annual DC energy yield for the PVUSA model was evaluated by again deriving the partial derivatives of the PVUSA model input variables. Specifically, the sensitivity coefficients of G_{POA}, T_{amb} and WS were evaluated based on the PVUSA equation:

$$P_{\mathrm{DC}} = G_{\mathrm{POA}} \cdot (a + b\, G_{\mathrm{POA}} + c\, T_{\mathrm{amb}} + d\, WS) \quad (4.12)$$

The combined uncertainty of each DC power data-point based on the absolute uncertainty parameters of irradiance, wind speed and ambient temperature for the PVUSA model is given by the RSS:

$$u_{\mathrm{C}} = \sqrt{\left[\left(\frac{\partial P_{\mathrm{DC}}}{\partial G_{\mathrm{POA}}} u_{G_{\mathrm{POA}}}\right)^2 + \left(\frac{\partial P_{\mathrm{DC}}}{\partial T_{\mathrm{Amb}}} u_{T_{\mathrm{amb}}}\right)^2 + \left(\frac{\partial P_{\mathrm{DC}}}{\partial WS} u_{WS}\right)^2\right]} \quad (4.13)$$

The combined annual DC energy yield uncertainty for the PVUSA model was evaluated by adding all calculated uncertainties of each power data-point over a year, for each PV technology.

In addition, the PVUSA model results are further associated with an uncertainty component due to fitting inaccuracies, as the model is first used to determine the regression coefficients *a*, *b*, *c* and *d* which are subsequently used in the annual DC energy yield estimation investigation. These coefficients were found by applying linear regression on real measurement data-sets over the period June 2007 - June 2008 after all technologies and especially the a-Si had stabilised. Statistically, the fitting accuracy of the regression coefficients was found using the coefficient of determination, R^2, from the difference

between the measured and estimated power data-points over the period June 2007 - June 2008. In general R^2 is defined as:

$$R^2 = 1 - \frac{\sum_i (X_i - F_i)^2}{\sum_i (X_i - \bar{X})^2} \tag{4.14}$$

where X_i are the observed values, F_i are the modelled values and $\bar{X}$ is the mean of the observed values of X. The fact that an uncertainty component due to fitting inaccuracies is also associated with this model, makes the uncertainty evaluation more elaborate compared to the single-point efficiency and single-point efficiency with temperature correction model uncertainty evaluations and must therefore be considered in order for the evaluations to be comparable.

Table 4.2 summarises the PVUSA regression coefficients, the R^2 value of the fit, the RMSE and model fit uncertainties over the period June 2007 - June 2008 for each PV technology. Most PV technologies exhibited good fit over the period under consideration and the model fit uncertainty of each PV technology was evaluated from the R^2 value. The total uncertainty was evaluated by adding the model fit uncertainty component, which for simplicity was assumed to be ±2 %, based on the average of all technologies, with the combined uncertainty due to the measurement errors in the model input variables.

Table 4.2. PVUSA regression coefficients over the period June 2007 - June 2008. The R^2, RMSE and model fit uncertainties are also given.

System	*a*	*b*	*c*	*d*	R^2 (%)	RMSE (W/kW_p)	Fit uncertainty (%)
Atersa (A-170M 24V)	1.2616	-0.0003	-0.0049	0.0135	98.7	35.5	±1.3
BP Solar (BP7185S)	1.2628	-0.0003	-0.0039	0.0112	94.6	68.4	±5.4
Sanyo (HIP-205NHE1)	1.2121	-0.0003	-0.0022	0.0053	98.5	37.5	±1.5
Suntechnics (STM 200 FW)	1.2059	-0.0002	-0.0041	0.0111	98.9	35.1	±1.1
Schott Solar (ASE-165-GT-FT/MC)	1.2573	-0.0003	-0.0039	0.0099	98.8	36.8	±1.2
Schott Solar (ASE-260-DG-FT)	1.2165	-0.0003	-0.0041	0.0090	98.7	35.6	±1.3
SolarWorld (SW165)	1.1824	-0.0003	-0.0043	0.0116	98.7	33.1	±1.3
Solon (P220/6+)	1.9049	-0.0005	-0.0067	0.0153	97.2	50.5	±2.8
MHI (MA100T2)	1.0330	-0.0003	0.0024	0.0052	98.5	36.8	±1.5
Schott Solar (ASIOPAK-30-SG)	1.0156	-0.0003	0.0006	0.0076	98.6	36.5	±1.4
Würth Solar (WS 11007/75)	1.1604	-0.0003	-0.0031	0.0086	97.6	51.3	±2.4
First Solar (FS60)	1.2126	-0.0003	0.0001	0.0029	98.8	39.9	±1.2
Average	**1.2438**	**-0.0003**	**-0.0028**	**0.0093**	**98.1**	**41.4**	**±1.9**

4.3 Modelling results

4.3.1 Measured and estimated annual DC energy yield

The measured and estimated annual DC energy yield, normalised to the data-sheet rated power of the PV technologies, was evaluated for the period June 2006 - June 2010. The measured annual solar irradiation over the period June 2006 - June 2010 in Cyprus is summarised in Table 4.3. The annual solar irradiation measurement uncertainty, based only on the expected daily uncertainty of the pyranometer (±2 %), was also calculated and shown in Table 4.3.

Table 4.3. Global irradiation in the POA and measurement uncertainty over the period June 2006 - June 2010.

Period	Global irradiation POA (kWh/m^2)	Global irradiation POA uncertainty (kWh/m^2)
June 2006 - June 2007	1988	39.8
June 2007 - June 2008	2054	41.1
June 2008 - June 2009	1997	39.9
June 2009 - June 2010	2006	40.1

The measured and estimated annual DC energy yield for all models over the period: June 2006 - June 2007, June 2007 - June 2008, June 2008 - June 2009 and June 2009 - June 2010 is summarised in Table 4.4, Table 4.5, Table 4.6 and Table 4.7, respectively. The single-point efficiency energy yield was evaluated by considering that the power of each PV system was equal to the product of the total irradiance in the POA, the PV array area and the STC efficiency provided from the manufacturer data-sheets. In practice some deviations from the nameplate power value were found, when evaluating the model by using the manufacturer provided area and STC efficiency, but those are not considered in this work. The estimation absolute percentage error (APE) was calculated for each technology by subtracting the estimated energy yield from the measured annual DC energy yield and normalising the result to the measured annual DC energy yield, given by:

$$\text{APE} = \frac{\text{Measured } E_{\text{DC}} - \text{Estimated } E_{\text{DC}}}{\text{Measured } E_{\text{DC}}} \cdot 100 \quad (4.15)$$

Both measured and estimated annual yield were normalised to the manufacturers' rated power, to allow the comparison between identical systems of 1 kW_p nominal power.

Table 4.4. Estimated and measured annual DC energy yield $E_{DC(Normalised)}$ normalised to the manufacturers' rated power over the period June 2006 - June 2007.

System	Measured	Single-point efficiency		Single-point efficiency and temperature		PVUSA		One-diode	
	$E_{DC(Normalised)}$ (kWh/kW$_p$)	$E_{DC(Normalised)}$ (kWh/kW$_p$)	APE (%)	$E_{DC(Normalised)}$ (kWh/kW$_p$)	APE (%)	$E_{DC(Normalised)}$ (kWh/kW$_p$)	APE (%)	$E_{DC(Normalised)}$ (kWh/kW$_p$)	APE (%)
Atersa (A-170M 24V)	**1753**	1988	-13.40	1860	-6.09	1864	-6.35	1812	-3.36
BP Solar (BP7185S)	**1612**	1988	-23.30	1794	-11.28	1753	-8.73	1784	-10.62
Sanyo (HIP-205NHE1)	**1790**	1988	-11.08	1879	-5.01	1864	-4.13	1803	-0.75
Suntechnics (STM 200 FW)	**1864**	1988	-6.67	1856	0.40	1959	-5.11	1795	3.68
Schott Solar (ASE-165-GT-FT/MC)	**1752**	1988	-13.46	1830	-4.45	1893	-8.05	1737	0.86
Schott Solar (ASE-260-DG-FT)	**1721**	1988	-15.51	1811	-5.23	1837	-6.74	1732	-0.66
SolarWorld (SW165)	**1731**	1988	-14.86	1806	-4.33	1786	-3.16	1717	0.77
Solon (P220/6+)	**1715**	1988	-15.91	1825	-6.40	1835	-6.97	1807	-5.33
MHI (MA100T2)	**1734**	1988	-14.66	1923	-10.90	1781	-2.70	2200	-26.92
Schott Solar (ASIOPAK-30-SG) *	**1599**	1988	-24.29	1915	-19.73	1724	-7.76	2230	-39.41
Würth Solar (WS 11007/75)	**1827**	1988	-8.80	1842	-0.83	1971	-7.85	1722	5.76
First Solar (FS60)	**1755**	1988	-13.27	1886	-7.44	1867	-6.40	2433	-38.63
Average	**1738**	1988	-14.60	1852	-6.77	1845	-6.16	1898	-9.55

Table 4.5. Estimated and measured annual DC energy yield $E_{DC(Normalised)}$ normalised to the manufacturers' rated power over the period June 2007 - June 2008.

System	Measured	Single-point efficiency		Single-point efficiency and temperature		PVUSA		One-diode	
	$E_{DC(Normalised)}$ (kWh/kW$_p$)	$E_{DC(Normalised)}$ (kWh/kW$_p$)	APE (%)	$E_{DC(Normalised)}$ (kWh/kW$_p$)	APE (%)	$E_{DC(Normalised)}$ (kWh/kW$_p$)	APE (%)	$E_{DC(Normalised)}$ (kWh/kW$_p$)	APE (%)
Atersa (A-170M 24V)	**1810**	2054	-13.47	1918	-5.96	1919	-6.02	1871	-3.35
BP Solar (BP7185S)	**1593**	2054	-28.93	1845	-15.84	1806	-13.38	1838	-15.39
Sanyo (HIP-205NHE1)	**1814**	2054	-13.25	1938	-6.86	1922	-5.98	1864	-2.77
Suntechnics (STM 200 FW)	**1890**	2054	-8.67	1912	-1.18	2012	-6.47	1853	1.98
Schott Solar (ASE-165-GT-FT/MC)	**1810**	2054	-13.45	1881	-3.92	1950	-7.72	1788	1.24
Schott Solar (ASE-260-DG-FT)	**1783**	2054	-15.23	1866	-4.70	1892	-6.13	1785	-0.16
SolarWorld (SW165)	**1772**	2054	-15.89	1858	-4.82	1838	-3.73	1773	-0.02
Solon (P220/6+)	**1761**	2054	-16.64	1878	-6.64	1889	-7.27	1859	-5.59
MHI (MA100T2)	**1734**	2054	-18.42	1982	-14.28	1844	-6.32	2283	-31.64
Schott Solar (ASIOPAK-30-SG) *	**1650**	2054	-24.46	1974	-19.63	1782	-8.01	2313	-40.16
Würth Solar (WS 11007/75)	**1863**	2054	-10.24	1877	-0.73	2031	-9.00	1756	5.78
First Solar (FS60)	**1752**	2054	-17.26	1944	-10.96	1930	-10.17	2523	-44.05
Average	**1769**	2054	-16.33	1906	-7.96	1901	-7.52	1959	-11.17

Table 4.6. Estimated and measured annual DC energy yield $E_{DC(Normalised)}$ normalised to the manufacturers' rated power over the period June 2008 - June 2009.

System	Measured	Single-point efficiency		Single-point efficiency and temperature		PVUSA		One-diode	
	$E_{DC(Normalised)}$ (kWh/kW$_p$)	$E_{DC(Normalised)}$ (kWh/kW$_p$)	APE (%)	$E_{DC(Normalised)}$ (kWh/kW$_p$)	APE (%)	$E_{DC(Normalised)}$ (kWh/kW$_p$)	APE (%)	$E_{DC(Normalised)}$ (kWh/kW$_p$)	APE (%)
Atersa (A-170M 24V)	**1744**	1997	-14.51	1865	-6.94	1859	-6.62	1817	-4.18
BP Solar (BP7185S)	**1457**	1997	-37.03	1796	-23.26	1751	-20.13	1787	-22.62
Sanyo (HIP-205NHE1)	**1731**	1997	-15.39	1884	-8.87	1865	-7.76	1808	-4.46
Suntechnics (STM 200 FW)	**1800**	1997	-10.92	1858	-3.22	1957	-8.68	1798	0.13
Schott Solar (ASE-165-GT-FT/MC)	**1736**	1997	-15.02	1832	-5.52	1891	-8.90	1740	-0.21
Schott Solar (ASE-260-DG-FT)	**1714**	1997	-16.53	1815	-5.93	1834	-7.04	1736	-1.30
SolarWorld (SW165)	**1689**	1997	-18.24	1809	-7.11	1781	-5.47	1721	-1.92
Solon (P220/6+)	**1681**	1997	-18.81	1828	-8.75	1831	-8.94	1809	-7.61
MHI (MA100T2)	**1644**	1997	-21.45	1917	-16.60	1787	-8.71	2213	-34.58
Schott Solar (ASIOPAK-30-SG) *	**1571**	1997	-27.14	1921	-22.31	1727	-9.93	2241	-42.70
Würth Solar (WS 11007/75)	**1748**	1997	-14.21	1839	-5.16	1969	-12.61	1717	1.80
First Solar (FS60)	**1645**	1997	-21.37	1891	-14.91	1873	-13.83	2445	-48.63
Average	**1680**	1997	-19.22	1855	-10.72	1844	-9.89	1903	-13.86

Table 4.7. Estimated and measured annual DC energy yield $E_{DC(Normalised)}$ normalised to the manufacturers' rated power over the period June 2009 - June 2010.

System	Measured	Single-point efficiency		Single-point efficiency and temperature		PVUSA		One-diode	
	$E_{DC(Normalised)}$ (kWh/kW$_p$)	$E_{DC(Normalised)}$ (kWh/kW$_p$)	APE (%)	$E_{DC(Normalised)}$ (kWh/kW$_p$)	APE (%)	$E_{DC(Normalised)}$ (kWh/kW$_p$)	APE (%)	$E_{DC(Normalised)}$ (kWh/kW$_p$)	APE (%)
Atersa (A-170M 24V)	**1719**	2006	-16.68	1866	-8.54	1852	-7.74	1817	-5.71
BP Solar (BP7185S)	**1510**	2006	-32.86	1798	-19.10	1746	-15.64	1789	-18.51
Sanyo (HIP-205NHE1)	**1703**	2006	-17.77	1887	-10.81	1863	-9.38	1811	-6.31
Suntechnics (STM 200 FW)	**1793**	2006	-11.86	1861	-3.78	1953	-8.91	1802	-0.46
Schott Solar (ASE-165-GT-FT/MC)	**1712**	2006	-17.19	1836	-7.24	1886	-10.17	1745	-1.94
Schott Solar (ASE-260-DG-FT)	**1688**	2006	-18.81	1818	-7.67	1829	-8.31	1742	-3.20
SolarWorld (SW165)	**1654**	2006	-21.25	1810	-9.41	1775	-7.27	1724	-4.19
Solon (P220/6+)	**1637**	2006	-22.57	1827	-11.64	1825	-11.49	1807	-10.43
MHI (MA100T2)	**1617**	2006	-24.07	1934	-19.60	1792	-10.82	2234	-38.17
Schott Solar (ASIOPAK-30-SG) *	**1554**	2006	-29.12	1926	-23.99	1728	-11.20	2264	-45.72
Würth Solar (WS 11007/75)	**1707**	2006	-17.53	1859	-8.93	1964	-15.07	1738	-1.82
First Solar (FS60)	**1605**	2006	-24.96	1894	-17.97	1875	-16.80	2465	-53.54
Average	**1658**	2006	-21.22	1860	-12.39	1841	-11.07	1912	-15.83

* The Schott Solar a-Si system had a broken module since October 2006.

** Partial shading had been affecting the performance of the BP Solar mono-c-Si and Solon multi-c-Si systems during the second, third and fourth years.

4.3.2 Annual DC energy yield model combined uncertainties

The total annual DC energy yield uncertainties for the single-point efficiency, single-point efficieny with temperature correction and PVUSA models, for each PV technology, over the period June 2006 - June 2010 are shown in Table 4.8.

Table 4.8. Single-point efficiency, single-point efficiency with temperature correction and PVUSA model combined uncertainties associated with the estimated annual DC energy yield, normalised to the manufacturers' rated power at STC, $E_{DC(Normalised)}$, over the period June 2006 - June 2010. The uncertainties are also shown as a percentage of the estimated annual DC energy yield of each model.

System	2006 - 2007 $E_{DC(Normalised)}$ uncertainty		2007 - 2008 $E_{DC(Normalised)}$ uncertainty		2008 - 2009 $E_{DC(Normalised)}$ uncertainty		2009 - 2010 $E_{DC(Normalised)}$ uncertainty	
	(kWh/kW$_p$)	(%)	(kWh/kW$_p$)	(%)	(kWh/kW$_p$)	(%)	(kWh/kW$_p$)	(%)
Single-point efficiency model								
All PV systems	±139.16	±7	±143.78	±7	±139.79	±7	±140.42	±7
Single-point efficiency with temperature correction model								
Atersa (A-170M 24V)	±104.73	±5.63	±107.72	±5.62	±105.18	±5.64	±104.99	±5.63
BP Solar (BP7185S)	±105.43	±5.88	±108.29	±5.87	±105.83	±5.89	±105.36	±5.86
Sanyo (HIP-205NHE1)	±105.11	±5.59	±108.14	±5.58	±105.48	±5.60	±105.49	±5.59
Suntechnics (STM 200 FW)	±104.97	±5.66	±107.97	±5.65	±105.37	±5.67	±105.22	±5.65
Schott Solar (ASE-165-MC)	±105.29	±5.75	±107.82	±5.73	±105.38	±5.75	±105.16	±5.73
Schott Solar (ASE-260-DG-FT)	±105.08	±5.80	±108.06	±5.79	±105.45	±5.81	±105.38	±5.80
SolarWorld (SW165)	±105.37	±5.83	±108.36	±5.83	±105.47	±5.83	±105.42	±5.82
Solon (P220/6+)	±105.07	±5.76	±108.05	±5.75	±105.37	±5.76	±105.41	±5.77
MHI (MA100T2)	±105.76	±5.50	±108.61	±5.48	±106.07	±5.53	±105.99	±5.48
Schott Solar (ASIOPAK-30-SG)	±105.88	±5.53	±108.97	±5.52	±106.45	±5.54	±106.15	±5.51
Würth Solar (WS 11007/75)	±105.31	±5.72	±107.97	±5.75	±104.92	±5.71	±107.39	±5.78
First Solar (FS60)	±104.66	±5.55	±107.82	±5.55	±105.03	±5.56	±105.20	±5.55
PVUSA model								
Atersa (A-170M 24V)	±67.68	±3.63	±69.56	±3.62	±67.42	±3.63	±67.02	±3.62
BP Solar (BP7185S)	±63.46	±3.62	±65.37	±3.62	±63.29	±3.62	±62.98	±3.61
Sanyo (HIP-205NHE1)	±66.75	±3.58	±68.84	±3.58	±66.73	±3.58	±66.51	±3.57
Suntechnics (STM 200 FW)	±73.58	±3.76	±75.56	±3.75	±73.45	±3.75	±73.22	±3.75
Schott Solar (ASE-165-MC)	±68.31	±3.61	±70.36	±3.61	±68.15	±3.60	±67.81	±3.60
Schott Solar (ASE-260-DG-FT)	±65.86	±3.59	±67.81	±3.58	±65.68	±3.58	±65.32	±3.57
SolarWorld (SW165)	±64.11	±3.59	±66.00	±3.59	±63.88	±3.59	±63.48	±3.58
Solon (P220/6+)	±65.23	±3.56	±67.15	±3.55	±65.01	±3.55	±64.51	±3.54
MHI (MA100T2)	±63.25	±3.55	±65.53	±3.55	±63.44	±3.55	±63.47	±3.54
Schott Solar (ASIOPAK-30-SG)	±60.92	±3.53	±63.02	±3.54	±60.97	±3.53	±60.86	±3.52
Würth Solar (WS 11007/75)	±70.32	±3.57	±72.46	±3.57	±70.17	±3.56	±69.82	±3.55
First Solar (FS60)	±67.18	±3.60	±69.43	±3.60	±67.32	±3.59	±67.27	±3.59

Between the three investigated models, the PVUSA showed the lowest combined uncertainties for the annual DC energy yield estimation. This is attributed to the fact that the input parameters of this model include the solar irradiance in the POA, ambient temperature and wind speed. Moreover, in contrast to the single-point efficiency and single-

point efficiency with temperature correction models, the PVUSA model is not associated with power tolerance uncertainties. The total combined uncertainty of the PVUSA model includes both the uncertatinty of the model fit, ±2 % approximate average of all technologies, and the combined uncertainty due to the measurement errors in the model input variables.

The annual DC energy yield uncertainties for the one-diode model were not evaluated in this work because the input parameters for this model were not acquired from measurements but instead were extracted from the computations of the INSEL simulation software, which calculated these parameters from manufacturer data-sheet values. Consequently, the uncertainties associated with the estimation of each respective one-diode model parameter for each technology by the software cannot be evaluated. The uncertainties of each parameter for this model can be only obtained by using equipment such as solar simulators that provide the I-V characteristic curve and diode parameters for each module.

4.3.3 Annual DC energy yield APE with single-point efficiency model

During the first year of operation, the single-point efficiency model estimated the annual DC energy yield of mono-c-Si technologies with an average APE of -14 %. For the same period, for both multi-c-Si and thin-film technologies the average APE was -15 %. The estimation APE results of the single-point efficiency model over the period June 2006 - June 2010 are shown in Figure 4.1, provided evidence that for all technologies, apart from the Solon multi-c-Si and the BP Solar mono-c-Si which suffered from shading, there was a gradual increase in deviation of estimated against real measured yield through the years. As this deviation increased every year, the source cannot be viewed as a seasonal loss factor but as a progressive loss which gets worse over time. The highest deviations progressively occurred for the thin-film technologies, which may be attributed to losses (such as faults of modules, as is the case for the Schott Solar a-Si system). The model annual DC energy yield combined uncertainty and ±0.765 % uncertainty for the annual DC energy yield are also shown in Figure 4.1.

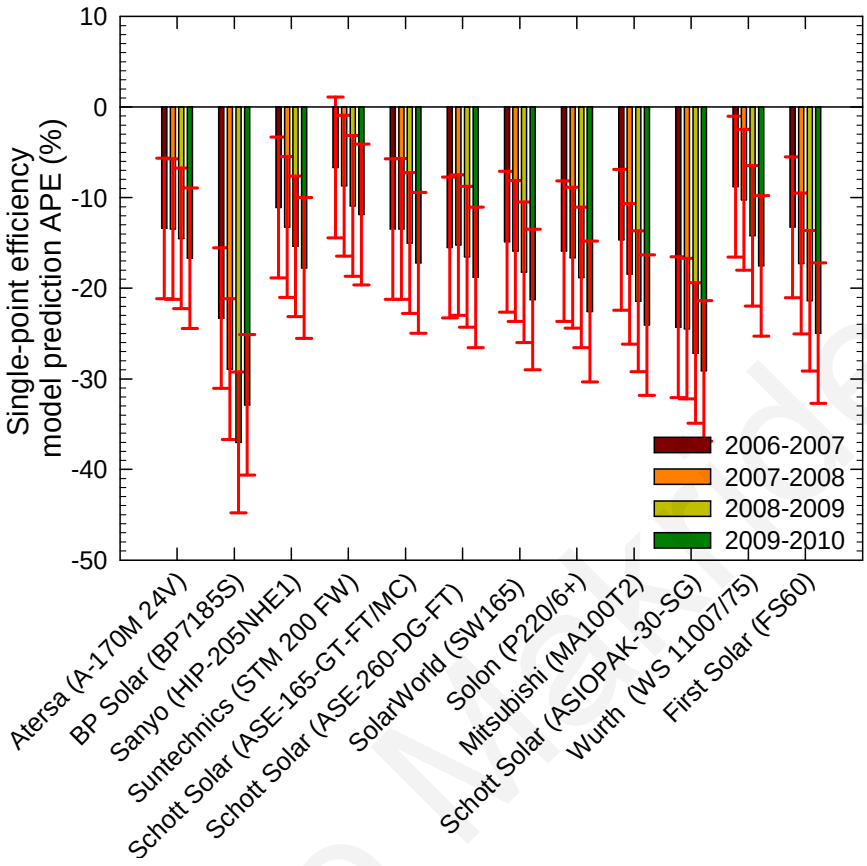

Figure 4.1. Single-point efficiency model annual DC energy yield estimation APE over the period June 2006 - June 2010. Model annual DC energy yield combined uncertainty and ±0.765 % uncertainty for the annual DC energy yield are also shown.

In addition, the degree of accuracy of each model was evaluated by the statistical test of the RMSE, which is a representative indicator of the quality of the model and its ability to describe the real behaviour of each system. More specifically, the RMSE of the monthly average residuals between the measured and single-point efficiency model estimated fifteen-minute average power data-points were evaluated on a monthly basis over a one year period. Figure 4.2 shows the monthly average RMSE of the residuals for each PV technology between June 2007 and June 2008.

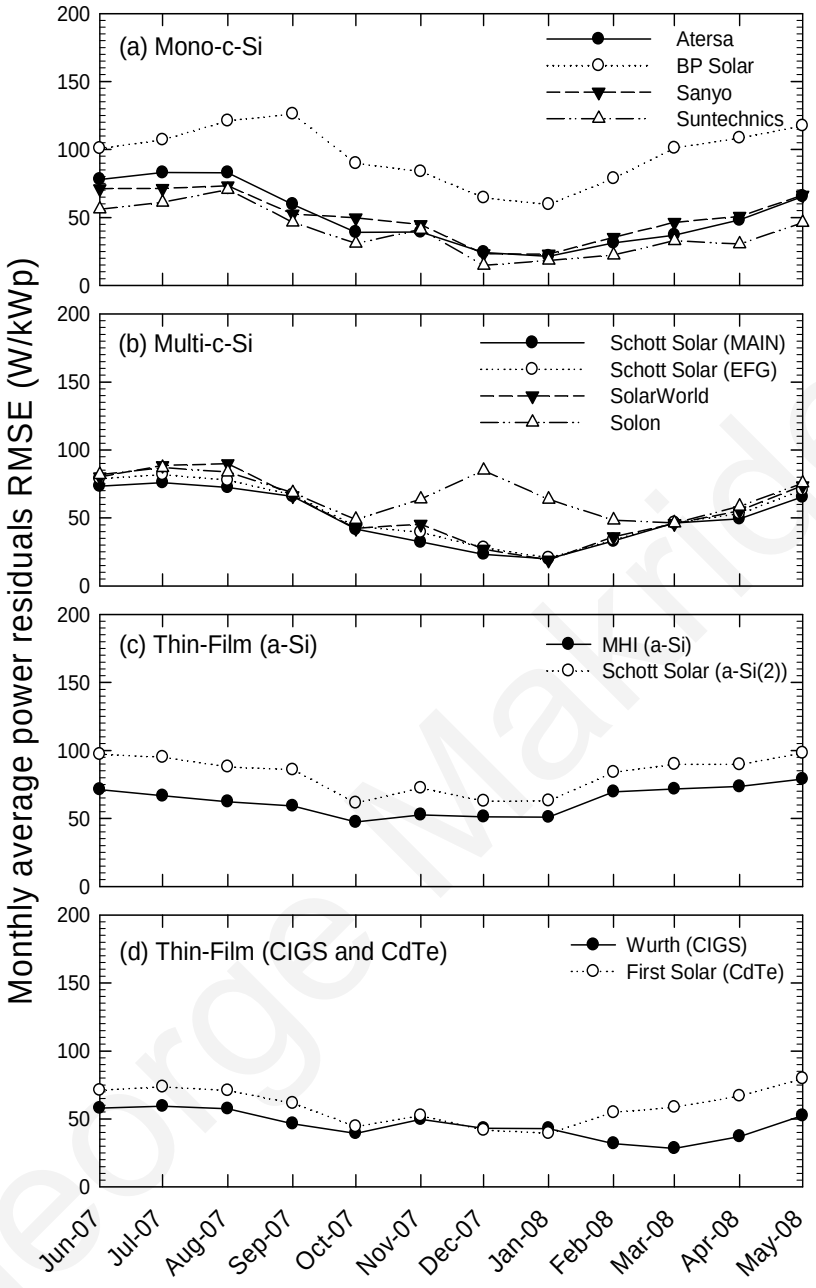

Figure 4.2. Single-point efficiency model monthly average RMSE of power data-point residuals of installed PV systems over the period June 2007 - June 2008.

It is obvious from Figure 4.2a and b that for both mono-c-Si and multi-c-Si technologies, the single-point efficiency model estimates the power with higher accuracy during the colder winter season, rather than during warmer periods, as higher estimation deviations (higher RMSE of monthly average DC power), particularly during summer and spring, are observed. This reveals further technology performance behaviours, such as seasonal

variations. The BP Solar mono-c-Si system showed the highest monthly RMSE values over the one year period due to shading loss, as shown in Figure 4.2b. Shading was the reason for the high RMSE values of the Solon multi-c-Si during the winter period depicted in Figure 4.2b. Similar model performance to the c-Si technologies was exhibited by the thin-film technologies, although the monthly average RMSE variations between summer and winter values are not as high. This suggests that thin-film technologies do not exhibit the same strong seasonal performance as c-Si technologies. The RMSE results of the thin-film a-Si technologies are depicted in Figure 4.2c, while for the CIGS and CdTe in Figure 4.2d.

4.3.4 Annual DC energy yield APE with single-point efficiency with temperature correction model

The annual DC energy yield estimation significantly improved for all PV technologies in Cyprus by incorporating temperature correction. In the present case, the annual DC energy yield for both mono-c-Si and multi-c-Si technologies was estimated with an average APE of approximately -5 % whereas the average APE was approximately -10 % for thin-film technologies over the first year. The improvement in DC energy yield estimation is due to the fact that, in the hot climate of Cyprus, temperature is a significant power loss factor. Figure 4.3 shows that there was again a gradual increase in the estimation APE deviation for the single-point efficiency with temperature correction model, over the period June 2006 - June 2010. Accordingly, for some of the technologies, which showed accurate estimation results (such as the Suntechnics mono-c-Si, Schott Solar MAIN multi-c-Si, Solarworld multi-c-Si and Würth CIGS) the uncertainty of the model exceeded the estimation error.

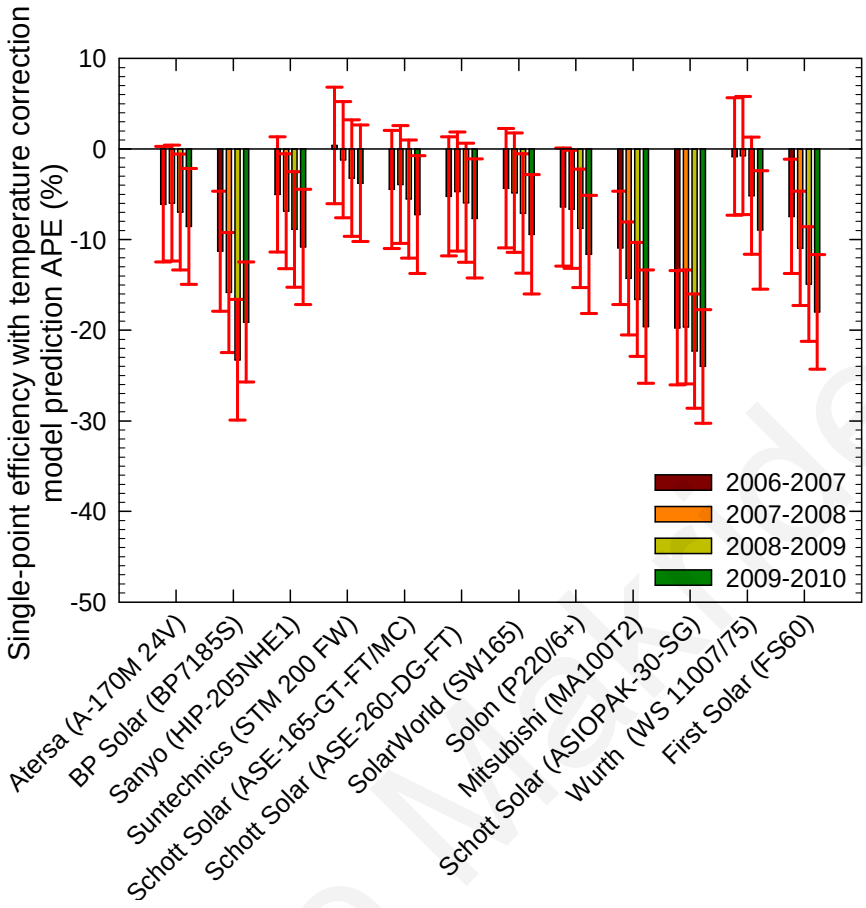

Figure 4.3. Single-point efficiency with temperature correction annual DC energy yield estimation APE over the period June 2006 - June 2010. Model annual DC energy yield combined uncertainty and ±0.765 % uncertainty for the annual DC energy yield are also shown.

The RMSE of the monthly average residuals between the measured and single-point efficiency with temperature correction model estimated fifteen-minute average power data were again evaluated over the period June 2007 - June 2008, and are shown in Figure 4.4. The monthly average RMSE of all technologies improved significantly when compared to the single-point efficiency model results, particularly during the warmer periods. Specifically, from Figure 4.4a and Figure 4.4b, it is obvious that for both mono-c-Si and multi-c-Si technologies the application of temperature correction improved the estimation accuracy of this model; the RMSE variations between winter and summer decreased and are lower compared to the variations shown in Figure 4.2 by the single-point efficiency model.

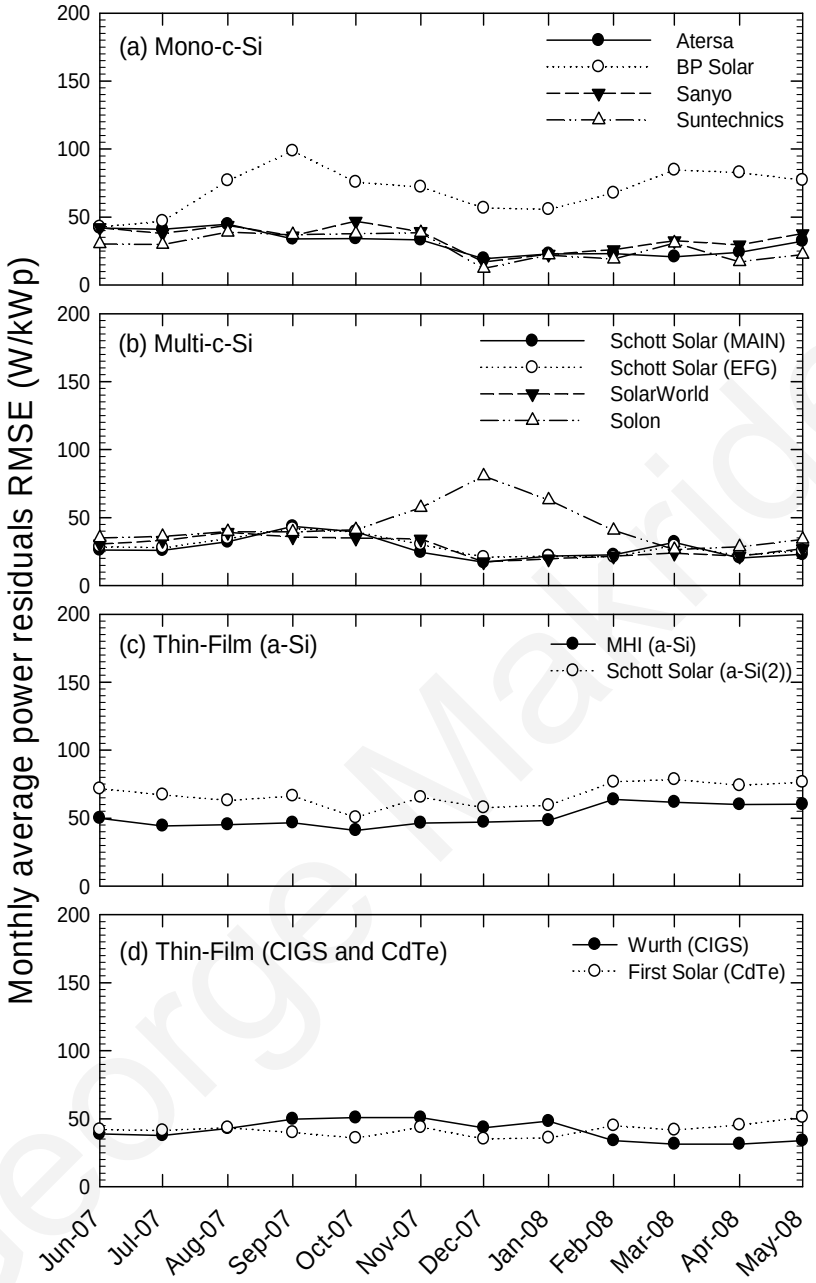

Figure 4.4. Single-point efficiency with temperature correction model monthly average RMSE of power data-point residuals of installed PV systems over the period June 2007 - June 2008.

Furthermore, the thin-film technologies of a-Si exhibited their highest RMSE during spring and late winter, as shown in Figure 4.4c. This may be attributed to spectral and thermal annealing effects that need to be considered, to increase the accuracy of this model for these technologies. The thin-film technologies of CdTe and CIGS exhibited a flat

RMSE behaviour, as shown in Figure 4.4d, with some minor variations, such as, increase in RMSE during winter for the CIGS system and spring for the CdTe, possibly due to spectral effects.

4.3.5 Annual DC energy yield APE with PVUSA model

The estimation accuracy for thin-film technologies improved when the PVUSA model was employed with the regression coefficients found over the period June 2007 - June 2008. Both model estimation APE and uncertainties are depicted in Figure 4.5. The PVUSA model was able to estimate the annual DC energy yield for thin-film technologies, with an APE in the range of -3 % to -8 % during the first year.

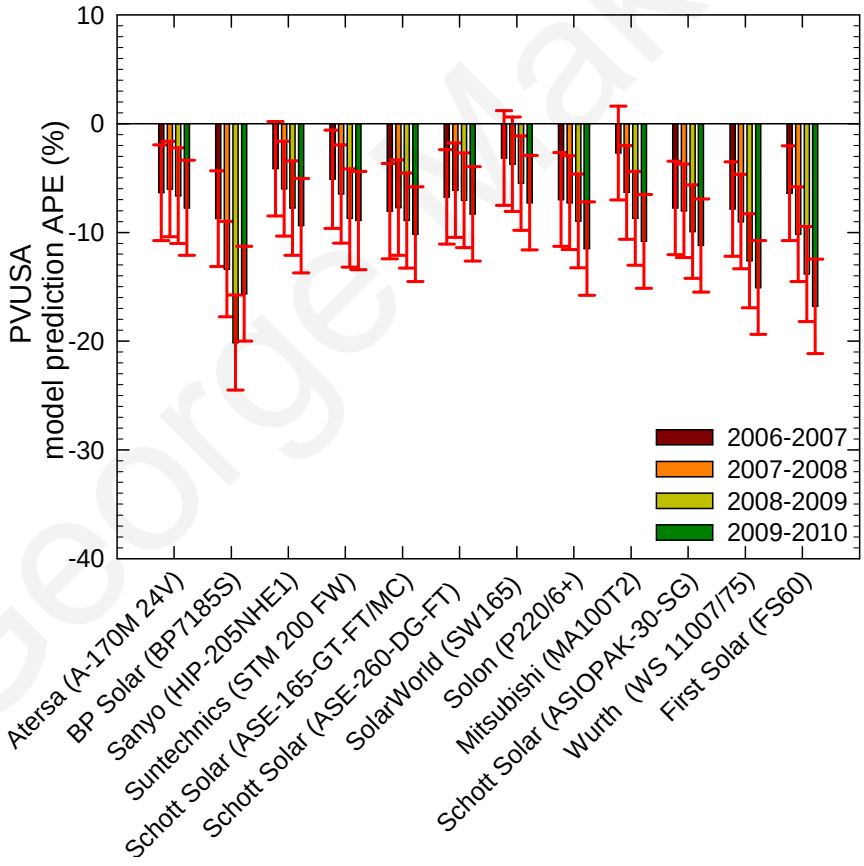

Figure 4.5. PVUSA model annual DC energy yield estimation APE over the period June 2006 - June 2010. Model annual DC energy yield combined uncertainty and ±0.765 % uncertainty for the annual DC energy yield are also shown.

The annual DC energy yield estimation APE of the PVUSA model over the period June 2006 - June 2010, again showed a gradual progressive increase in deviation of estimated against real measured yield, for all the technologies.

In order to obtain more information about the PVUSA model performance, the RMSE between the measured and PVUSA model estimated fifteen-minute average power data-point residuals were again evaluated over a one-year period. The results in Figure 4.6 show that for the c-Si technologies the model behaved better during the colder winter season rather than the summer; as lower monthly average RMSE were observed during the winter compared to the summer for these technologies.

The same applied for the thin-film technologies of a-Si, as shown in Figure 4.6c, as a higher RMSE was observed during the summer and early autumn compared to the winter. The higher RMSE for these technologies during this time of the year is attributed to thermal annealing during the warm season. In the case of the thin-film CIGS system, the model behaved better during spring, while the CdTe system showed the lowest RMSE during winter, as shown in Figure 4.6d.

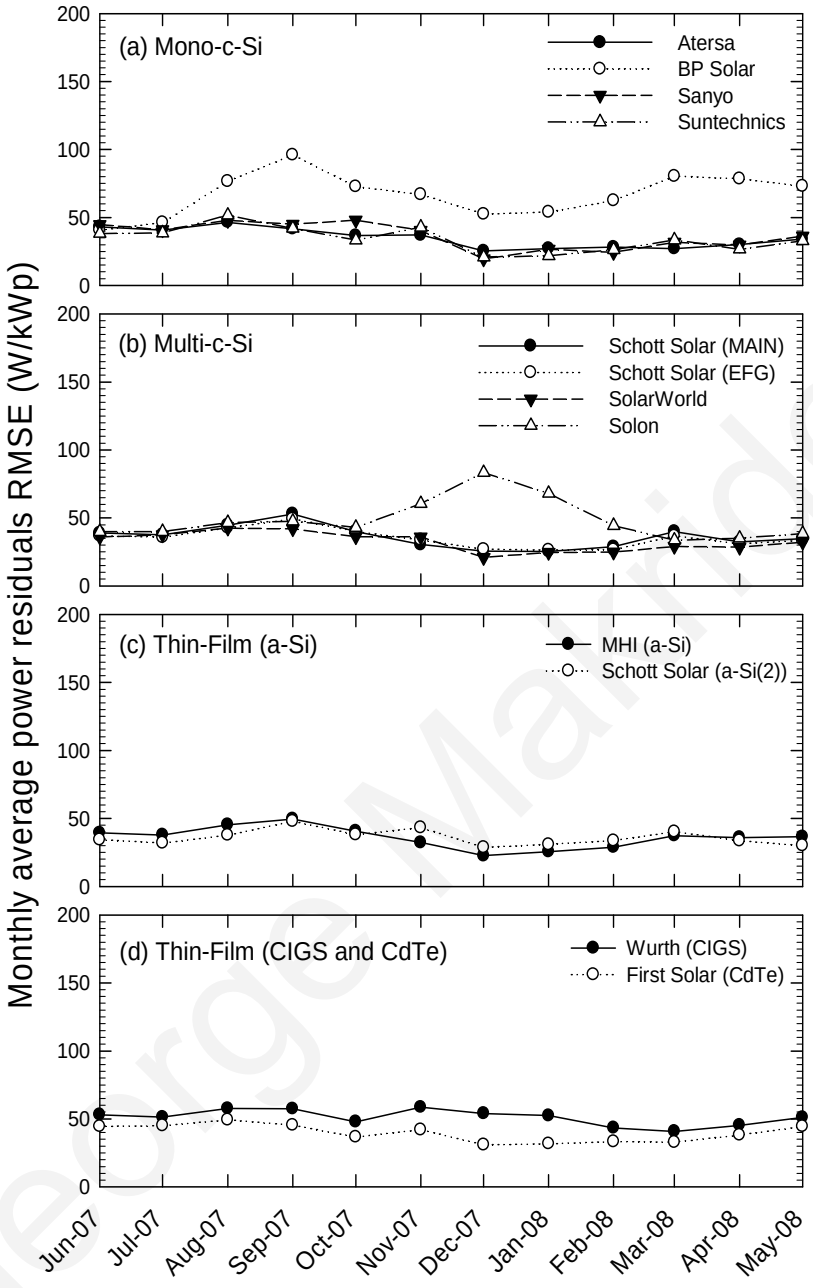

Figure 4.6. PVUSA model monthly average RMSE of power data-point residuals of installed PV systems over the period June 2007 - June 2008.

4.3.6 Annual DC energy yield APE with one-diode model

During the four year evaluation period, the best agreement between the modelled results and outdoor data for mono-c-Si and multi-c-Si technologies, was obtained from the one-diode model. In the case of thin-film technologies, the one-diode model provided the

weakest estimations in comparison to the other models. Figure 4.7 shows that over the period June 2006 - June 2010, the one-diode model provided accurate estimation APE results for c-Si, but not for thin-film technologies.

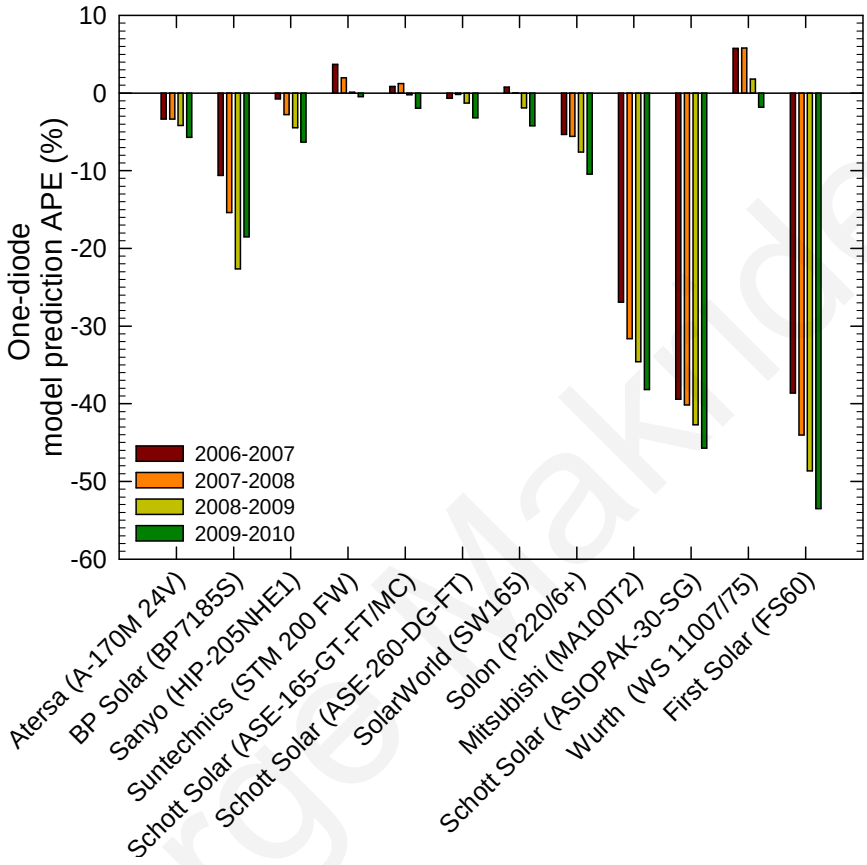

Figure 4.7. One-diode model annual DC energy yield estimation APE over the period June 2006 - June 2010.

The only thin-film technology accurately estimated was the Würth CIGS. Again, a gradual increase in deviation of estimated against real measured yield was observed.

Figure 4.8 shows the RMSE between the measured and one-diode model estimated fifteen-minute average power data-point residuals over the period June 2007 - June 2008.

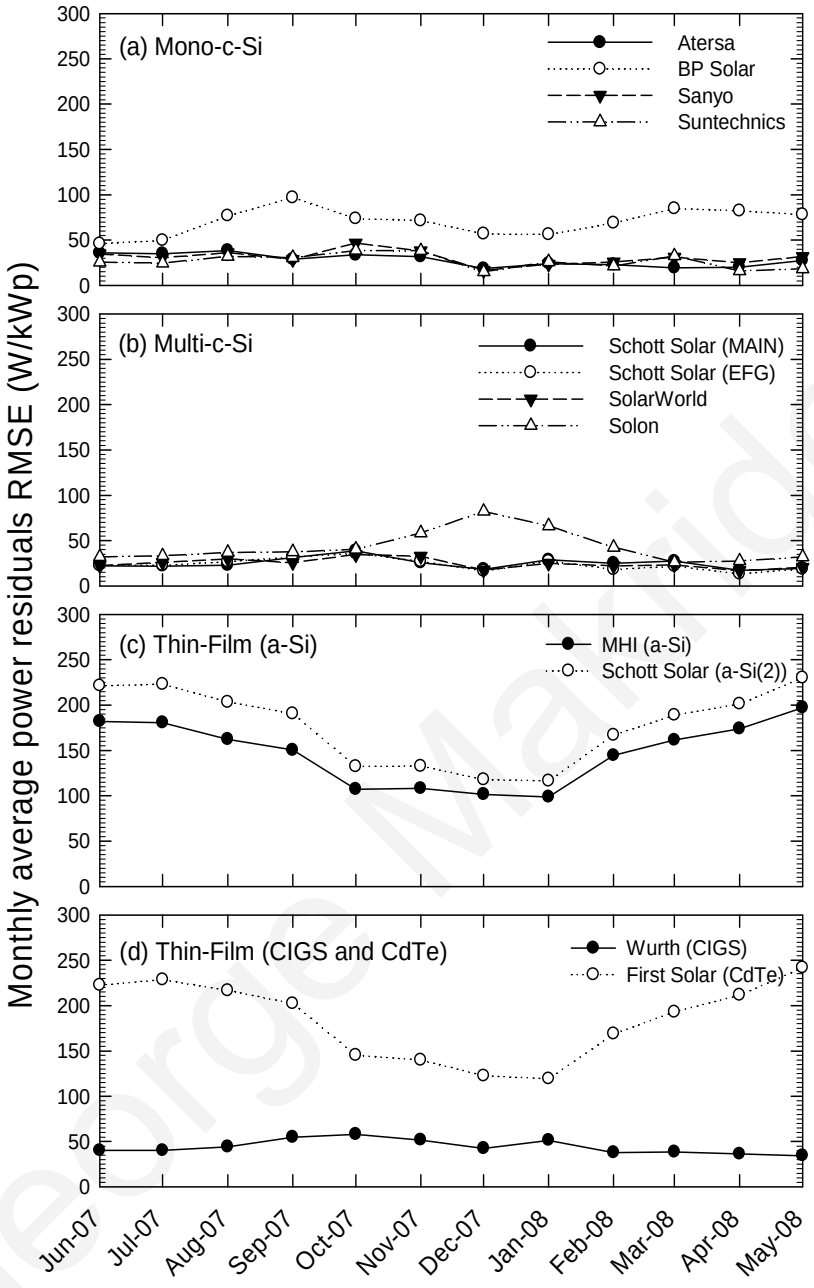

Figure 4.8. One-diode model monthly average RMSE of power data-point residuals of installed PV systems over the period June 2007 - June 2008.

It is obvious from the monthly average RMSE of the mono-c-Si and multi-c-Si technologies, shown in Figure 4.8a and Figure 4.8b, respectively, that the one-diode model accurately estimated with low RMSE the power for each month. The RMSEs for the c-Si technologies are lower compared to previous model results, indicating fairly close agreement with measured data.

Conversely, amongst the thin-film technologies, only the CIGS system showed good performance for this model, with low RMSE residual results. All other thin-film technologies exhibited high RMSE results for this model.

4.3.7 PV technology model estimation benchmark

Figure 4.9 shows the annual DC energy yield normalised to rated power estimation APE results of all models over the periods June 2006 - June 2010. The results demonstrate that the models employed in this study exhibited different estimation performance for the different technologies considered. For all PV technologies the single-point efficiency model showed the highest estimation errors. The technology which showed the lowest estimation error for this model was the Suntechnics mono-c-Si, which was attributed to the low performance losses of this technology throughout the evaluation period.

The application of temperature correction assisted the estimation performance for most c-Si technologies and for the Würth CIGS, demonstrating the significance of the temperature effect on these technologies. This model was not particularly accurate for the remaining thin-film technologies, signifying the presence of a more important loss factor than temperature for thin-films. This loss factor was more prominent in a-Si, in comparison to the CdTe technology as during the first year the CdTe system showed better estimation accuracy when applying temperature correction. Other effects such as the spectrum and light induced degradation need to be accounted for, in order to improve the model accuracy for a-Si.

The one-diode model showed the best estimation accuracies for all c-Si technologies and can, therefore, be used in conjunction with manufacturer provided data-sheets; in order to estimate the one-diode model parameters and to provide accurate estimations of the annual DC energy yield. Figure 4.9c further shows that the one-diode model estimated the Würth CIGS with the highest accuracy amongst all models used for the third year. Shading on the BP Solar mono-c-Si was a reason why the one-diode model did not accurately estimate the energy yield for this technology.

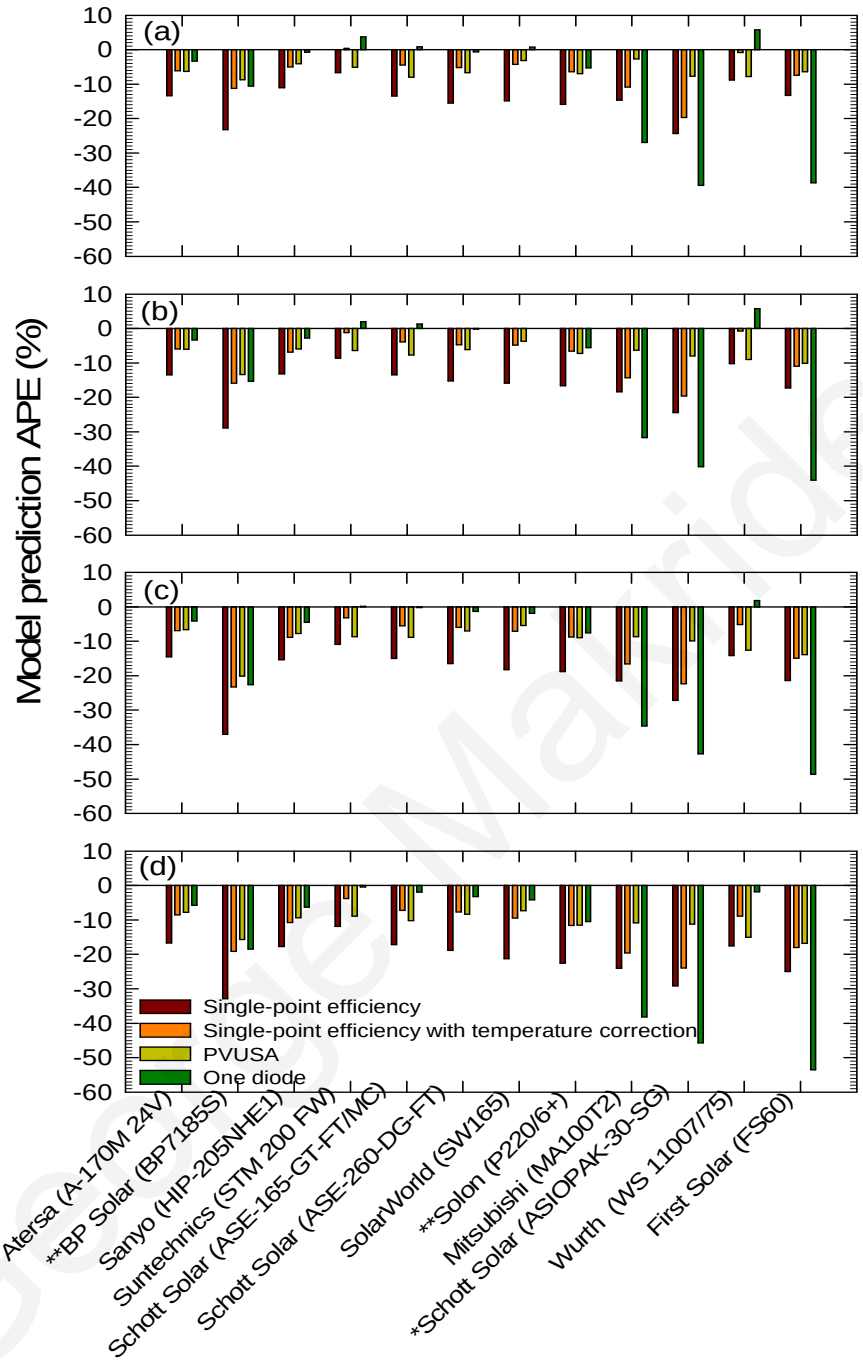

Figure 4.9. Single-point efficiency, single-point efficiency with temperature correction, PVUSA and one-diode model annual DC energy yield normalised to manufacturers' rated power, estimation APE over the period a) June 2006 - June 2007, b) June 2007 - June 2008, c) June 2008 - June 2009 and d) June 2009 - June 2010 for all PV technologies.

* The Schott Solar a-Si system had a broken module since October 2006.

** Partial shading had been affecting the performance of the BP Solar mono-c-Si and Solon multi-c-Si systems during the second, third and fourth years.

With the exception of Würth CIGS, the annual DC energy yield of all other thin-film technologies was better estimated with the PVUSA model due to the fact that for this model the input parameters are directly fitted to the measured power data-sets over a period of a year. Figure 4.9b-d show that after the first year, the estimation error of all the investigated models increased for the a-Si and CdTe technologies. This provides evidence that the loss factor is not predominately seasonal (e.g. spectrum) but other effects such as degradation or individual module power loss (e.g. the case for the Schott Solar a-Si system, which had a broken module since October 2006) are responsible for the poor energy estimation of the above models and have to be accounted for in the models.

The evaluation of different model energy yield estimations in comparison with outdoor measurements is very important in assessing the credibility and accuracy of each modelling approach. The obtained results indicate that the different models estimate the energy yield of different PV technologies, with various degrees of accuracy. In the following chapters, the outdoor performance of the PV systems is analysed and the main loss factors and reasons why the models deviated from the real energy yield measurements are investigated.

Chapter 5

Seasonal performance assessment

5.1 Introduction

Even though seasonal performance evaluations have already been presented in the literature [41], [47], [49], [51], [53], [64], [112], [116], the work outlined in this chapter is one of the first attempts to investigate the outdoor performance behaviour of different grid-connected PV technologies, installed side-by-side, in two different locations. The test-sites in Nicosia and Stuttgart have been operating since June 2006 and the locations selected cover the climatic exposure to the warm climatic conditions of Cyprus, typical of the Mediterranean region and also the moderate climatic conditions of Germany, typical of central Europe.

Specifically, this chapter presents the evaluation of the weather conditions and the seasonal performance of the PV technologies installed in Cyprus over a four-year period, while it also outlines an initial comparison of the outdoor performance of each technology based on measured operational and meteorological data. The monthly DC energy yield, E_{DC}, and the DC PR, PR_{DC}, were used to obtain the seasonal behaviour that each technology exhibited.

Although the seasonal patterns are evident in the plots of both E_{DC} and PR_{DC} monthly time series, further insight into the trend and seasonality of each PV technology can be obtained by analyzing and extracting the seasonal behaviour using statistical methods. The concept of extracting the seasonality from a time series is useful, as important

information about the periodicity of the time series is gained, which can be further applied in forecasting techniques. In addition, the presence of seasonality makes it difficult to determine the underlying trend of the time series hence information about the trend is usually acquired by first extracting the seasonal component from the data. Decomposition techniques such as classical series decomposition (CSD) described in [117], [118] can be used to extract the seasonality and trend from time series that exhibit seasonal behaviour. Moreover, decomposition is in general the preferred method for simple seasonal adjustment [119]. An advantage of this technique over other time series modelling approaches is that it can be easily applied and readily provide a perspective on the underlying variations and relationships. On the other hand, due to the fact that the particular decomposition technique is predefined and selected without previous analysis on the time series, this may result in increasing the influence of variations which may be modelled as part of the seasonality and trend. For this purpose, the monthly average DC PR time series of each PV technology was further decomposed, with the extracted seasonality subsequently processed to acquire the standard deviation, σ, of the CSD extracted seasonal indices throughout the year. The standard deviation provides information and illustrates the seasonal performance variation of each PV technology.

Additionally, a comparison of the seasonal performance exhibited by the same technologies installed both in Nicosia, Cyprus and Stuttgart, Germany was further carried out from the acquisition and analysis of real PV operating and climatic data. The performance fluctuations exhibited by each PV technology were obtained from the monthly average AC performance ratio, PR_{AC}, constructed time series over the period June 2006 - June 2009 for both locations. In addition, the AC PR peak-to-peak variations of each year were also calculated, with the results demonstrating that each technology provided different performance variations throughout a year, at each location.

Finally, a comparison of the outdoor performance of each technology based on the monthly AC energy yield normalised to the manufacturers' nameplate power, $E_{AC(Normalised)}$, was also carried out between the two locations. Again, the results showed significant performance differences amongst the various technologies, as a function of location.

5.2 Methodology

5.2.1 Performance parameters

The first step in the analysis of the PV seasonal performance was to extract the DC energy yield and PR on a monthly basis. The extracted parameters include the normalised final monthly PV system energy yield, Y_f (kWh/kW$_p$), which is defined as the total energy produced by a PV system during a period of a month, with the energy yield E (kWh) further normalised to the nameplate manufacturer power at STC, P_{STC} (kW$_p$), in order to allow for comparison between the different installed PV technologies [104]. The final yield, Y_f, is given by:

$$Y_f = \frac{E}{P_{STC}} \tag{5.1}$$

Additionally, the normalised AC energy yield, $E_{AC(Normalised)}$, is defined as the total AC energy yield produced in a given time period, E_{AC}, further normalised to the nameplate manufacturer power at STC, P_{STC} and is given by:

$$E_{AC(Normalised)} = \frac{E_{AC}}{P_{STC}} \tag{5.2}$$

For the analysis in this study the normalising factor P_{STC} was the rated power as provided from the manufacturers' datasheets. The normalisation step was performed using the rated power provided from the manufacturers' datasheets and not the power measured using a flasher or from field measurements because this is the power that is readily known and which investors pay for.

Furthermore, the PR was calculated and used as a general measure of PV performance which takes into account the overall losses due to PV module temperature, spectrum, module mismatch and other factors such as optical reflection, soiling and downtime failures. The DC PR, PR_{DC}, is defined as the ratio between the real DC energy production, E_{real} (kWh), and the DC energy which the PV array would produce if it had no losses due to deviations from STC, E_{STC} (kWh) [111]:

$$PR_{DC} = \frac{E_{\text{real}}}{E_{\text{STC}}} = \frac{E}{H \cdot A \cdot \eta_{\text{STC}}} \tag{5.3}$$

where H (kWh/m^2) is the global irradiation, A (m^2) is the area of the PV array and η_{STC} (%) is the PV module efficiency at STC.

5.2.2 Seasonal performance evaluation using classical series decomposition (CSD)

CSD was applied to the monthly average DC PR time series of all installed PV technologies, in order to extract the trend, the seasonality and the irregular component. The trend was obtained from the time series by using a two step centred moving average (MA). For the PV performance data it is more appropriate to use a centred twelve month moving average, so as to include all the seasonal variations that occur over a period of one year. For a 2 x k moving average, where k is the MA order (k=12 because of the number of months of a year), the centred average at time t was found as [120]:

$$T_{\text{t}} = \frac{1}{2}\left(\frac{1}{k}\sum_{i=t-m}^{t+m-1} Y_{\text{i}} + \frac{1}{k}\sum_{i=t-m+1}^{t+m} Y_{\text{i}}\right) \tag{5.4}$$

where T_{t} is the trend at time t, ($t > m$), and m is defined as the half-width of a moving average, $m = \frac{k}{2}$. The calculated moving averages formed a smoother series, the trend of each time series.

Subsequently, the seasonality component was obtained by subtracting the trend from the original data, for each respective month, throughout the four-year evaluation period. The function used to extract the crude seasonality component was:

$$S_{\text{t}} = Y_{\text{t}} - T_{\text{t}} \tag{5.5}$$

where the seasonality, S_{t}, is defined as the difference from the original data and the trend at time t. A more statistically useful estimate was then determined from the seasonality in terms of a normalised value. This normalised seasonality, $S_{\text{t(normalised)}}$, was obtained by

averaging each respective month of the extracted seasonality. It ultimately comprises twelve average seasonality indices for each respective month of the year.

As an example of the application of CSD to estimate the trend, seasonality and irregularity, the analysis for the Atersa mono-c-Si system is shown in Figure 5.1. The constructed monthly average DC PR time series is first shown in Figure 5.1a, while the extracted trend and coefficient of determination, R^2, are depicted in Figure 5.1b. The annual performance loss rates were obtained by applying a linear least square fit to the extracted trend. The fitted trend line for the Atersa mono-c-Si time series, shown in Figure 5.1b is given by:

$$Y = a + bX = 89.98 - 0.062X \tag{5.6}$$

In addition, the gradient of the fit represents the linear monthly performance loss, which can be multiplied by 12 to find the annual performance loss rate. The R^2 values of the trend and linear fit comparison was also obtained to provide a measure of how reliably the trend is described by the linear fit (high R^2 value shows good agreement between curve and fit while low R^2 value shows that the curve cannot be adequately described by the linear fit and hence the gradient used to describe the performance loss may be inaccurately used). It is further shown in Figure 5.1b that the annual performance loss rate was -0.75 % and the R^2 value of the trend and linear fit was 63 %. The normalised seasonality of the technology is shown in Figure 5.1c while Figure 5.1d shows the irregularities.

This chapter focuses on the extracted seasonality of each PV technology. The performance loss rates evaluated using CSD are presented in chapter 7.

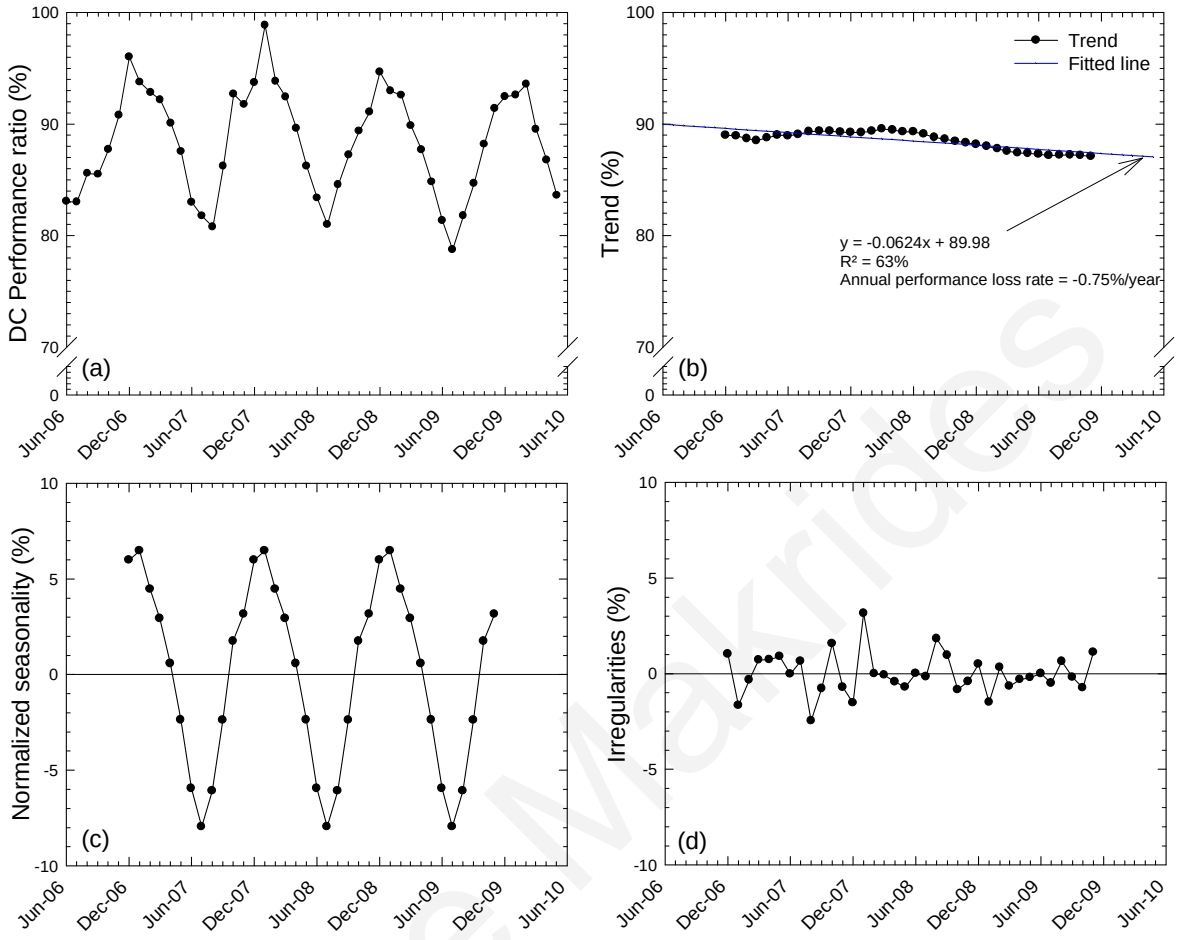

Figure 5.1. (a) Monthly average DC PR time series for the Atersa mono-c-Si system over the period June 2006 - June 2010. (b) CSD extracted trend, linear least square fit, R^2 value and annual performance loss rate. (c) CSD extracted normalised seasonality. (d) CSD extracted irregularities.

5.3 Results

The seasonal performance results both in Nicosia, Cyprus and Stuttgart Germany are summarised in this section.

5.3.1 Environmental conditions

The monthly global irradiation in the POA of 27.5° and the monthly average ambient temperature, measured over the four-year period at the outdoor test facility at the University of Cyprus, are plotted in Figure 5.2a and Figure 5.2b, respectively. It is clear from Figure 5.2a that the global irradiation in the POA exhibits seasonality, with the

highest irradiation occurring during summer and the lowest during winter. The summer and winter seasons of June 2009 - June 2010 showed the highest and lowest irradiation, respectively, over the whole evaluation period. From Figure 5.2b, it is evident that the summer seasons were the warmest, while the lowest monthly average ambient temperatures occurred during winter.

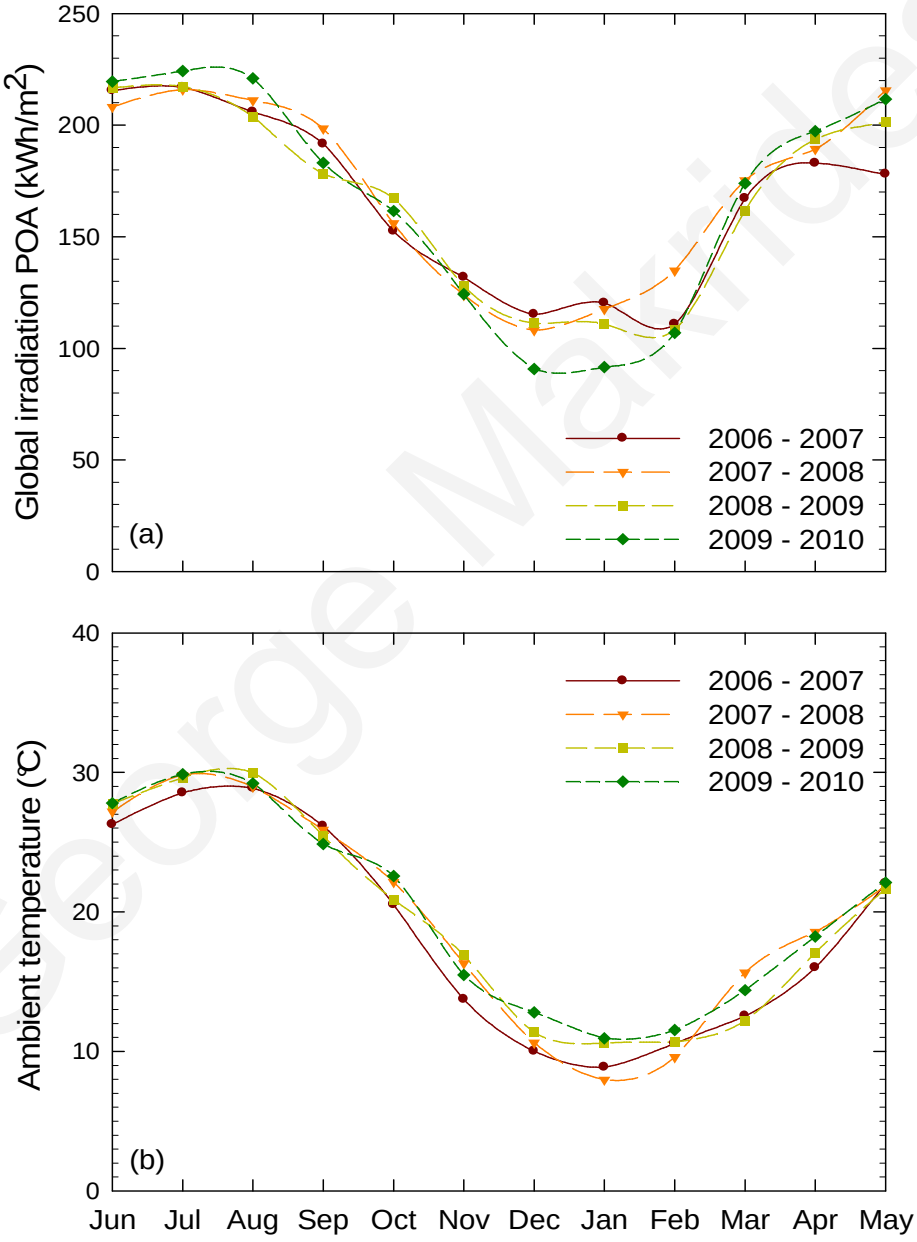

Figure 5.2. (a) Monthly total irradiation in the POA and (b) Monthly average ambient temperature over the period June 2006 - June 2010.

The measured annual global irradiation in the POA of 27.5 ° in Cyprus between June 2006 and June 2010, is summarised in Table 5.1.

Table 5.1. Annual global irradiation in the POA over the period June 2006 - June 2010

Period	Global irradiation in the POA (kWh/m^2)
June 2006 - June 2007	1988
June 2007 - June 2008	2054
June 2008 - June 2009	1997
June 2009 - June 2010	2006

5.3.1.1 Comparison of environmental conditions in Nicosia, Cyprus and Stuttgart, Germany

The monthly global irradiation in the POA for the test-sites in Nicosia and Stuttgart, was measured over the three-year period, using the pyranometer installed in the POA at each site (shown in Figure 5.3a and Figure 5.3b, respectively). It is evident from Figure 5.3 that the irradiation of both locations exhibits a seasonal pattern, with the highest irradiation occurring during summer and the lowest during winter. In addition, the measured annual total irradiation in the POA at the test-site in Nicosia was approximately 33 % higher than that measured in Stuttgart. The monthly global irradiation plots in Stuttgart demonstrated more oscillations compared to the ones in Nicosia, attributed to the overcast weather in the climatic conditions of Stuttgart. The solar irradiation in the POA of 27.5° in Nicosia averages over 5.5 peak sun hours (PSH) each day, varying from 3.9 PSH during winter, to 6.9 PSH during the summer season. Accordingly, in the POA of 33° in Stuttgart, the average daily solar irradiation is over 3.7 PSH, varying from 1.7 PSH during winter, to 5.2 PSH during the summer season.

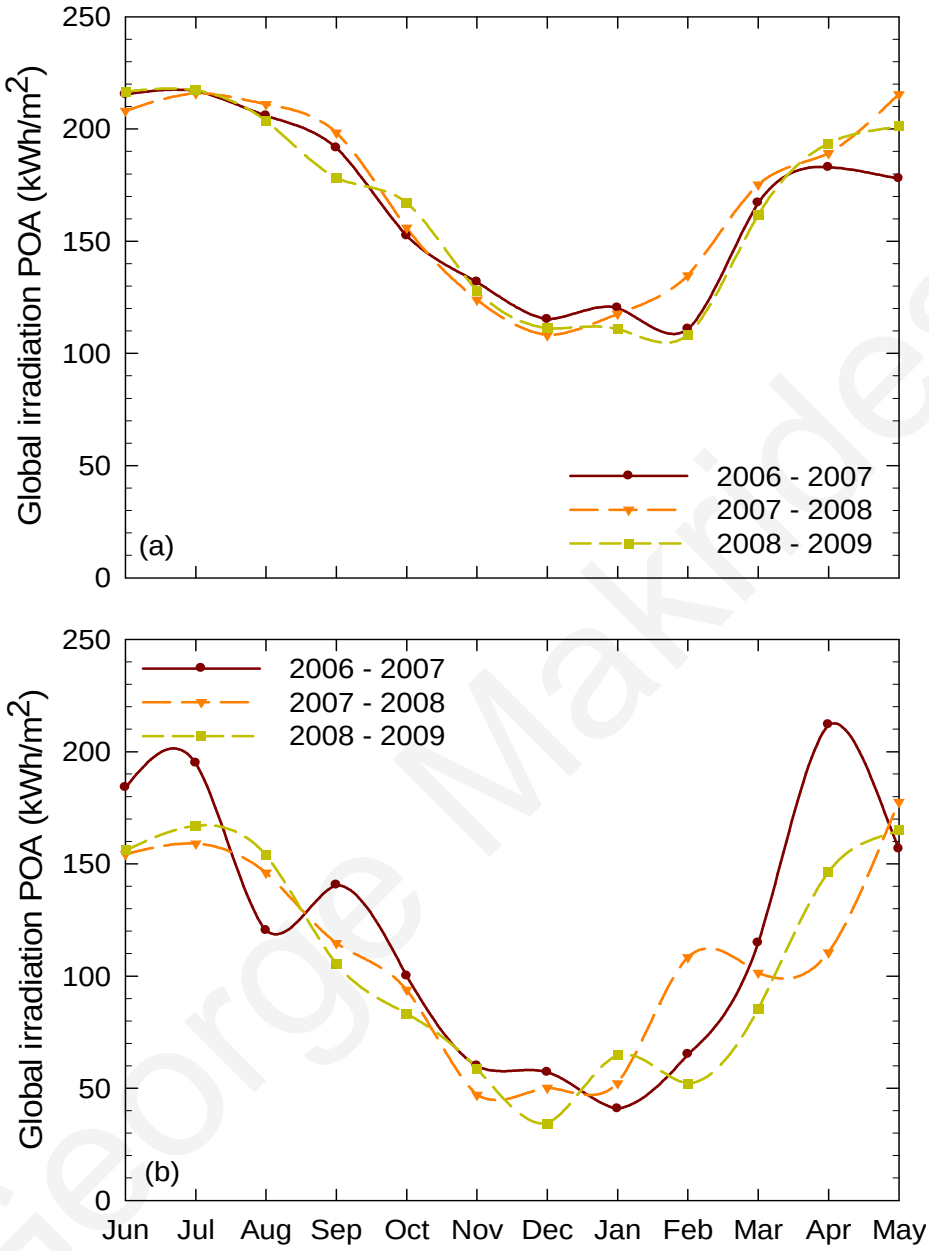

Figure 5.3. Monthly global irradiation in the POA over the period June 2006 - June 2009 in (a) Nicosia, Cyprus and (b) Stuttgart, Germany.

The measured annual global irradiation in the POA, between June 2006 and June 2009, in Nicosia and Stuttgart, is summarised in Table 5.2. In Nicosia, the period of highest annual solar irradiation was the second year of investigation, June 2007 - June 2008, while in Stuttgart, this was the first year, June 2006 - June 2007.

Table 5.2. Annual global irradiation in the POA over the period June 2006 - June 2009, measured at the test-sites in Nicosia, Cyprus and Stuttgart Germany.

Period	Annual global irradiation POA in Nicosia (kWh/m^2)	Annual global irradiation POA in Stuttgart (kWh/m^2)
June 2006 - June 2007	1988	1446
June 2007 - June 2008	2054	1315
June 2008 - June 2009	1997	1272
Average of three-years	**2013**	**1344**

In addition, the monthly average ambient temperatures of both sites are also shown in Figure 5.4. From the plot of Figure 5.4a, it is evident that the summer season was the warmest in Nicosia, while the lowest monthly average ambient temperatures occurred during winter. The monthly average ambient temperatures ranged between 8 °C and 30 °C. Similarly, at the test-site in Stuttgart, the highest temperatures occurred during the summer (as shown in Figure 5.4b). However, in general lower temperatures were recorded throughout the year compared to the test-site in Cyprus, with the monthly average ambient temperatures in Stuttgart ranging between -2 °C and 23 °C.

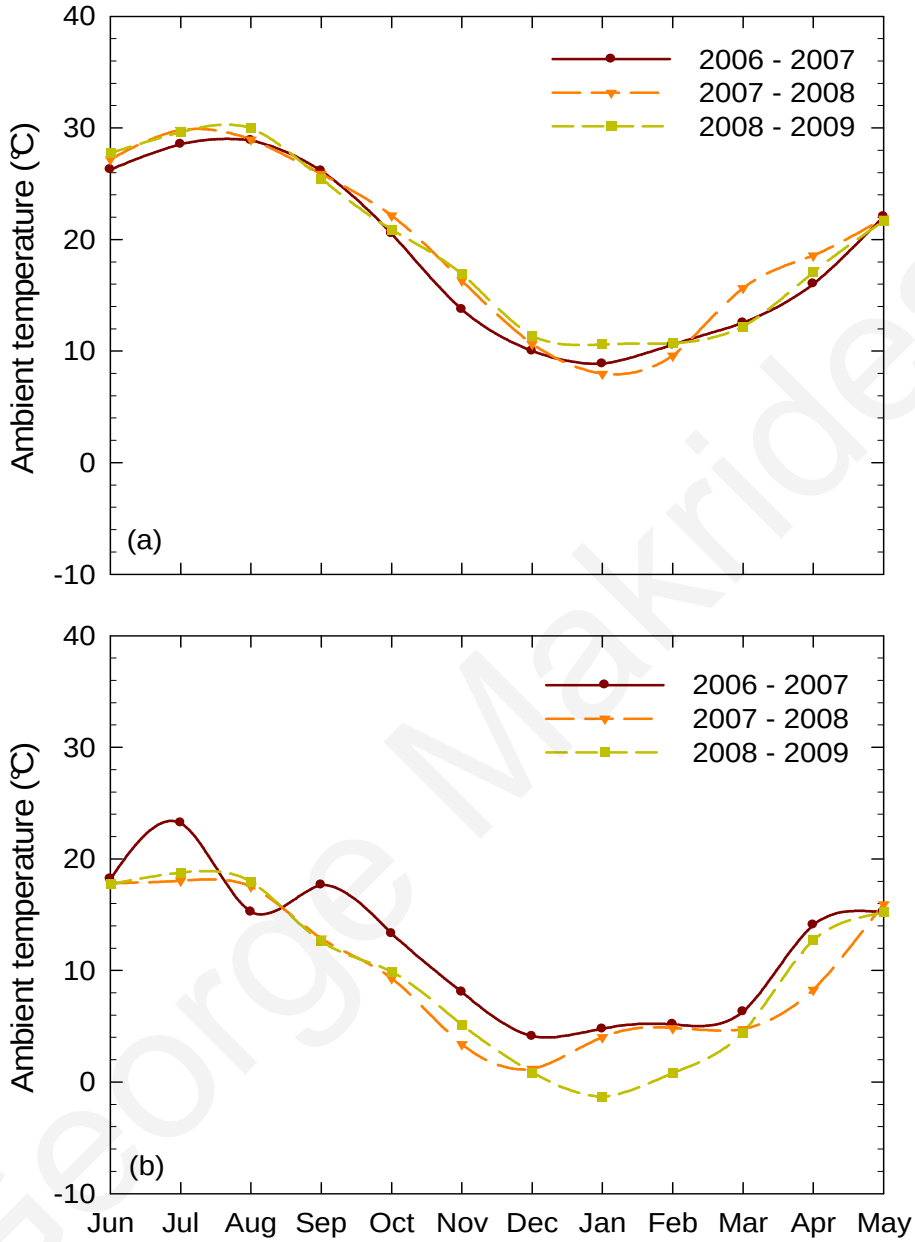

Figure 5.4. Monthly average ambient temperature over the period June 2006 - June 2009 in (a) Nicosia, Cyprus and (b) Stuttgart, Germany.

5.3.2 Energy yield

During the first year of operation, the fixed plane PV systems showed an average annual DC energy yield of 1738 kWh/kW$_p$. During the second year of operation and for the same

systems, the average DC energy yield was 1769 kWh/kW$_p$, showing an increase of 1.8 % in comparison to the first year. The average DC energy yield was lower during the third and fourth year, with 1680 kWh/kW$_p$ and 1658 kWh/kW$_p$, respectively. The annual DC energy yield normalised to the manufacturers' rated power over the period June 2006-June 2010 in Nicosia, Cyprus, is shown in Table 5.3.

Table 5.3. Annual DC energy yield normalised to the manufacturers' rated power at STC over the period June 2006 - June 2010 in Nicosia, Cyprus.

System	**Normalised DC energy yield, $E_{DC(Normalised)}$ (kWh/kW$_p$)**			
	2006 - 2007	**2007 - 2008**	**2008 - 2009**	**2009 - 2010**
Atersa (A-170M 24V)	1753	1810	1744	1719
BP Solar (BP7185S)	1612	1593	1457	1510
Sanyo (HIP-205NHE1)	1790	1814	1731	1703
Suntechnics (STM 200 FW)	1864	1890	1800	1793
Schott Solar (ASE-165-GT-FT/MC)	1752	1810	1736	1712
Schott Solar (ASE-260-DG-FT)	1721	1783	1714	1688
SolarWorld (SW165)	1731	1772	1689	1654
Solon (P220/6+)	1715	1761	1681	1637
MHI (MA100T2)	1734	1734	1644	1617
Schott Solar (ASIOPAK-30-SG)	1599	1650	1571	1554
Würth Solar (WS 11007/75)	1827	1863	1748	1707
First Solar (FS60)	1755	1752	1645	1605

During the first year of operation, the best performing technologies in Cyprus, based on their annual DC energy yield, were the Suntechnics mono-c-Si, the Würth Solar CIGS, the Sanyo HIT mono-c-Si and the First Solar CdTe. During the second year, the mono-c-Si technologies of Sanyo, Suntechnics and the CIGS retained their high energy yield. During the third year, the highest energy yield was produced by the Suntechnics mono-c-Si, Würth Solar CIGS and Atersa mono-c-Si system. During the fourth year, the three technologies which produced the highest yield were entirely c-Si; the Suntechnics, Atersa mono-c-Si and the Schott Solar MAIN multi-c-Si, while the Würth Solar CIGS system followed.

A comparison of the annual DC energy yield produced by the same technology modules, Atersa mono-c-Si fixed-plane, installed in the POA of 27.5° and also mounted on a two-axis tracker is shown in Figure 5.5. Over a four-year period, the tracker provided on average 21 % higher energy yield compared to the fixed-plane system. During the first year, the solar irradiation collected by the reference cell installed at the tracker was 2532 kWh/m^2, while, during the second year, it was 2606 kWh/m^2.

Subsequently, during the third and fourth year, the solar irradiation collected by the tracker was 2510 kWh/m^2 and 2483 kWh/m^2, respectively.

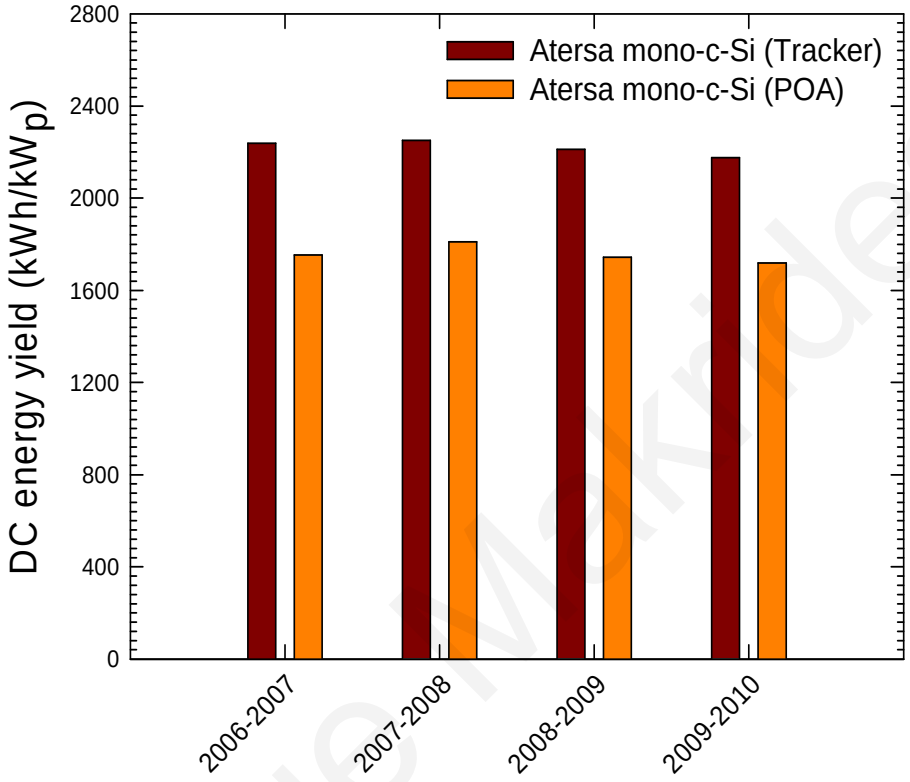

Figure 5.5. Comparison of the annual DC energy yield of the tracker and fixed-plane Atersa mono-c-Si systems, normalised to the manufacturers' rated power at STC over the period June 2006 - June 2010.

Table 5.4 shows the annual AC energy yield normalised to the manufacturers' rated power at STC.

Table 5.4. Annual AC energy yield normalised to the manufacturers' rated power at STC over the period June 2006 - June 2010 in Nicosia, Cyprus.

System	Normalised AC energy yield, $E_{AC(Normalised)}$ (kWh/kW$_p$)			
	2006 - 2007	**2007 - 2008**	**2008 - 2009**	**2009 - 2010**
Atersa (A-170M 24V)	1593	1646	1583	1564
BP Solar (BP7185S)	1463	1445	1320	1370
Sanyo (HIP-205NHE1)	1630	1659	1581	1555
Suntechnics (STM 200 FW)	1692	1717	1641	1638
Schott Solar (ASE-165-GT-FT/MC)	1588	1642	1575	1552
Schott Solar (ASE-260-DG-FT)	1562	1620	1554	1532
SolarWorld (SW165)	1573	1613	1535	1500
Solon (P220/6+)	1567	1609	1533	1495
MHI (MA100T2)	1573	1575	1495	1466
Schott Solar (ASIOPAK-30-SG)	1462	1506	1433	1419
Würth Solar (WS 11007/75)	1653	1691	1581	1543
First Solar (FS60)	1599	1600	1500	1461

Figure 5.6 presents the annual AC energy yield normalised to the nameplate manufacturer power, $E_{AC(Normalised)}$, of the different PV technologies installed in both locations. In Nicosia, the Suntechnics mono-c-Si system produced the highest annual $E_{AC(Normalised)}$ over the entire three-year evaluation period. The three-year average $E_{AC(Normalised)}$ of the systems installed in Nicosia was 1572 kWh/kW$_p$. In Stuttgart, the technology that produced the highest energy yield during the first year was the Würth Solar CIGS, while, during the second and third year, this technology was outperformed by the Suntechnics mono-c-Si system (shown in Figure 5.6b and Figure 5.6c, respectively). The three-year average $E_{AC(Normalised)}$ of the systems installed in Stuttgart was 1097 kWh/kW$_p$.

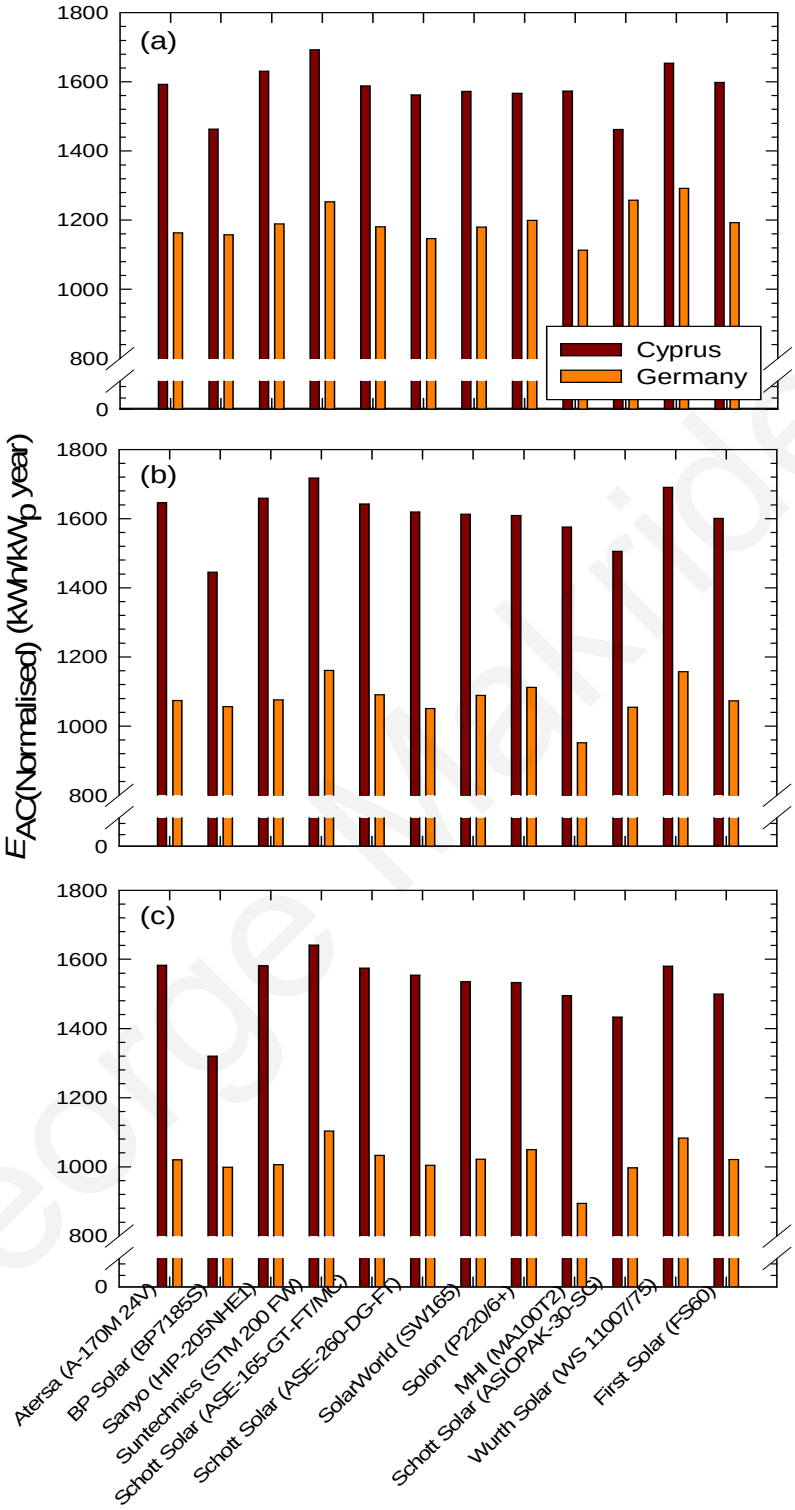

Figure 5.6. Annual $E_{AC(Normalised)}$ over the period June 2006 - June 2009 for the different PV technologies in Nicosia, Cyprus and Stuttgart, Germany. (a) Over the period June 2006 - June 2007. (b) Over the period June 2007 - June 2008. (c) Over the period June 2008 - June 2009.

5.3.3 Seasonal performance

The seasonal performance of the installed technologies in Nicosia, Cyprus and Stuttgart, Germany is summarised in this section.

5.3.3.1 Seasonality using outdoor measurements in Cyprus

The constructed monthly DC energy yield plots of each PV technology were investigated over the four-year evaluation period and the results clearly show that the technologies exhibit seasonality in their energy yield. The highest amount of energy was produced during summer while the lowest during the winter seasons for all installed PV technologies (shown in Figure 5.7). All PV technologies exhibit a seasonal energy yield behaviour that follows the total irradiation pattern previously shown in Figure 5.2a. For some technologies, such as the BP solar mono-c-Si, this is not always the case and the main reason for this is attributed to the shading the technology had experienced over the evaluation period depicted in Figure 5.7f. Another important observation from Figure 5.7 is that the annual DC energy yield for all technologies decreased during the fourth year when compared to the first year, despite the fact that the total irradiation was higher during the period June 2009 - June 2010, as compared to June 2006 - June 2007.

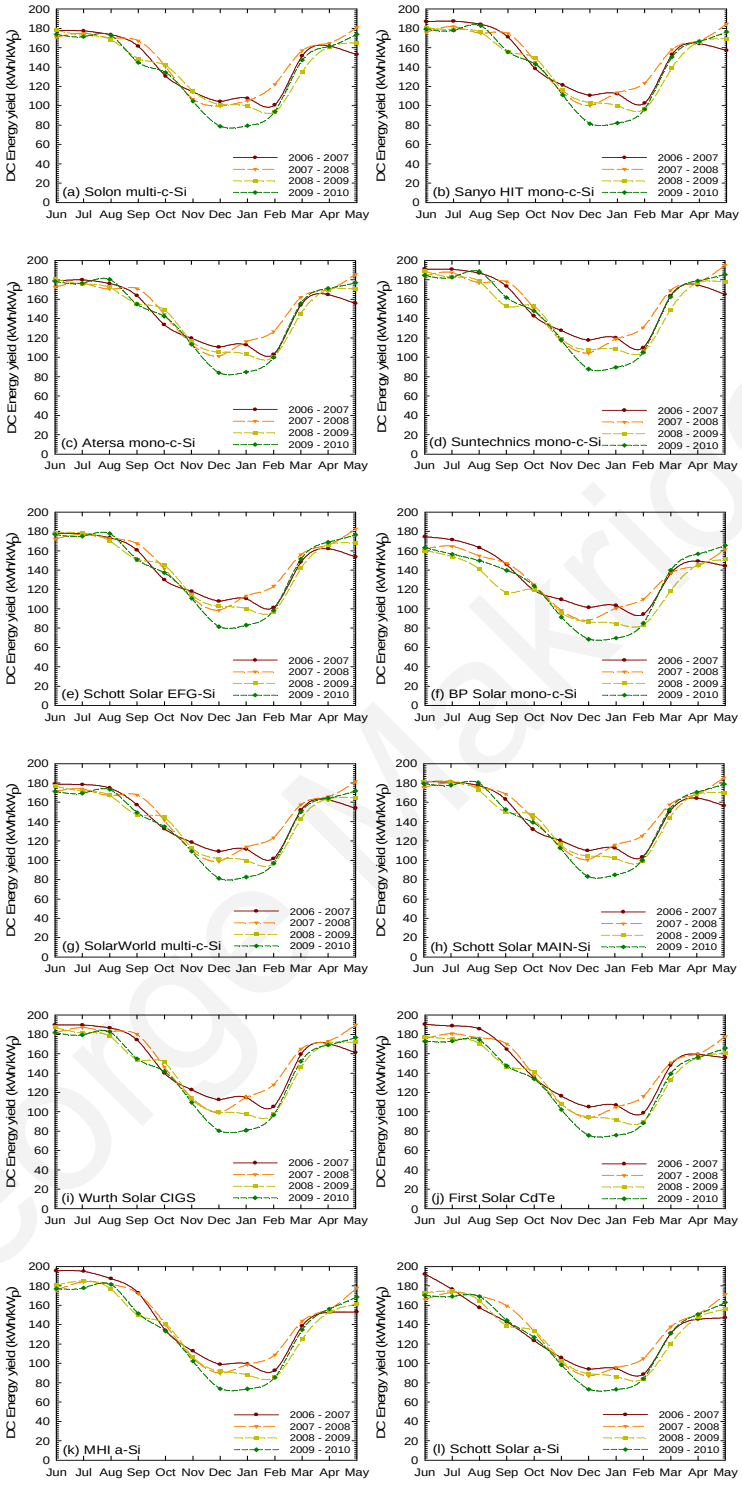

Figure 5.7. Monthly DC energy yield over the period June 2006 - June 2010 for the different PV technologies. (a) Solon multi-c-Si. (b) Sanyo HIT mono-c-Si. (c) Atersa mono-c-Si. (d) Suntechnics mono-c-Si. (e) Schott Solar EFG-Si. (f) BP Solar mono-c-Si. (g) SolarWorld multi-c-Si. (h) Schott Solar MAIN-Si. (i) Würth Solar CIGS. (j) First Solar CdTe. (k) MHI a-Si. (l) Schott Solar a-Si.

During the four-year period, the a-Si technologies showed the highest monthly DC energy yield, which reached 198 kWh/kW$_p$ and 192 kWh/kW$_p$ for the single-junction and tandem-junction technologies in June 2006 depicted in Figure 5.7k and Figure 5.7l, respectively. The high initial monthly energy yield of the a-Si technologies is primarily attributed to the fact that during the first month of installation, these technologies had not yet stabilised [121].

Noticeable seasonal behaviour was also observed from the average monthly PR_{DC} plots, with both mono-c-Si and multi-c-Si technologies exhibiting PR peaks during the cold winter season and performance decrease during the warm summer months as depicted in Figure 5.8. The same seasonal performance pattern exhibited for c-Si technologies, Figure 5.8a-h, was observed for the Würth Solar CIGS and First Solar CdTe technologies and shown in Figure 5.8i and Figure 5.8j, respectively. It is further shown in Figure 5.8j that in the case of the First Solar CdTe system a narrower peak-to-peak PR variation between the seasons was observed, when compared to the c-Si and CIGS seasonal behaviour shown in Figure 5.8a-i. Furthermore, Figure 5.8d shows that the Suntechnics mono-c-Si exhibited high monthly PR, which approached optimum (PR of 100 %) during the winter seasons while in one case, in December 2006, this value was even exceeded. This can occur because of the associated power rating and irradiation uncertainties which are present also in the calculated monthly PR value. Additionally, from the PR plot of Figure 5.8k for the MHI a-Si technology it was obvious that during the summer and early autumn, the performance was higher than in the winter. The higher performance of the a-Si technologies during warm periods is partly due to thermal annealing and to the more favorable spectrum during the warm summer season, compared to the less favorable spectrum during the cold winter months [55], [122].

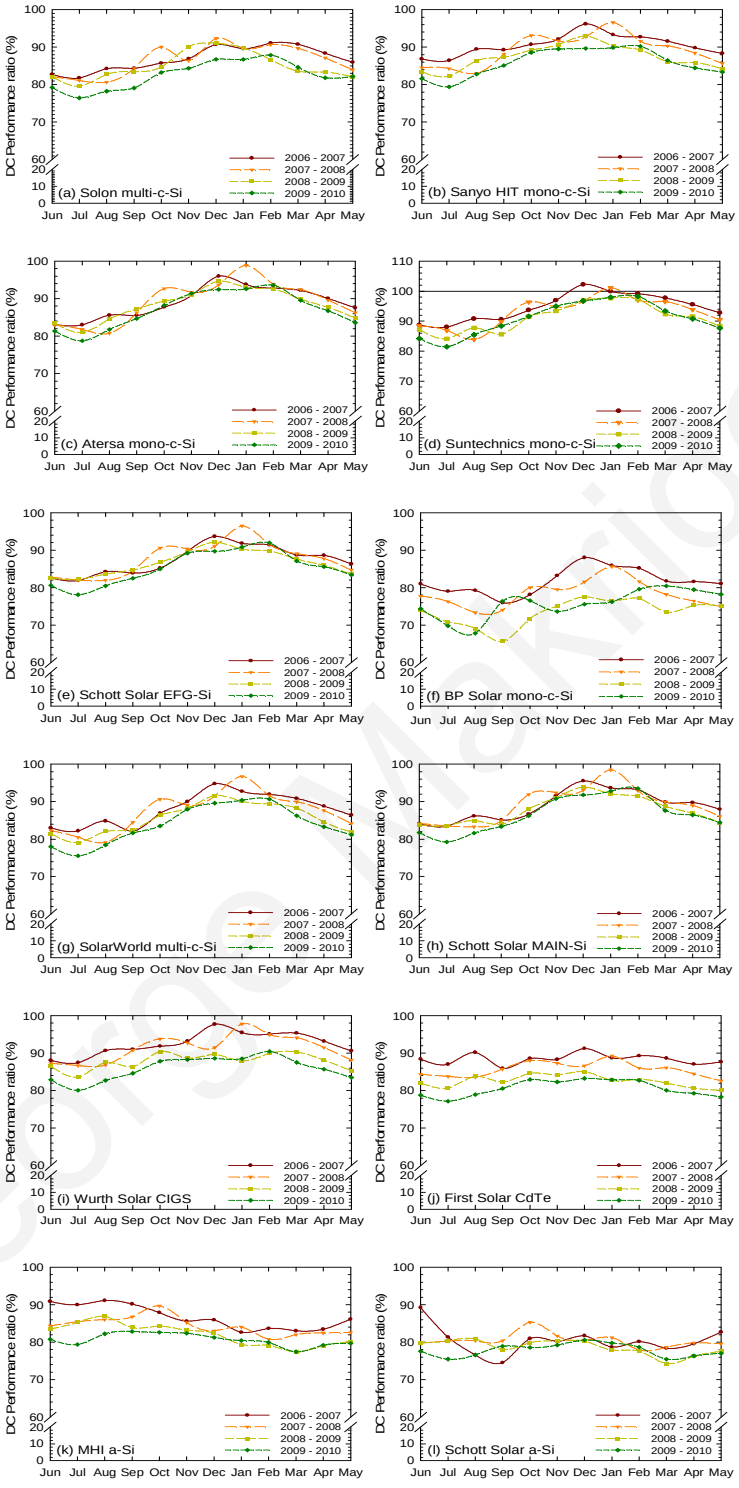

Figure 5.8. Monthly DC PR over the period June 2006 - June 2010 for the different PV technologies. (a) Solon multi-c-Si. (b) Sanyo HIT mono-c-Si. (c) Atersa mono-c-Si. (d) Suntechnics mono-c-Si. (e) Schott Solar EFG-Si. (f) BP Solar mono-c-Si. (g) SolarWorld multi-c-Si. (h) Schott Solar MAIN-Si. (i) Würth Solar CIGS. (j) First Solar CdTe. (k) MHI a-Si. (l) Schott Solar a-Si.

The seasonal PR peak-to-peak variations, $PR_{\text{peak-peak}}$, extracted from the monthly average PR_{DC} plots of all PV technologies, are summarised in Table 5.5. All c-Si PV technologies showed higher peak-to-peak PR variations when compared to thin-film technologies, with the exception of the Schott Solar a-Si in the first year due to the high PR the technology exhibited during its initial stabilisation phase in June 2006. The $PR_{\text{peak-peak}}$ variations increased for most c-Si technologies, particularly during warm periods in the second and fourth year, June 2007 - June 2008 and June 2009 - June 2010, respectively. Amongst the mono-c-Si technologies the Sanyo HIT showed the lowest $PR_{\text{peak-to-peak}}$ variations, while the Atersa and Suntechnics showed the highest. For all installed technologies, the lowest seasonal $PR_{\text{peak-to-peak}}$ was exhibited by the thin-film technologies and, particularly, the First Solar CdTe and Schott Solar a-Si technologies.

Table 5.5. Seasonal $PR_{\text{peak-peak}}$ variations of PV technologies over the period June 2006 - June 2010 in Nicosia, Cyprus.

System	2006 - 2007 $PR_{\text{peak-peak}}$ (%)	2007 - 2008 $PR_{\text{peak-peak}}$ (%)	2008 - 2009 $PR_{\text{peak-peak}}$ (%)	2009 - 2010 $PR_{\text{peak-peak}}$ (%)
Atersa (A-170M 24V)	13.01	18.08	13.68	14.84
BP Solar (BP7185S)	12.06	12.31	11.94	12.61
Sanyo (HIP-205NHE1)	9.75	13.60	10.70	10.82
Suntechnics (STM 200 FW)	14.23	17.25	13.55	16.82
Schott Solar (ASE-165-GT-FT/MC)	12.12	15.23	10.32	14.28
Schott Solar (ASE-260-DG-FT)	11.75	14.51	9.90	13.84
SolarWorld (SW165)	12.67	17.59	12.55	15.12
Solon (P220/6+)	9.30	11.69	11.46	11.42
MHI (MA100T2)	8.49	8.95	9.51	5.41
Schott Solar (ASIOPAK-30-SG)	14.72	7.40	6.60	5.12
Würth Solar (WS 11007/75)	10.25	11.14	6.79	10.40
First Solar (FS60)	5.32	6.63	5.05	6.09

5.3.3.2 Seasonality using CSD in Cyprus

The seasonal behaviour was further investigated through examining the normalised seasonality indices and standard deviation, obtained by using CSD on the four-year monthly average PR_{DC} time series of each PV technology. Figure 5.9 depicts the monthly average PR_{DC} normalised seasonality indices, calculated over the four-year evaluation period for each PV technology. The plots of the normalised seasonality indices of the mono-c-Si, multi-c-Si and thin-film technologies of CdTe and CIGS are presented in

Figure 5.9a, Figure 5.9b and Figure 5.9d, respectively, clearly revealing that these technologies peaked in PR during winter.

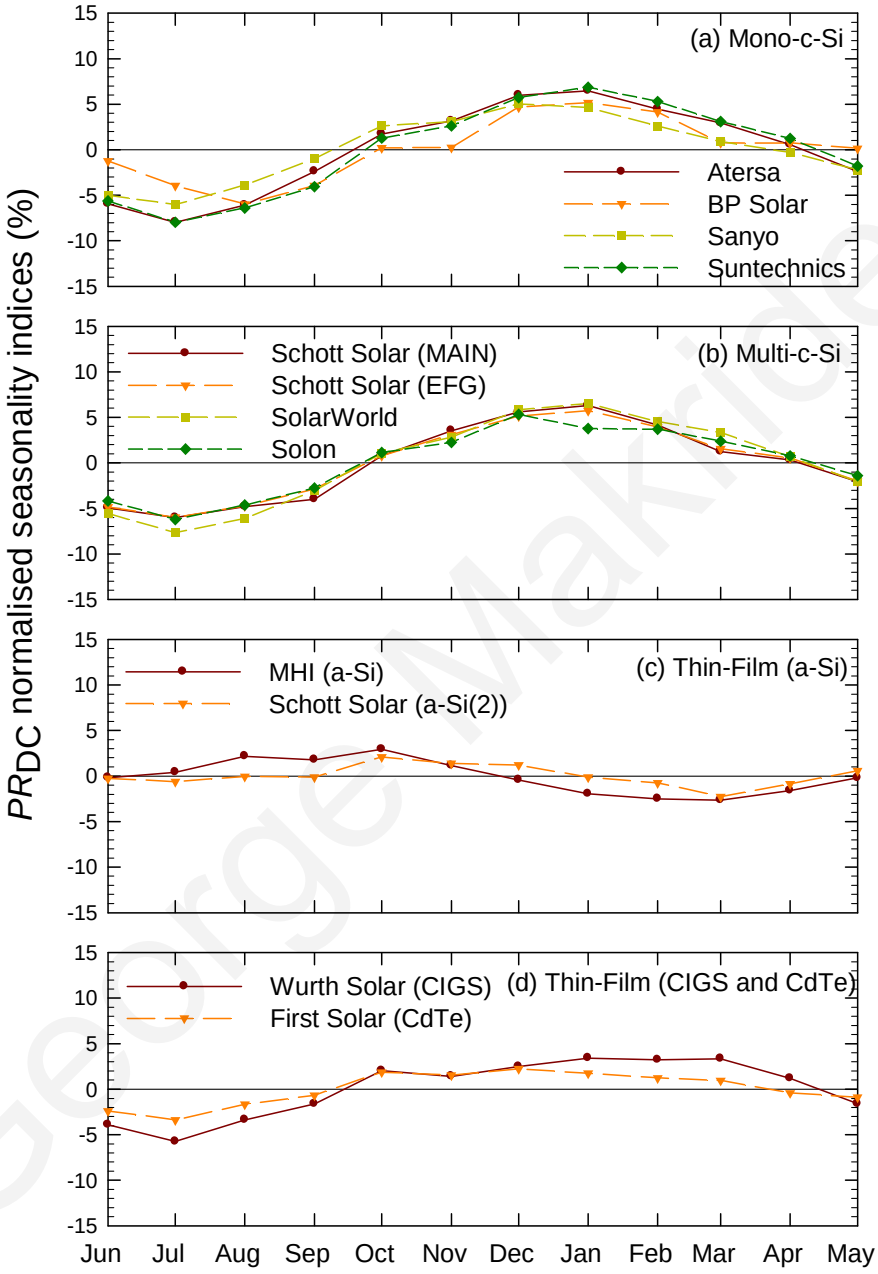

Figure 5.9. PR_{DC} normalised seasonality indices over the period June 2006 - June 2010 for the different PV technologies. (a) Mono-c-Si installed technologies. (b) Multi-c-Si installed technologies. (c) Thin-film installed technologies of a-Si. (d) Thin-film installed technologies of CIGS and CdTe.

The a-Si technologies showed a PR increase starting from spring and progressing through to summer and early autumn, as shown in Figure 5.9c. The a-Si and CdTe technologies also showed lower peak-to-peak PR seasonality variations, compared to the c-Si and CIGS technologies.

The maximum, minimum and the standard deviation of the normalised seasonality indices of all installed PV technologies were evaluated and are summarised in Table 5.6. An unequal absolute maximum and minimum of the normalised seasonality demonstrates that the specific technology performs differently during the seasons throughout the year. This difference is attributed to the response of each technology to the seasonal effects of temperature, spectrum and irradiance. Furthermore, the standard deviation of the normalised seasonality indices provides information about the variation of the performance of each technology from the annual average performance, with smaller standard deviation values indicating smaller variations due to seasonal effects. In the course of a year, both mono-c-Si and multi-c-Si technologies showed similar average normalised seasonality indices, minima and maxima ranging from -6.98 % to 5.89 % and -6.42 % to 5.90 %, respectively. The average standard deviation of mono-c-Si and multi-c-Si technologies was 4.31 % and 4.25 %, respectively. The thin-film technologies exhibited average normalised seasonality indices minima and maxima within the narrower range of -3.51 % to 2.67 % and a lower average standard deviation of 2.02 % compared to the c-Si technologies.

Table 5.6. Absolute minimum and maximum PR_{DC} normalised seasonality indices for the PV systems in Nicosia, Cyprus over the period June 2006 - June 2010. The standard deviation of each PV technology evaluated from the PR_{DC} normalised seasonality indices is also shown.

System	Minimum normalised seasonality (%)	Maximum normalised seasonality (%)	Normalised seasonality standard deviation σ (%)
Atersa (A-170M 24V)	-7.96	6.47	4.92
BP Solar (BP7185S)	-5.96	5.17	3.50
Sanyo (HIP-205NHE1)	-6.03	5.04	3.73
Suntechnics (STM 200 FW)	-7.96	6.86	5.07
Schott Solar (ASE-165-GT-FT/MC)	-6.00	6.28	4.33
Schott Solar (ASE-260-DG-FT)	-5.98	5.75	4.07
SolarWorld (SW165)	-7.67	6.53	4.85
Solon (P220/6+)	-6.03	5.04	3.76
MHI (MA100T2)	-2.65	2.94	1.86
Schott Solar (ASIOPAK-30-SG)	-2.27	2.09	1.17
Würth Solar (WS 11007/75)	-5.75	3.42	3.19
First Solar (FS60)	-3.37	2.23	1.85

5.3.4 Performance comparison in Nicosia and Stuttgart

For comparison, the monthly average PR_{AC} of the mono-c-Si technologies in both locations, over the period June 2006 - June 2009, were plotted and depicted in Figure 5.10. The PV field monthly average PR_{AC} which was calculated from the monthly average PR_{AC} values of all installed systems, was also plotted and used as a general indicator of how well each technology performed, compared to the field average. In general, as the climatic conditions in Stuttgart were not as stable as in Nicosia, mainly due to the overcast weather and snow, significant variations in the performance were observed.

In both locations, the best performing mono-c-Si technology based on the average PR_{AC} of the three-year evaluation period, was the Suntechnics mono-c-Si system. In addition, Figure 5.10 shows that most mono-c-Si systems in Nicosia exhibited higher monthly average PR_{AC} compared to the field average, whereas, in Stuttgart, only the Suntechnics mono-c-Si clearly outperformed the field average. In addition, the mono-c-Si systems in Nicosia exhibited higher and more pronounced seasonal variations, with lower performance during the summer seasons compared to the systems in Stuttgart (without considering the periods of snow in Stuttgart). The high performance variations of the mono-c-Si technologies in Nicosia are due to the warm climatic conditions.

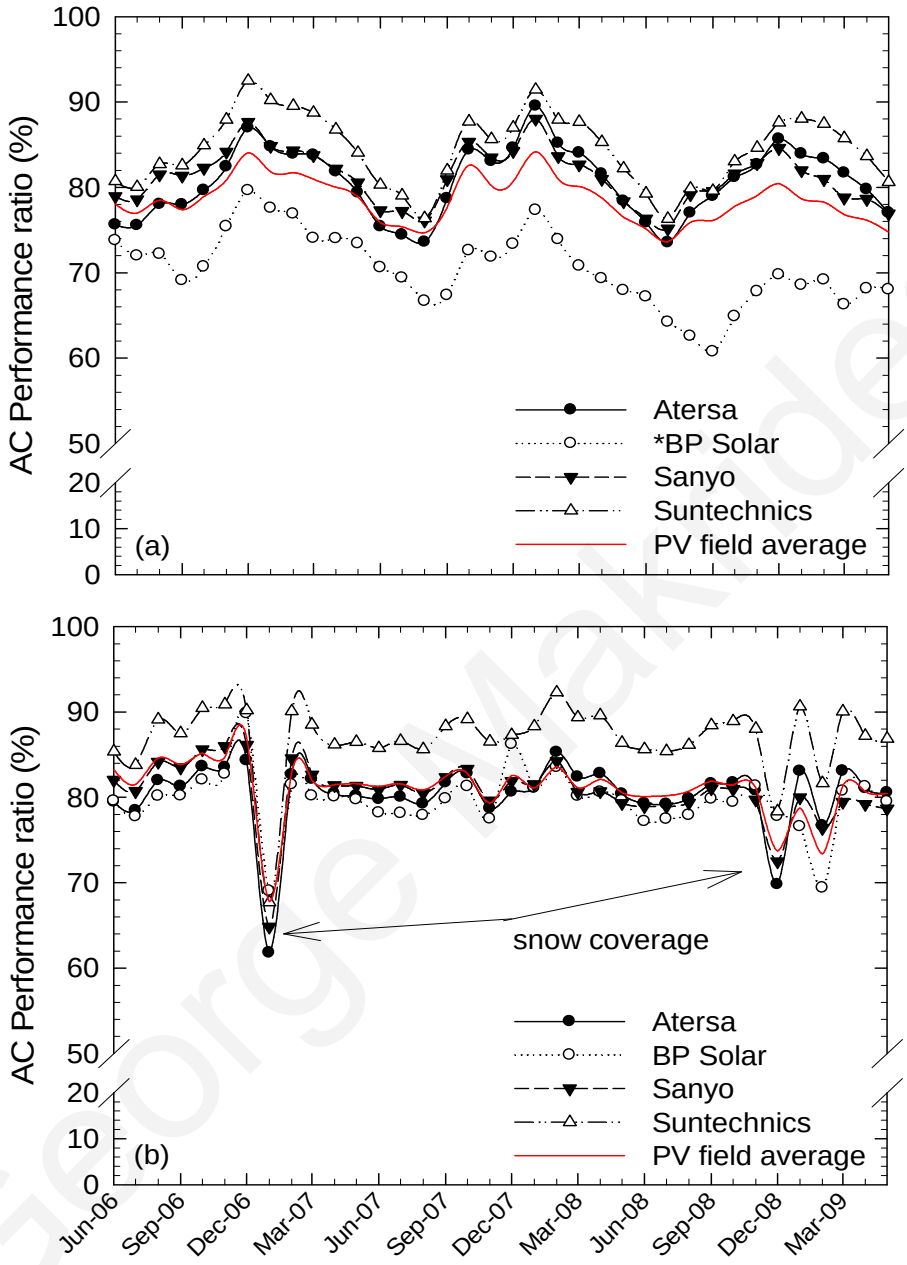

Figure 5.10. Monthly average PR_{AC} over the period June 2006 - June 2009 for the mono-c-Si PV technologies in (a) Nicosia, Cyprus and (b) Stuttgart, Germany.
* The BP Solar mono-c-Si system in Nicosia was affected by partial shading during the second and third year.

The multi-c-Si technologies also showed higher variations in Nicosia compared to Stuttgart. In particular, the monthly average PR_{AC} was lower during the warmer summer periods in Nicosia compared to Stuttgart as depicted in Figure 5.11. During the summer

months, the multi-c-Si technologies in Stuttgart demonstrated higher monthly average PR_{AC} values compared to the respective ones in Nicosia. In addition, the multi-c-Si technologies demonstrated good performance agreement with the field average in both locations.

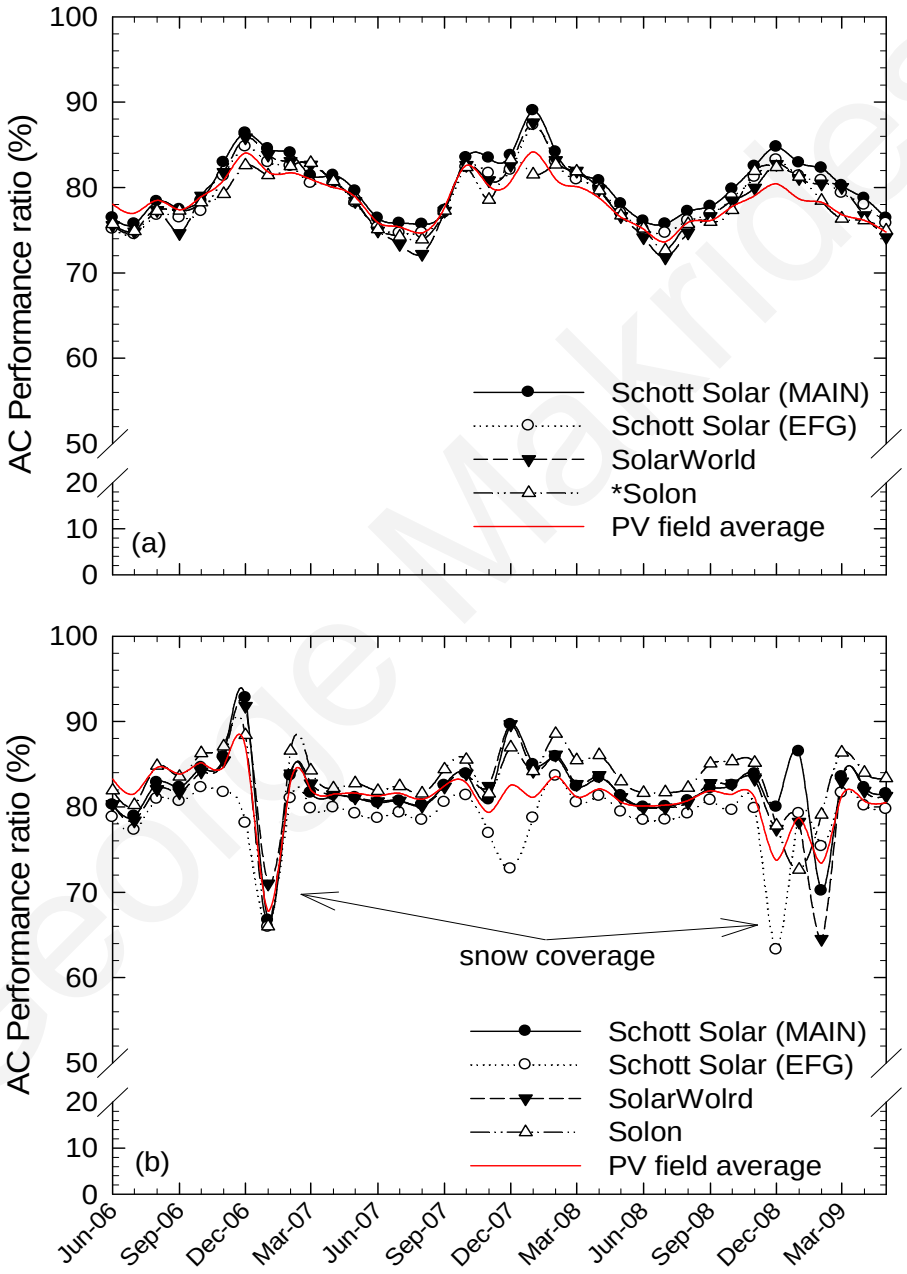

Figure 5.11. Monthly average PR_{AC} over the period June 2006 - June 2009 for the multi-c-Si PV technologies in (a) Nicosia, Cyprus and (b) Stuttgart, Germany.
* The Solon multi-c-Si system in Nicosia was affected by partial shading during the second and third year.

Furthermore, the thin-film technologies of CIGS and CdTe, generally showed higher monthly average PR_{AC} values in Stuttgart, compared to the respective systems installed in Nicosia as shown in Figure 5.12.

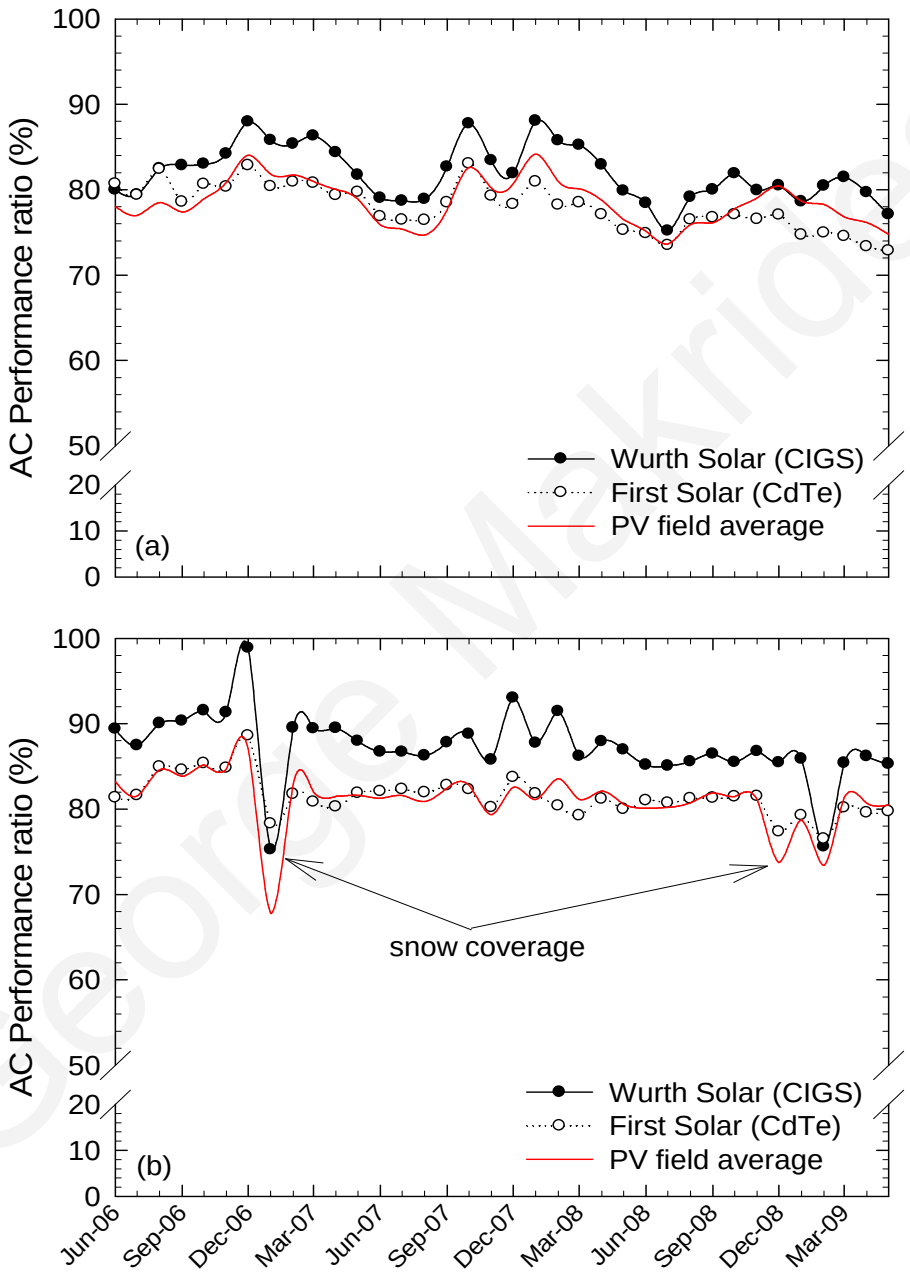

Figure 5.12. Monthly average PR_{AC} over the period June 2006 - June 2009 for the thin-film CIGS and CdTe PV technologies in (a) Nicosia, Cyprus and (b) Stuttgart, Germany.

It was more evident in Nicosia because of the warm conditions, that these technologies exhibited seasonal behaviour very similar to the c-Si systems, whereas, in Stuttgart, variations during the seasons were less obvious. In both locations, the CIGS technology exhibited higher performance than the CdTe and the PV field average.

Finally, from the plots of the monthly average PR_{AC} of the a-Si technologies presented in Figure 5.13, it was obvious that systems installed in Stuttgart exhibited a higher seasonal peak-to-peak performance, compared to the a-Si technologies installed in Nicosia. The MHI a-Si, which outperformed the Schott Solar a-Si system in Nicosia, showed lower performance in Stuttgart due to the climatic conditions. Figure 5.13, therefore, clearly shows that the best performing system in Nicosia was not the best performing system in Stuttgart. A reason for this may be the fact that the Schott Solar system in Nicosia had a broken module since October 2006. Another reason the Schott Solar a-Si may have outperformed the MHI a-Si system in Stuttgart could be that the spectral conditions were more favourable for the tandem-junction rather than for the single-junction technology. In Nicosia, the Schott Solar a-Si system performed worse compared to the average PV field monthly average PR_{AC}, while, in Stuttgart, the field performance was higher than the MHI a-SI system. Additionally, the MHI a-Si in Nicosia and the Schott Solar a-Si in Stuttgart occasionally exhibited higher monthly average PR_{AC} values during the summer seasons, as compared to the field average.

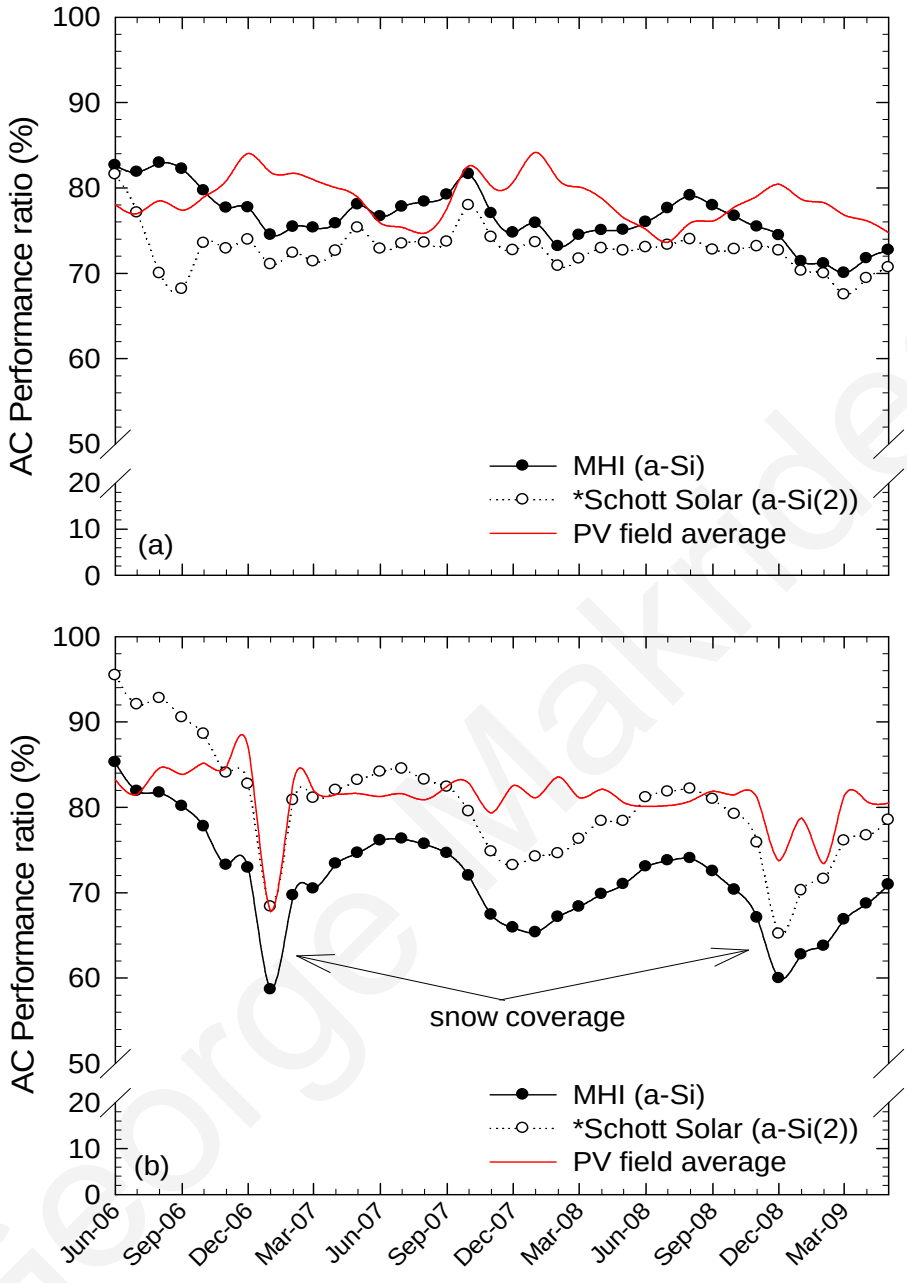

Figure 5.13. Monthly average PR_{AC} over the period June 2006 - June 2009 for the thin-film a-Si PV technologies in (a) Nicosia, Cyprus and (b) Stuttgart, Germany.

* The Schott Solar a-Si system in Nicosia, Cyprus had a broken module since October 2006.
The Schott Solar a-Si system in Stuttgart, Germany had a broken module since the 9th of May 2008.

Chapter 6

Thermal effects

6.1 Introduction

Important information can be extracted through the evaluation of temperature coefficients in correlation to the performance of the installed systems. In order to accurately characterise the temperature behaviour of PV modules at a wide range of operating conditions, it is important to derive the temperature coefficients for short-circuit current, I_{SC}, MPP current, I_{MPP}, open-circuit voltage, V_{OC}, MPP voltage, V_{MPP} and MPP power, P_{MPP}. Temperature coefficients are usually determined through indoor laboratory measurements, using a standard solar spectral distribution at 1000 W/m^2 irradiance.

A useful technique to obtain temperature coefficient information at other irradiance levels, and under real operating conditions, is by employing outdoor field test measurements. Both techniques are used by manufacturers and professionals within the field. However, as the STC are not common under real conditions, outdoor measurements are therefore more suitable to provide information for the behaviour of such systems at the environmental conditions they are installed. The application of outdoor testing has a number of advantages over indoor performed tests: primarily, there is no need for expensive artificial light sources, no limitation in the size of the samples to be investigated and, most importantly, an indication of the coefficients is provided under real environmental conditions where the modules are installed.

This chapter outlines the temperature coefficients of the installed grid-connected PV systems, which were measured under real outdoor conditions employing an outdoor evaluation technique. In parallel to the outdoor technique, a second procedure to evaluate the temperature coefficients by extensive manipulation of the data, as collected from the installed sensors at the test sites, is further described for both the test sites in Nicosia, Cyprus and Stuttgart, Germany. The results were also compared to the temperature coefficients provided by the manufacturers, demonstrating agreement in the majority of the cases.

Furthermore, the thermal losses on the annual DC energy yield of each of the different PV technologies were evaluated, by comparing the annual energy lost due to temperature to the optimum annual energy yield. The optimum annual energy yield is defined as the annual energy produced at STC, with all incident irradiation converted into energy from the PV system without any contributing losses. The thermal losses of the annual DC energy yield were calculated by employing the manufacturer and outdoor evaluated temperature coefficients, along with outdoor fifteen-minute average module temperature measurements, over the period June 2006 - June 2010. In countries such as Cyprus, with a high solar resource and warm climate the extent to which PV technologies are affected by temperature is an important criterion for their selection.

Finally, the thermal annealing effect for the a-Si technologies was also studied and described in this chapter. This was carried out by filtering DC MPP power measurements for irradiance levels greater than 800 W/m^2 and $1 \leq$ geometric AM ≤ 1.5. An important step in this procedure was to differentiate between the associated spectral and thermal annealing effects. The single-junction a-Si technology showed an increase in power, with a maximum of 7.5 %, while the tandem-junction a-Si technology showed a maximum power increase of 8.4 % from March to September.

6.2 Methodology

The procedure employed to evaluate the MPP power temperature coefficients and to calculate the thermal effects of the installed technologies is outlined in this section.

6.2.1 Temperature coefficient investigation

The investigations into the effect of temperature were based on an outdoor and data-evaluation procedure for the extraction of the MPP power temperature coefficients of the installed technologies [61].

For the outdoor procedure, the temperature coefficients at the MPP power were extracted from a series of acquired *I-V* curve measurements, over a range of temperatures (from ambient to maximum module temperature during the period of outdoor measurements). The temperature coefficient measurements were performed outdoors during periods of the day with conditions of stable sunshine and calm winds (2 m/s), around solar noon. More specifically, the temperature coefficients at the open-circuit and maximum power point voltage, short circuit and maximum power point current were determined from a number of *I-V* curve measurements, obtained for a range of temperatures (from ambient to maximum module temperature during the period of outdoor measurements). All the PV systems were equipped with back surface temperature sensors that were mounted at the centre of the investigated modules. Initially, the module was shaded with a reflective cover, specially made to cover the entire module under test, allowing at the same time airflow to pass, in order for the module to cool. The cover was carefully positioned above the photovoltaic module under investigation, shading it and decreasing in this way its temperature. After the reflective cover was removed, the module temperature rose up to the stable operating temperature. During the rise in temperature, a series of data and *I-V* traces were taken, using an outdoor *I-V* curve acquisition device shown in Figure 6.1.

Figure 6.1. Outdoor temperature coefficient evaluation apparatus. The modules under investigation are first shaded and after the cover is removed, *I-V* curves are stored at different temperatures, using the connected PVPM1000.

The *I-V* curves obtained as the module temperature rose were processed to evaluate the respective coefficients. The measured I_{SC} was adjusted by multiplying the measured values by the ratio of the reference irradiance at STC, G_{STC} (1000 W/m^2) to the measured POA irradiance G_{POA}, as measured during the experiments. The short-circuit current I_{SC} is proportional to the irradiance, at fixed temperatures, with the temperature dependence given by

$$I_{SC} = I_{SC\,STC} \cdot [1 + \alpha \cdot (T_{module} - T_{STC})] \cdot \frac{G_{POA}}{G_{STC}} \tag{6.1}$$

where $I_{SC\ STC}$ is the short-circuit current at STC, α, the short-circuit current temperature coefficient, T_{module}, the module temperature and T_{STC} is the STC module temperature at 25 °C. The plot of the measured I_{SC} values, normalised to the module respective I_{SC} at STC values, against temperature and, in particular, the slope, provides the current temperature coefficients.

Accordingly, the temperature coefficients for V_{OC} were determined in a similar manner, using the obtained *I-V* curves. The open-circuit voltage is proportional to the logarithm of the irradiance, with this dependence being assumed as constant, as there is typically less than 5 % change in the voltage coefficients over the change in irradiance from 100 W/m^2 to 1000 W/m^2 [25] – thus making the voltage dependent primarily on temperature, given by:

$$V_{\mathrm{OC}} = V_{\mathrm{OC\,STC}} \cdot [1 + \beta \cdot (T_{\mathrm{module}} - T_{\mathrm{STC}})] \tag{6.2}$$

where $V_{\mathrm{OC\ STC}}$, is the open-circuit current at STC and β is the open-circuit voltage temperature coefficient. The obtained V_{OC} values were plot against the module temperature and the slope of the linear regression provided the temperature coefficients for the voltage [61].

In parallel to the measured outdoor results, the temperature coefficients were also calculated, through analysis of the data obtained by the installed sensors (data-evaluation technique). In this analysis, measured data (fifteen-minute averages) between June 2006 and June 2007 were used. As the systems were in continuous grid-connected operation, it was only possible to evaluate the temperature coefficients of V_{MPP}, I_{MPP}, and P_{MPP}. Data sets where the global irradiance was between 700 and 1100 W/m² were chosen, to minimise the influence of high AM in the morning and the evening. Linear normalisation as a function of the irradiance was also performed, for all collected P_{MPP} measurements, and the resulting data were plot against the measured module temperatures. A linear fit provides the temperature coefficient [61].

6.2.2 Thermal influence on energy yield

The analytical calculation of the annual DC energy produced by a PV system, including the energy lost due to high temperatures, was obtained using the nominal power of the PV system, the irradiance incident on the surface of the PV systems, measured by a pyranometer installed at the POA and a temperature deviation factor, η_T. The evaluation relied on fifteen-minute average measurements, acquired and calculated for the POA irradiance and temperature deviation factor, respectively. More specifically, the following

equation was used to calculate the energy produced including losses due to temperature:

$$E_{\text{DC (STC yield and temperature loss)}} = \sum_{\text{year}} [(\eta_{\text{STC}} \cdot \eta_{\text{T}} \cdot A \cdot G_{\text{POA}})\Delta t] \quad (6.3)$$

where $E_{\text{DC (STC yield and temperature loss)}}$ is the annual DC energy yield at STC, including the associated losses due to temperature, η_{STC} is the nominal STC DC efficiency of the PV modules as provided by the manufacturer, G_{POA} is the solar irradiance at the POA, A is the total area of the PV array and Δt is the period of time. Each power data-set was then integrated over a period of one year, to obtain the annual DC energy yield calculated at STC and incorporating the thermal loss. The temperature deviation factor, η_{T}, arises from the product of the manufacturer-provided P_{MPP} temperature coefficient, γ, and the difference between the measured module temperature and the STC temperature of 25 °C. The temperature deviation coefficient is given below:

$$\eta_{\text{T}} = \begin{cases} 1 + \gamma \cdot (T_{\text{module}} - T_{\text{STC}}), & T_{\text{module}} > 25\ ^{\circ}\text{C} \\ 1, & T_{\text{module}} \leq 25\ ^{\circ}\text{C} \end{cases} \quad (6.4)$$

where T_{module} is the measured module temperature and T_{STC} is the STC temperature of 25 °C. For data-sets where the measured T_{module} was less than 25 °C, the η_{T} was considered as unity, in order to only account for the losses due to temperatures higher than the STC. The energy yield was also calculated using the same methodology, but with the MPP power temperature coefficients, which were evaluated using the outdoor technique previously performed at the University of Cyprus.

6.2.2 Thermal annealing of amorphous silicon technologies

For this investigation on grid-connected PV systems, DC MPP power data-sets of the installed a-Si systems were constructed. These were filtered at high irradiance levels (over 800 W/m^2), at 1 ≤ geometric AM ≤ 1.5, over a period of two years. The data-sets were then linearly corrected for irradiance to 1000 W/m^2 and temperature to 25 °C, using the MPP power temperature coefficients provided by the manufacturers and the measured

module temperatures. Since the data-sets were filtered at $1 \leq$ geometric AM ≤ 1.5, any observed increase in power is likely to be attributed to the thermal annealing effect.

Although this technique can provide an indication of the effect of thermal annealing, it was difficult to determine the exact conditions of thermal annealing and to observe the memory effect associated with the annealing procedure. Subsequently, the accuracy of the result could be affected by the spectrum, soiling, progressive degradation and solar irradiation sensor uncertainties. The soiling effect was minimised during the evaluation period of December 2007 - December 2009, as all the systems were occasionally cleaned by intermediate rainfall, as well as manually cleaned on the 24th of July 2009. In an attempt to further validate the results, the investigation was also carried out by using the irradiance measurements acquired from a c-Si reference cell installed next to the pyranometer, to filter and correct the DC MPP power data-sets.

Finally, in order to calculate the magnitude of the thermal annealing effect and to determine if the periodic and seasonal increase in performance was due to temperature and not spectral effects, the same investigation was carried out; this time by selecting only DC MPP power measurements at a different geometric AM range, between 1.4 and 1.6, and then correcting for irradiance to 1000 W/m^2 and temperature to 25 °C. By then applying a linear least square fit to the corrected DC MPP power measurements data-sets, the power increase was evaluated over the period of evident increase in power output, from March to September, for each year of the evaluation.

6.3 Results

The results of the temperature coefficient, thermal effect and annealing investigations are summarised in this section.

6.3.1 Temperature distribution

Prior to obtaining the outdoor measurements, the thermal distribution of all modules near the mounting, junction and centre were investigated. Infrared images were taken, clearly showing that the temperature distribution in a module is uniform, apart from areas around the junction box and the main busbar interconnection point. These points tend to accumulate more heat than the rest of the module and are, hence, at higher temperature than expected (around 2 - 3 °C higher in this case), as shown in Figure 6.2.

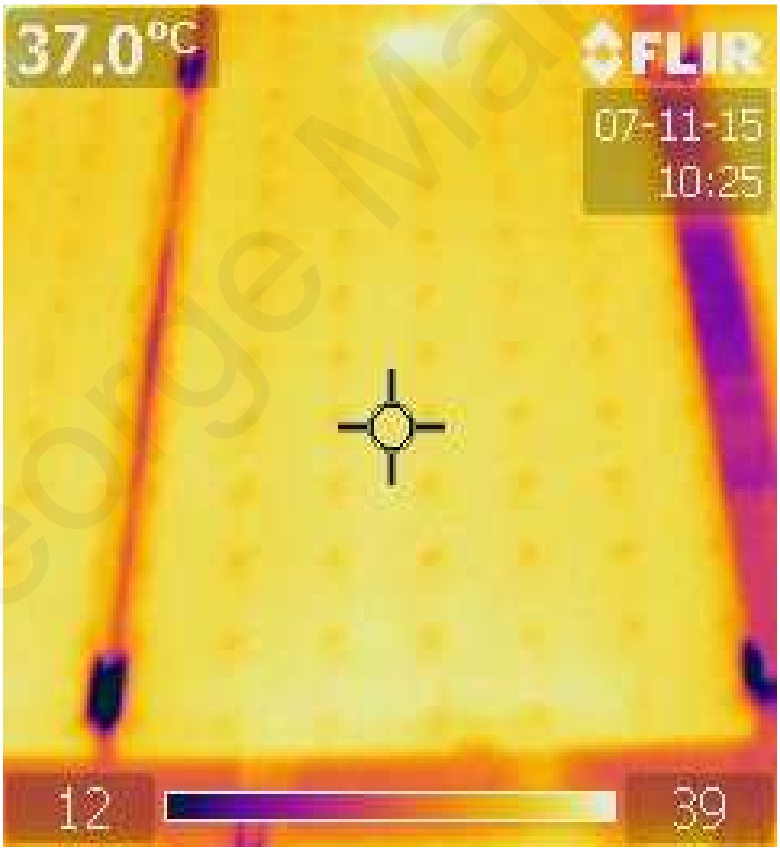

Figure 6.2. Infrared photograph of mono-c-Si module. Higher temperature (around 2 - 3 °C) was obtained near the junction box.

6.3.2 Temperature coefficients

A large number of outdoor tests for all systems were performed in Cyprus, to provide more reliable results for the temperature coefficients. Table 6.1 summarises the results of the outdoor measured α, β and γ temperature coefficients in Cyprus. The results indicate that multi-c-Si technologies showed larger V_{OC} temperature coefficients, in comparison to the thin-film and mono-c-Si high efficiency technologies.

Table 6.1. Installed PV technology outdoor measurement α, β and γ temperature coefficients in Cyprus.

Module	α I_{SC} **(%/K)**	β V_{OC} **(%/K)**	γ P_{MPP} **(%/K)**
Atersa mono-c-Si	0.08	-0.44	-0.56
BP Solar mono-c-Si	0.07	-0.43	-0.53
Sanyo HIT-Si	0.01	-0.29	-0.42
Suntechnics mono-c-Si	0.03	-0.32	-0.45
Schott Solar MAIN-Si	0.13	-0.48	-0.50
Schott Solar EFG-Si	0.17	-0.43	-0.42
SolarWorld multi-c-Si	0.05	-0.36	-0.49
Solon multi-c-Si	0.02	-0.38	-0.40
MHI a-Si	0.18	-0.36	-0.19
Schott Solar a-Si	0.05	-0.31	-0.20
First Solar CdTe	0.04	-0.36	-0.22
Würth Solar CIGS	0.03	-0.14	-0.42

Furthermore, the P_{MPP} temperature coefficients, for both mono-c-Si and multi-c-Si technologies, were higher than the respective coefficients for thin-film technologies.

Figure 6.3 summarises the measured, calculated and manufacturer provided MPP power temperature coefficients obtained by both techniques. For most PV technologies, the outdoor evaluated results showed satisfactory agreement when compared to manufacturer provided data. The difference in some cases arises mainly due to the systematic errors of the different measurement sensors and the equipment used to measure the results, as well as the effects of dust, which is a more obvious phenomenon in Cyprus. The highest deviations were observed for the thin-film amorphous silicon technologies, possibly because of the spectral effects [123].

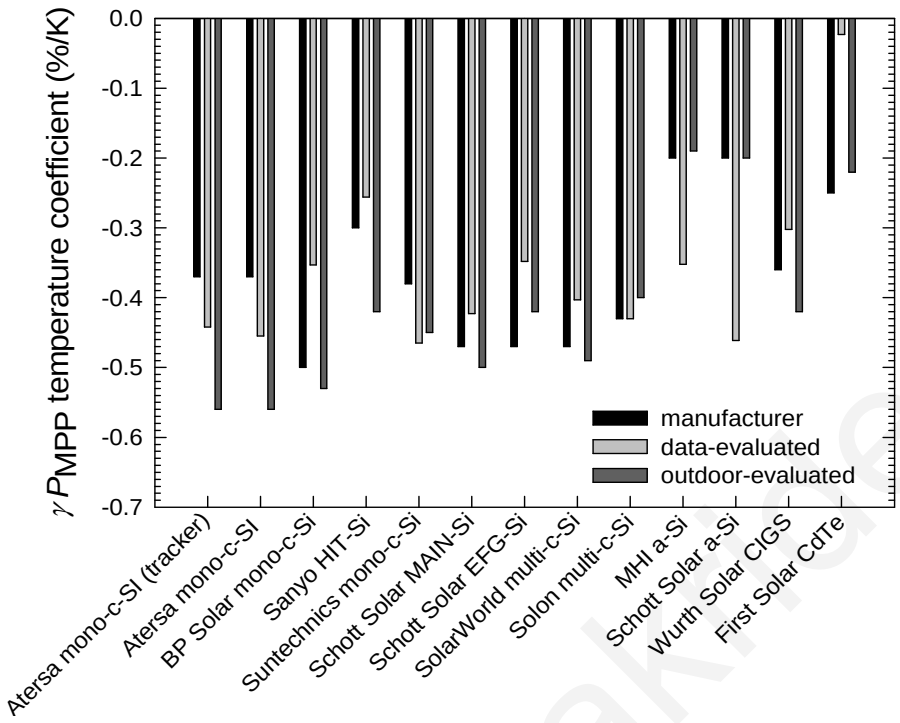

Figure 6.3. Comparison of the γ MPP power temperature coefficients (%/K), obtained by the two methods outlined above (outdoor and data-evaluated) and the manufacturers' data for the installed systems.

Additionally, comparisons of the temperature coefficients obtained through data analysis show that the coefficients are approximately the same for the systems installed in Germany and Cyprus as can be seen in Table 6.2. Some deviations, however, are evident for the MHI and First Solar systems.

Table 6.2. Calculated γ P_{MPP} temperature coefficients in Cyprus and Germany.

Module	**Cyprus γ P_{MPP} (%/K)**	**Germany γ P_{MPP} (%/K)**
Atersa mono-c-Si	-0.455 ± 0.006	-0.437 ± 0.004
BP Solar mono-c-Si	-0.353 ± 0.006	-0.358 ± 0.011
Sanyo HIT-Si	-0.256 ± 0.007	-0.262 ± 0.004
Suntechnics mono-c-Si	-0.465 ± 0.009	-0.437 ± 0.004
Schott Solar MAIN-Si	-0.423 ± 0.014	-0.418 ± 0.011
Schott Solar EFG-Si	-0.348 ± 0.006	-0.367 ± 0.008
SolarWorld multi-c-Si	-0.403 ± 0.006	-0.424 ± 0.010
Solon multi-c-Si	-0.430 ± 0.006	-0.502 ± 0.010
MHI a-Si	-0.352 ± 0.052	-0.290 ± 0.016
Schott Solar a-Si	-0.461 ± 0.012	-0.039 ± 0.014
First Solar CdTe	-0.023 ± 0.009	-0.074 ± 0.011
Würth Solar CIGS	-0.302 ± 0.012	-0.320 ± 0.011

6.3.3 Influence of temperature on PV performance

Important conclusions about the performance of the PV technologies, in relation to warm weather conditions, were deducted by plotting the monthly average DC PR for all installed PV technologies and the ambient temperature over the four-year evaluation period.

The results showed that both mono-c-Si and multi-c-Si technologies exhibited better performance during winter, in comparison to summer. The c-Si technologies showed the lowest PR during the hot summer period, as shown in Figure 6.4 and Figure 6.5. On the other hand, the peaks in performance during winter occurred when the ambient temperature was minimum, signifying that there is a clear correlation between the performance of c-Si technologies and the temperature.

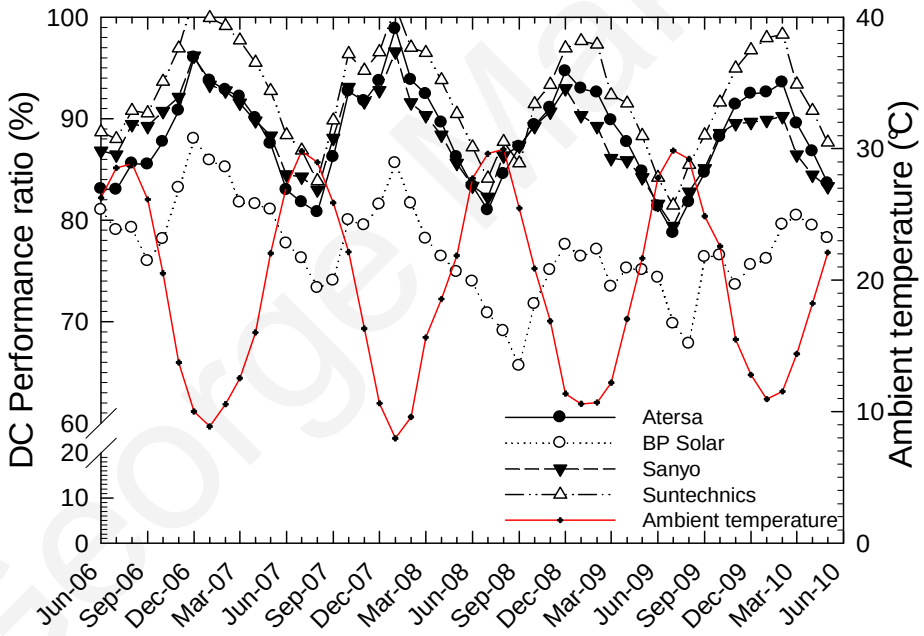

Figure 6.4. Monthly average DC PR for mono-c-Si systems over the period June 2006 - June 2010 in Nicosia, Cyprus (partial shading of the BP Solar system occurred during the second, third and fourth years).

Similar seasonal performance to the c-Si technologies was observed for the Würth Solar CIGS and the First Solar CdTe, as shown in Figure 6.6.

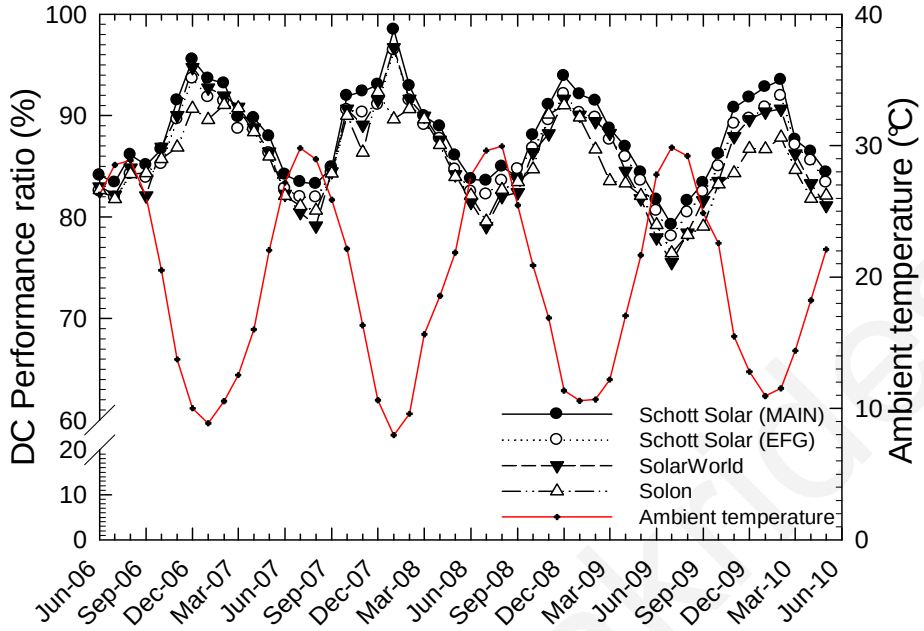

Figure 6.5. Monthly average DC PR for multi-c-Si systems over the period June 2006 - June 2010 in Nicosia, Cyprus (partial shading of the Solon system occurred during the second, third and fourth years).

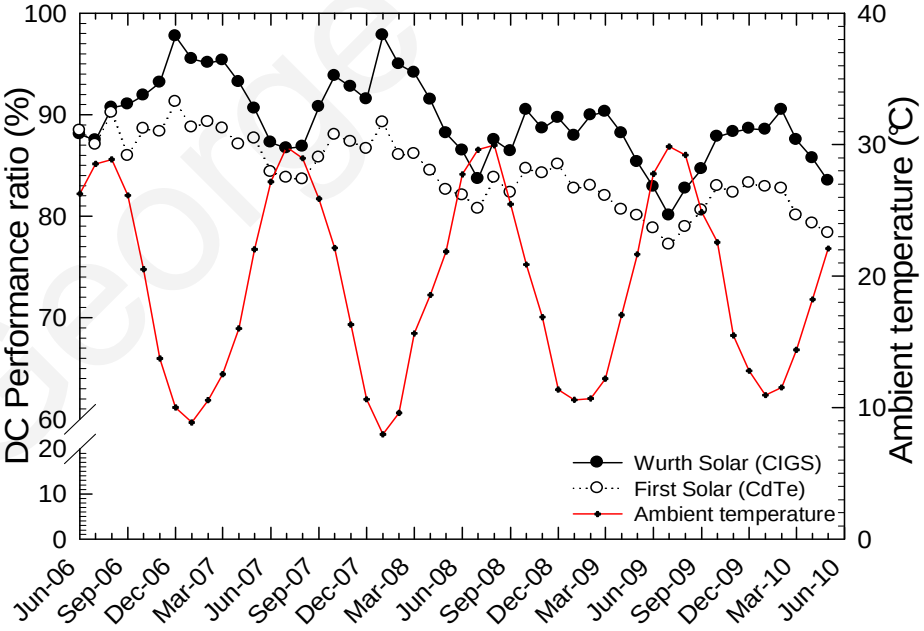

Figure 6.6. Monthly average DC PR for thin-film CIGS and CdTe systems over the period June 2006 - June 2010 in Nicosia, Cyprus.

On the other hand, Figure 6.7 shows that the a-Si thin-film technologies showed relatively better performance during the warmer months (starting from spring to autumn) than during the winter.

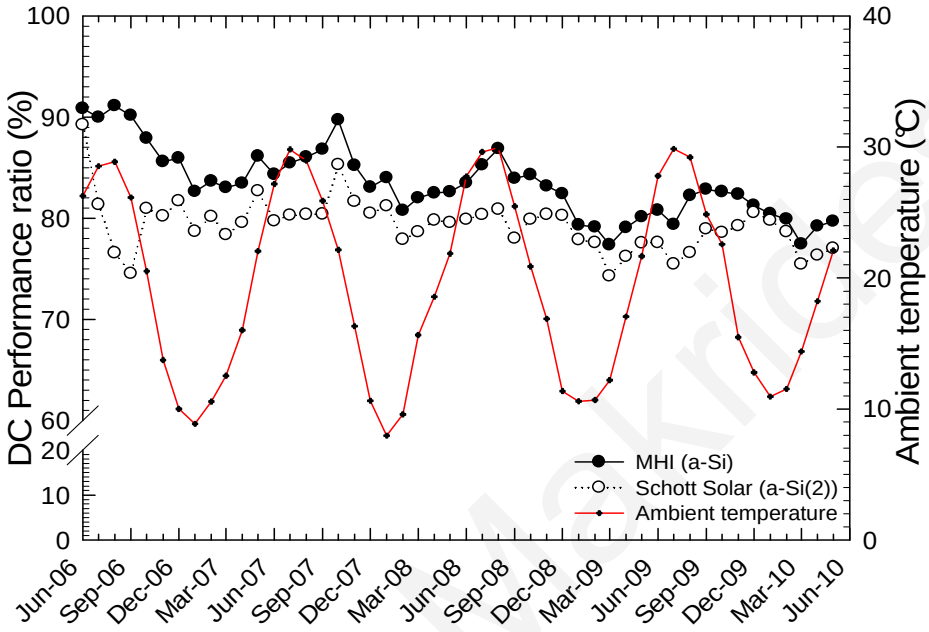

Figure 6.7. Monthly average DC PR for thin-film a-Si systems over the period June 2006 - June 2010 in Nicosia, Cyprus (one of the Schott Solar a-Si modules has been broken since the 4th of October 2006).

The annual losses caused by high module temperatures were first accounted for by applying corrections based on the manufacturers' γ. In this case, the highest average APE of the thermal losses on the annual DC energy yield, in comparison to the annual DC energy yield at STC efficiency were 8 % and 9 %, for the mono-c-Si and multi-c-Si technologies, respectively; whereas this was 5 % for thin-film technologies. The annual thermal losses of the a-Si technologies were the lowest because their temperature coefficients were the lowest amongst the installed PV technologies. Table 6.3 summarises the results.

Table 6.3. Annual DC energy yield thermal losses APE using the manufacturers' MPP power temperature coefficients over the period June 2006 - June 2010 in Nicosia, Cyprus.

System	Manufacturer γ (%/K)	2006 - 2007 APE (%)	2007 - 2008 APE (%)	2008 - 2009 APE (%)	2009 - 2010 APE (%)
Atersa (A-170M 24V)	-0.37	6.44	6.61	6.60	6.97
BP Solar (BP7185S)	-0.50	9.75	10.16	10.05	10.36
Sanyo (HIP-205NHE1)	-0.30	5.47	5.64	5.64	5.91
Suntechnics (STM 200 FW)	-0.38	6.63	6.90	6.94	7.22
Schott Solar (ASE-165-GT-FT/MC)	-0.47	7.94	8.40	8.26	8.49
Schott Solar (ASE-260-DG-FT)	-0.47	8.90	9.14	9.09	9.37
SolarWorld (SW165)	-0.47	9.16	9.55	9.42	9.77
Solon (P220/6+)	-0.43	8.20	8.57	8.46	8.92
MHI (MA100T2)	-0.20	3.28	3.50	4.00	3.60
Schott Solar (ASIOPAK-30-SG)	-0.20	3.67	3.88	3.80	3.98
Würth Solar (WS 11007/75)	-0.36	7.33	8.63	7.92	7.32
First Solar (FS60)	-0.25	5.15	5.37	5.32	5.59

Likewise, the thermal losses using the outdoor evaluated temperature coefficients produced similar results, with the exception of Sanyo HIT and Atersa mono-c-Si (due to the fact that the outdoor evaluated coefficients were found to be higher than the manufacturers' coefficients for these two systems). Table 6.4 lists the APE of the annual DC energy yield thermal losses over the period June 2006 - June 2010, for all PV technologies, using the outdoor evaluated MPP power temperature coefficients.

Table 6.4. Annual DC energy yield thermal losses APE using the outdoor evaluated MPP power temperature coefficients over the period June 2006 - June 2010 in Nicosia, Cyprus.

System	Outdoor evaluated γ (%/K)	2006 - 2007 APE (%)	2007 - 2008 APE (%)	2008 - 2009 APE (%)	2009 - 2010 APE (%)
Atersa (A-170M 24V)	-0.56	9.76	10.01	10.00	10.54
BP Solar (BP7185S)	-0.53	10.34	10.77	10.65	10.98
Sanyo (HIP-205NHE1)	-0.42	7.66	7.88	7.91	8.26
Suntechnics (STM 200 FW)	-0.45	7.86	8.17	8.22	8.55
Schott Solar (ASE-165-GT-FT/MC)	-0.50	8.45	8.93	8.79	9.03
Schott Solar (ASE-260-DG-FT)	-0.42	7.95	8.17	8.12	8.37
SolarWorld (SW165)	-0.49	9.55	9.96	9.82	10.18
Solon (P220/6+)	-0.40	7.63	7.98	7.87	8.30
MHI (MA100T2)	-0.19	3.12	3.32	3.80	3.42
Schott Solar (ASIOPAK-30-SG)	-0.20	3.67	3.88	3.80	3.98
Würth Solar (WS 11007/75)	-0.42	8.56	10.07	9.25	8.53
First Solar (FS60)	-0.22	4.53	4.73	4.68	4.92

6.3.4 Thermal annealing effect on PV performance

The effect of temperature on the DC MPP power of the MHI and Schott Solar a-Si and two c-Si technologies (namely, the Atersa mono-c-Si and Schott Solar (MAIN) multi-c-Si) was first investigated by extracting DC MPP power and module temperature measurements at POA irradiance levels in the range $980 \leq$ POA irradiance ≤ 1020 W/m^2, over the period June 2007 - June 2010. The extracted data-sets were first normalised to the manufacturers' rated peak power and then plotted without applying any other corrections. From the power against module temperature plots obtained and shown in Figure 6.8 - Figure 6.10, it was evident that the c-Si technologies showed a decrease in performance with increasing temperature, while this was not always the case for the a-Si technologies. The gradient of the applied linear least square fit can also provide information about the MPP power temperature coefficient, although the values obtained from this investigation on a one year data-set for each technology can be obscured by effects such as the spectrum, degradation and soiling. From the extracted data-sets of the period June 2007 - June 2008, as shown in Figure 6.8a, the MHI a-Si showed almost steady performance, with a very small decrease, while an evident decrease in power as temperature increased was observed for the c-Si technologies (shown in Figure 6.8c-d). In Figure 6.8b the Schott Solar a-Si showed a performance decrease which was smaller than the manufacturers' MPP power temperature coefficient.

For subsequent years (June 2008 - June 2009 and June 2009 - June 2010), both a-Si technologies showed no evident decrease in performance with the increased temperature, while this was not the case for the c-Si technologies. The results are depicted in Figure 6.9 and Figure 6.10. During this period, the MHI a-Si showed a positive temperature coefficient, while the Schott Solar a-Si showed a positive temperature coefficient for the period June 2008 - June 2009 and a very small negative coefficient during the period June 2009 - June 2010.

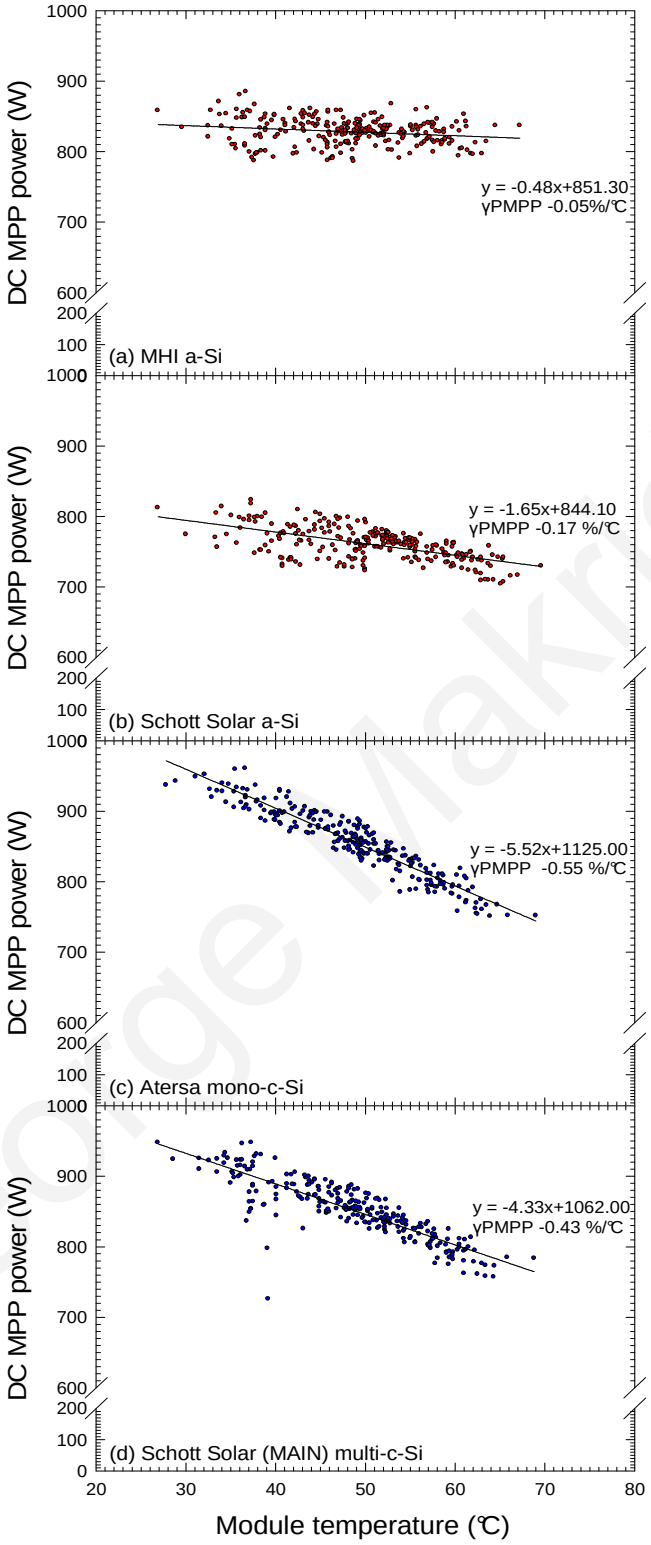

Figure 6.8. Filtered DC MPP power at irradiance in the range 980 ≤ POA irradiance ≤ 1020 W/m^2 over the period June 2007 - June 2008.

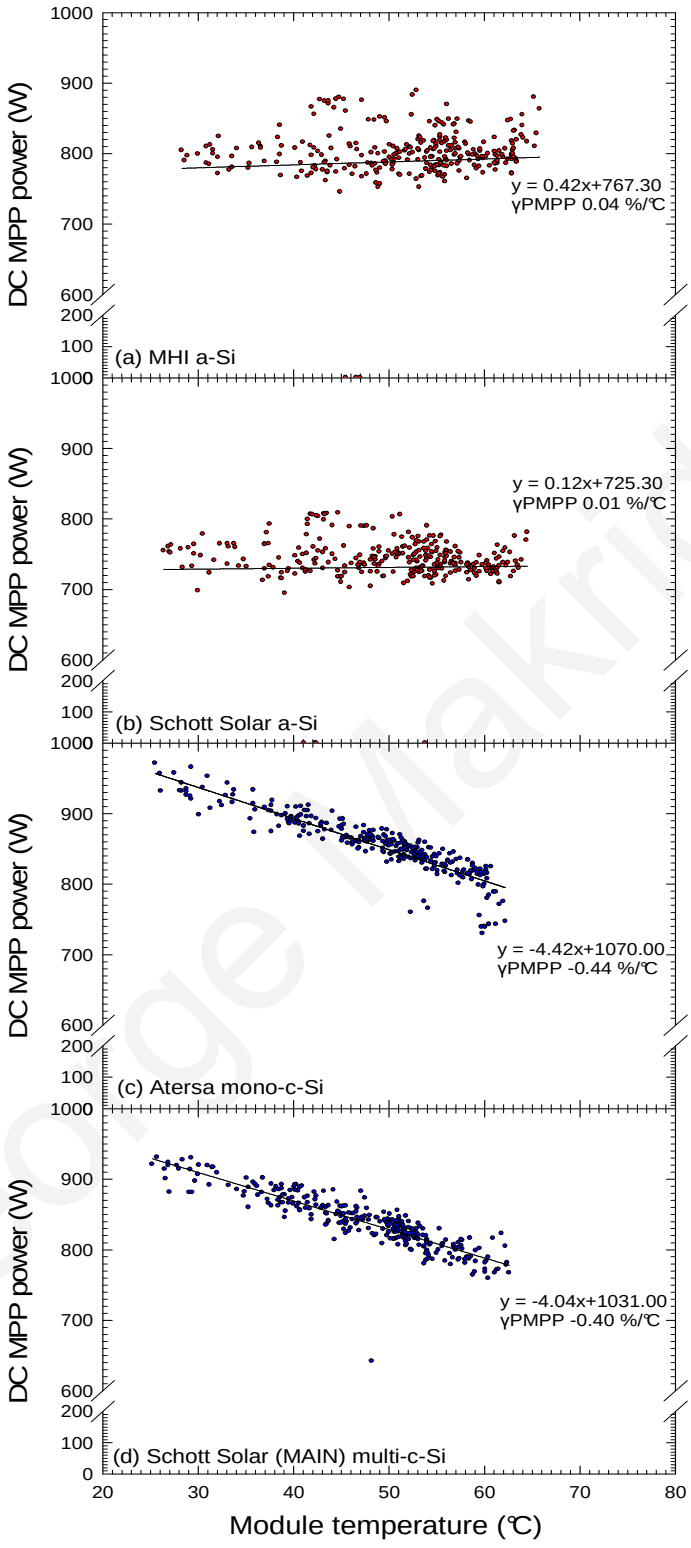

Figure 6.9. Filtered DC MPP power at irradiance in the range 980 ≤ POA irradiance ≤ 1020 W/m^2 over the period June 2008 - June 2009.

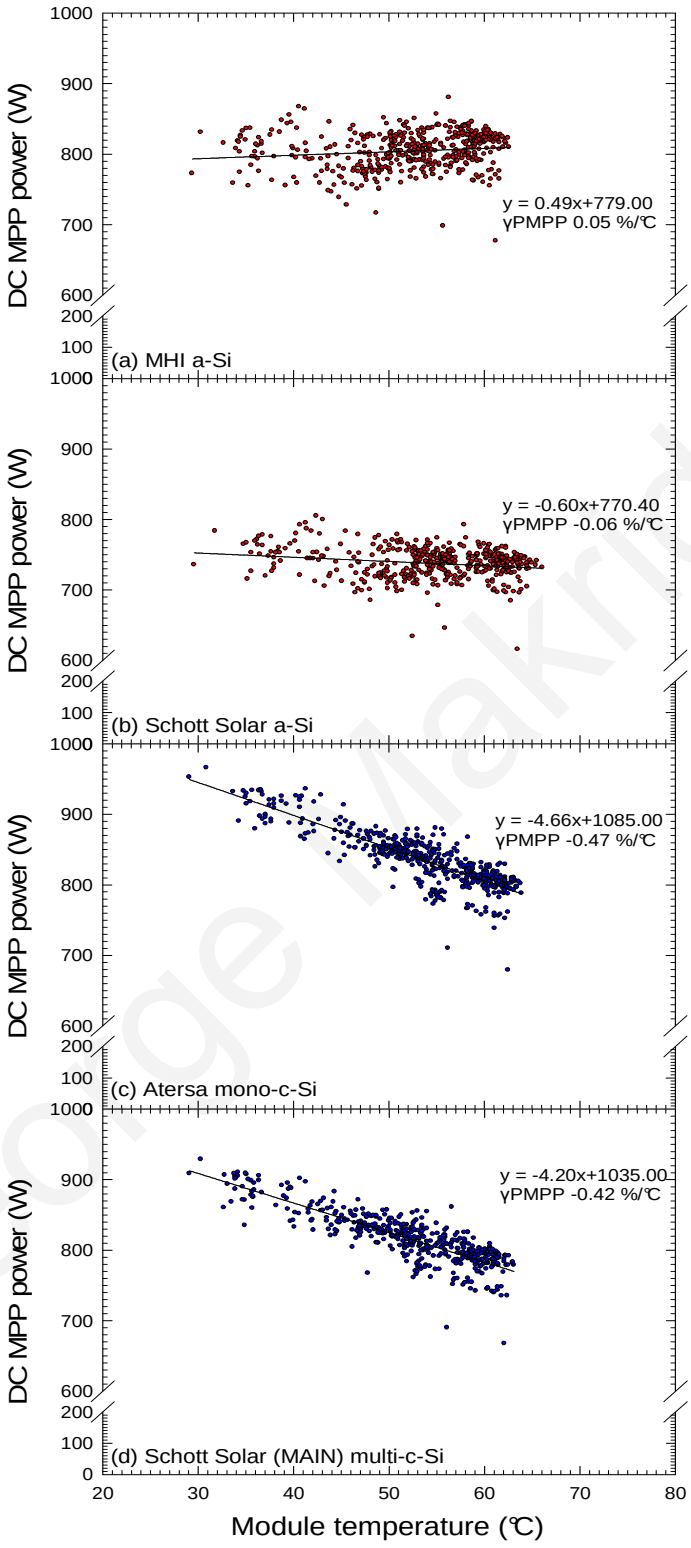

Figure 6.10. Filtered DC MPP power at irradiance in the range 980 ≤ POA irradiance ≤ 1020 W/m^2 over the period June 2009 - June 2010.

The effect of thermal annealing became more evident for the a-Si technologies from the plots of the filtered and corrected DC MPP power data-sets, given a progressive increase in power from early spring until early autumn, from March to September, due to the increased module temperatures and is shown in Figure 6.11 and Figure 6.12, for the MHI and Schott Solar a-Si, respectively. After this period there was a tendency for the power to decrease. Similarly, for validation purposes and more specifically, in order to account for uncertainties associated with the pyranometer or soiling on the sensor itself, the same investigation was performed. However, instead of filtering and correcting the DC MPP power data-sets based on the POA pyranometer measurements, the measurements acquired from a c-Si reference cell installed next to the pyranometer were used. The power increase over early spring and autumn was again evident for the a-Si technologies. For clarity, the DC MPP power data-sets were divided into groups of 0.1 geometric AM intervals, in the filtered range $1 \leq$ geometric AM ≤ 1.5, in order to show the geometric AM levels and occurrence of each power data-set.

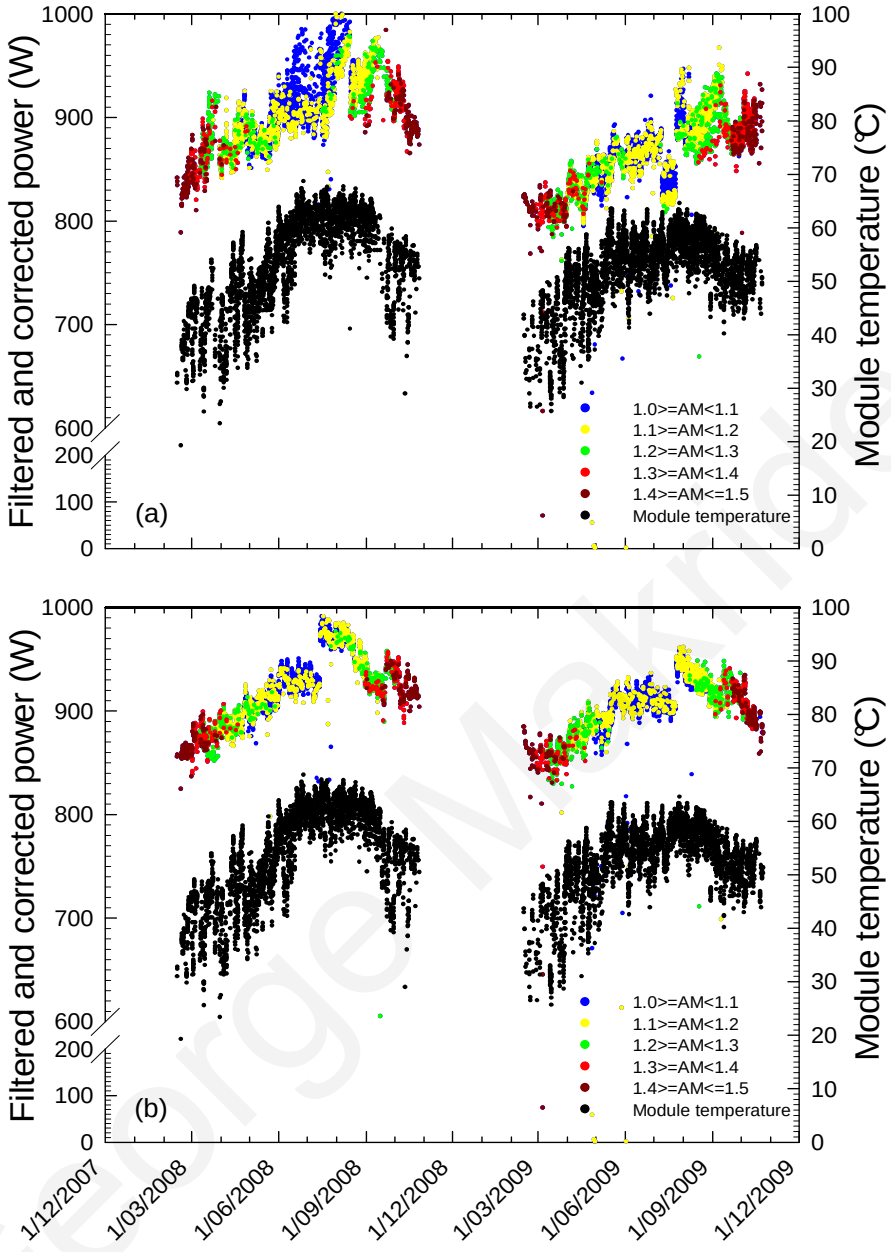

Figure 6.11. Filtered and corrected DC MPP power, grouped into AM ranges, over the period December 2007 - December 2009 for MHI a-Si (single-junction) and correcting power to irradiance measurements of a) the pyranometer and b) the c-Si reference cell. Module temperatures of the filtered data are also shown.

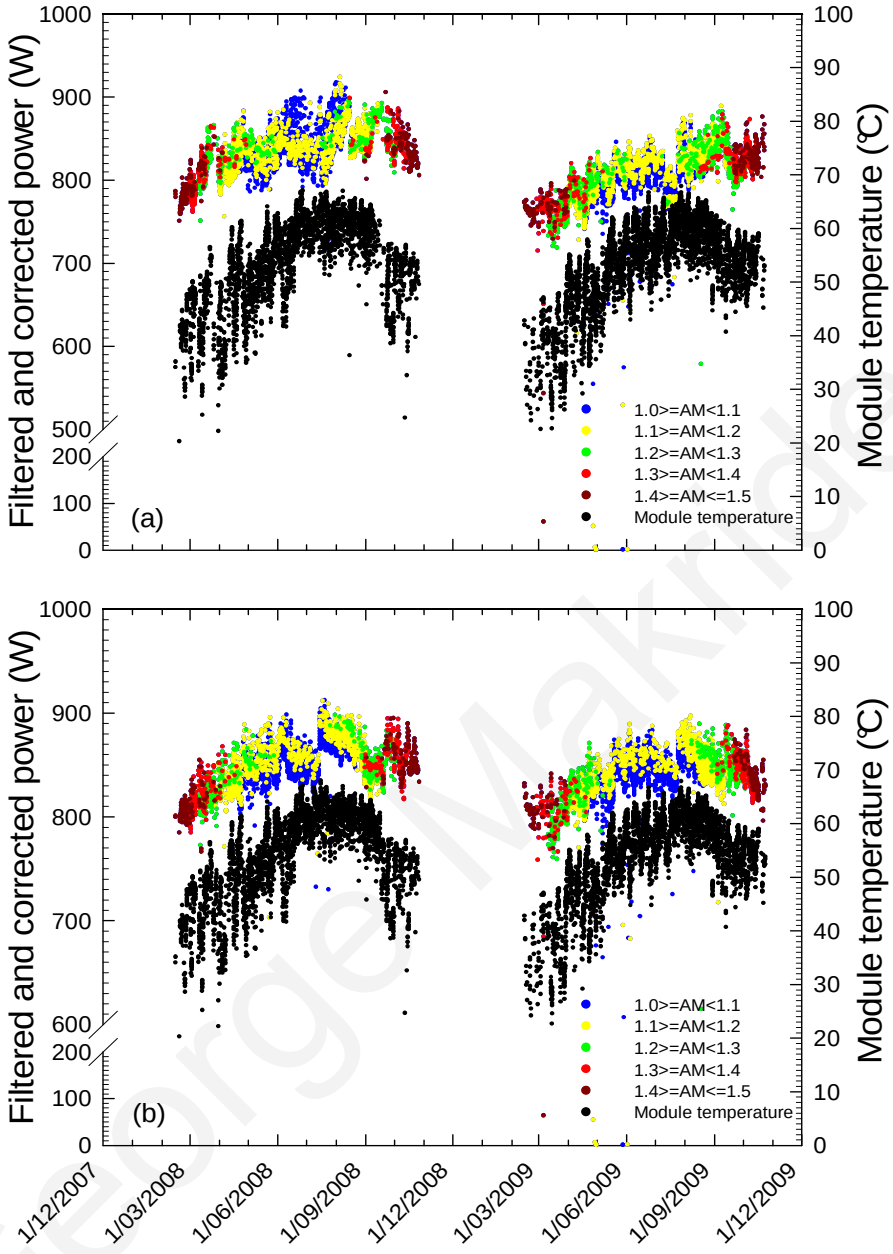

Figure 6.12. Filtered and corrected DC MPP power, grouped into AM ranges, over the period December 2007 - December 2009 for Schott Solar a-Si (tandem) and correcting power to irradiance measurements of a) the pyranometer and b) the c-Si reference cell. Module temperatures of the filtered data are also shown.

For comparison, the same investigation was carried out for the Atersa mono-c-Si and Schott Solar MAIN multi-c-Si systems. The plots in Figure 6.13a and Figure 6.13b show that, contrary to the a-Si behaviour, the c-Si technologies showed no evident progressive increase in power, particularly throughout the investigation period, March to September;

with the exception of cases when there was rainfall and when the modules were cleaned (24th July 2009).

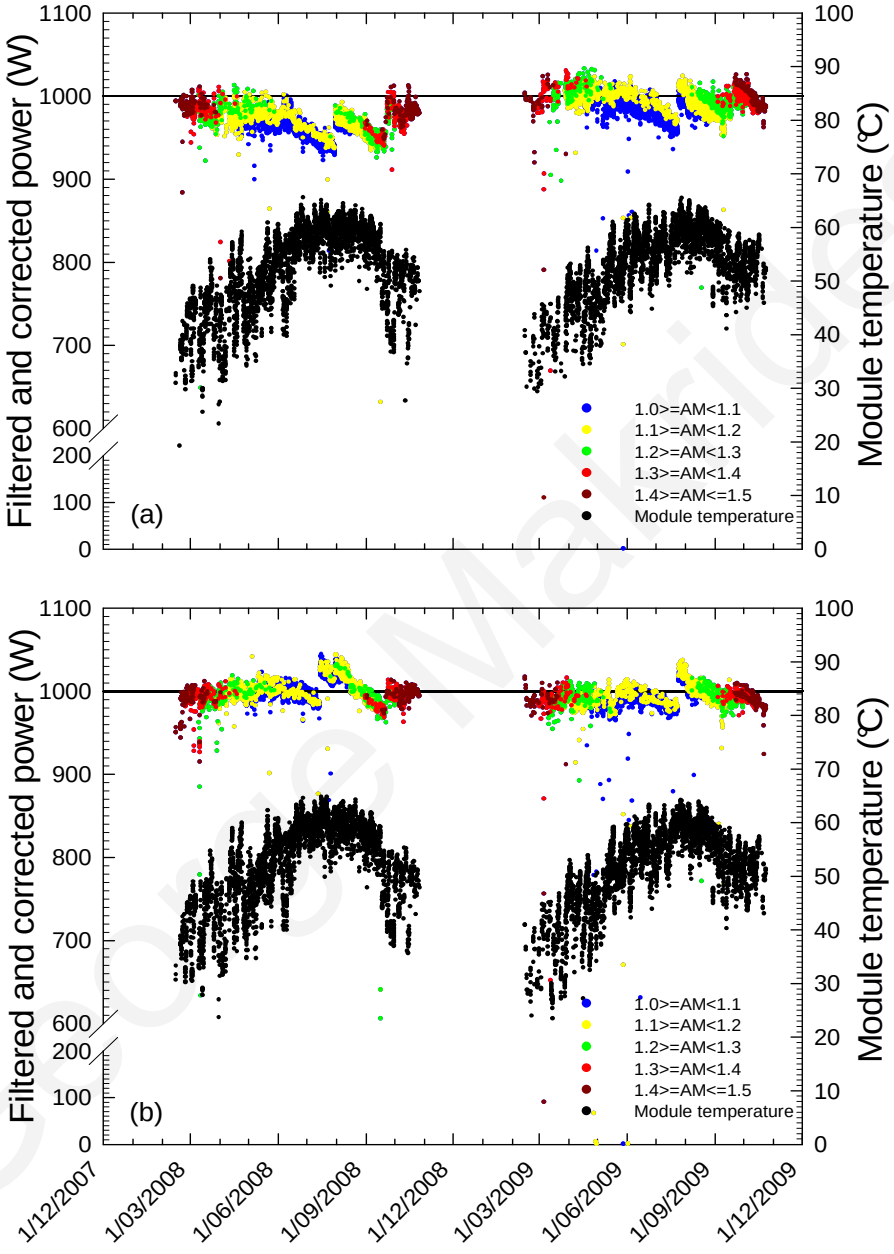

Figure 6.13. Filtered and corrected DC MPP power, grouped into AM ranges, over the period December 2007 - December 2009 for the a) Atersa mono-c-Si and b) Schott Solar MAIN multi-c-Si systems. Power was corrected based on irradiance measurements of the c-Si cell. Module temperatures of the filtered data are also shown.

The same investigation was carried out by filtering and correcting the power data-sets that occurred at a different geometric AM range, 1.4 ≤ geometric AM ≤ 1.6. Figure 6.14 shows the presence of a thermal annealing effect for both a-Si technologies because a performance increase is still obvious during periods with increased module temperature.

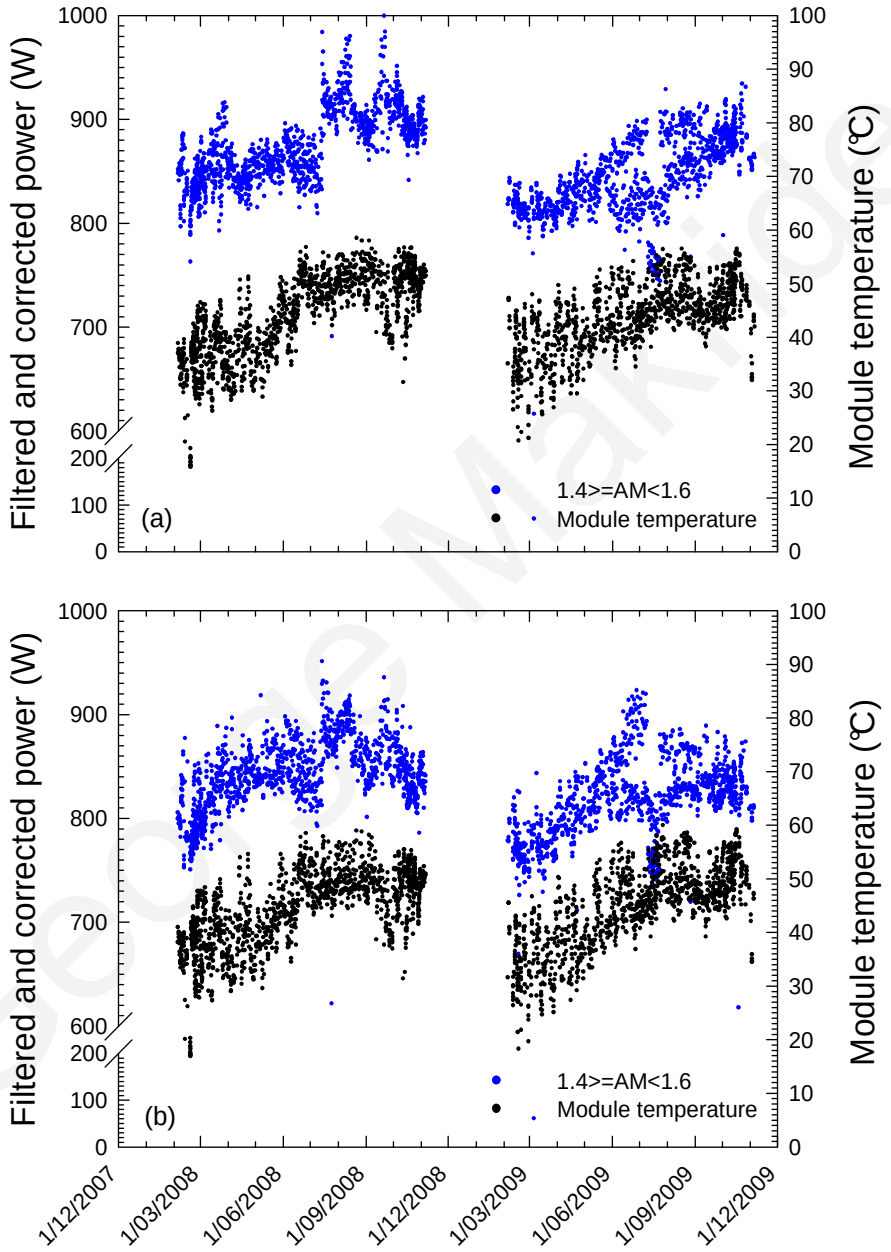

Figure 6.14. Filtered and corrected DC MPP power, using irradiance measurements of the POA pyranometer, over the period December 2007 - December 2009 for a) MHI a-Si (single-junction) and b) Schott Solar a-Si (tandem-cell). Module temperatures of the filtered data are also shown.

The amount of thermal annealing over the period March 2008 - September 2008 was found by first applying a linear least square fit over the filtered and corrected DC MPP power data-sets and then, comparing the DC MPP power at the beginning and end of this period (at fifteen-minute time intervals). The MHI and Schott Solar a-Si technologies exhibited a power increase of 7.5 % and 7.2 %, respectively, in September 2008, in comparison to the DC MPP power at the beginning of March 2008 as shown in Figure 6.15.

Figure 6.16 demonstrates the increase in power for both the MHI and the Schott Solar a-Si technologies, between March 2009 and September 2009. The MHI and the Schott Solar a-Si showed a 7 % and 8.4 % increase in power, respectively, over this period.

Soiling was the reason for the decrease in performance during July 2009, however, following the cleaning of the modules on the 24th July 2009, there was again a substantial increase in performance. All results are summarised in Table 6.5. The effect of thermal annealing was previously found to have contributed to an approximately 7 % increase in power from winter to summer months for an outdoor a-Si module [53], which is consistent with the obtained results.

Table 6.5. Power increase evaluated over the period March 2008 - September 2008 and March 2009 - September 2009 in Nicosia, Cyprus.

System	**Power increase from March - September 2008 (%)**	**Power increase from March - September 2009 (%)**
MHI (MA100T2)	7.5	7.0
Schott Solar (ASIOPAK-30-SG)	7.2	8.4

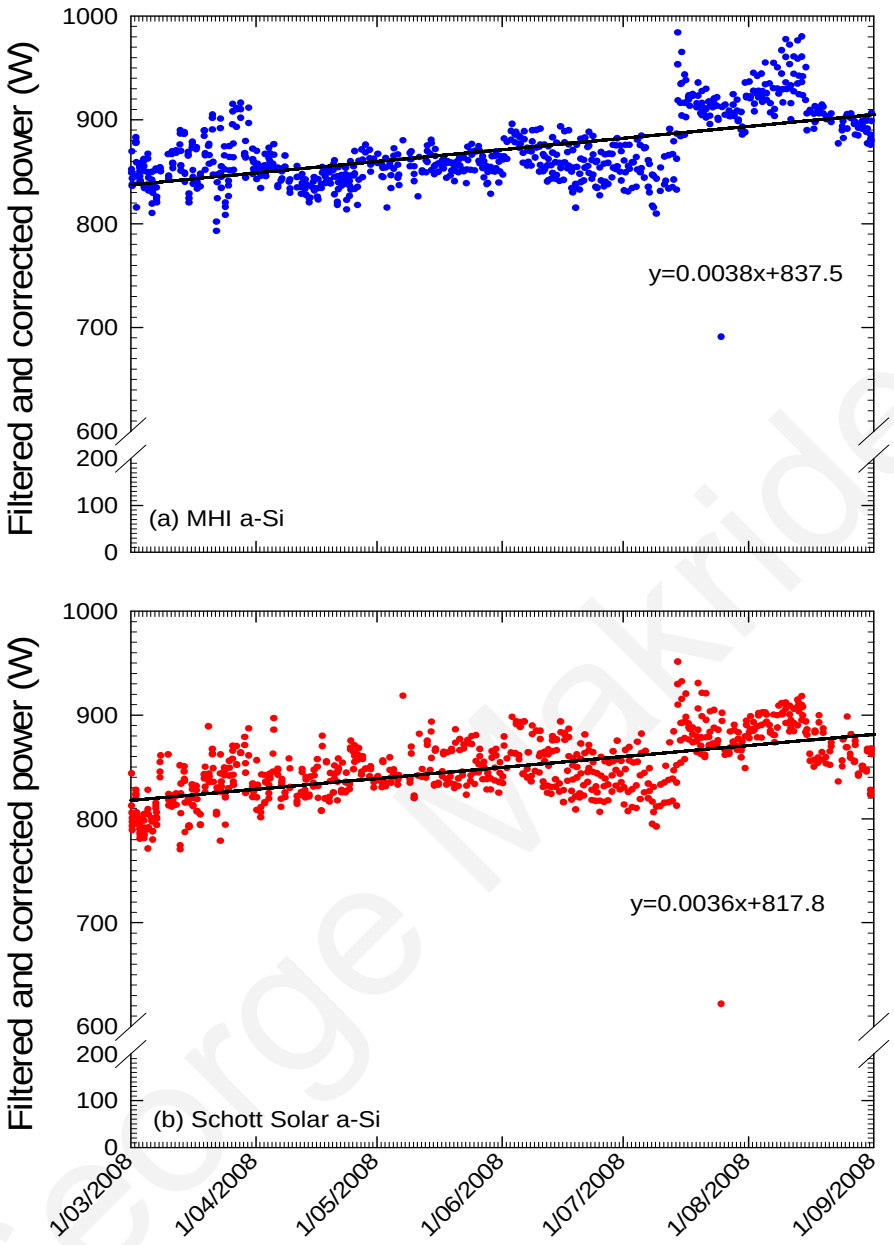

Figure 6.15. Filtered and corrected DC MPP power over the period March 2008 - September 2008.

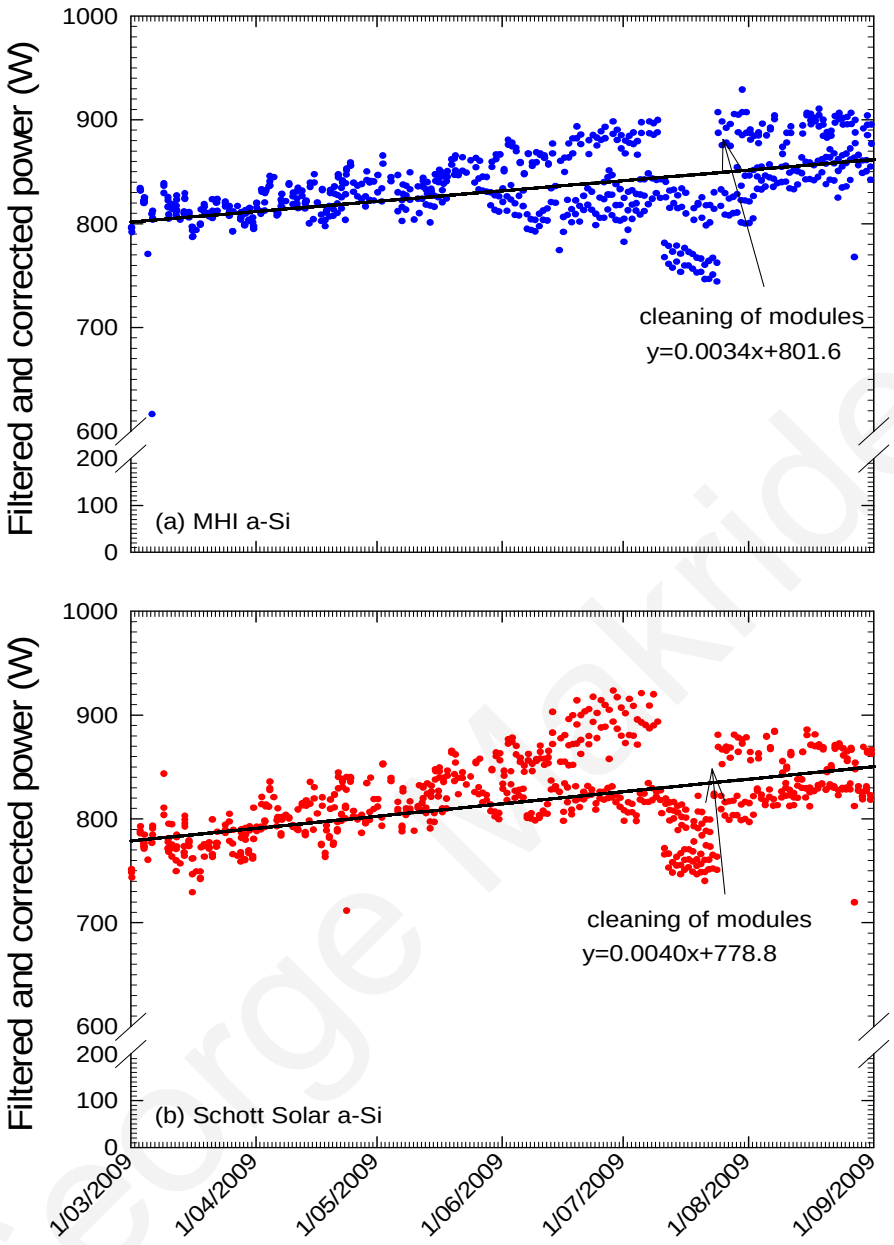

Figure 6.16. Filtered and corrected DC MPP power over the period March 2009 - September 2009.

This chapter analysed the effects of temperature on the performance of PV systems installed in Cyprus. For most technologies, both the outdoor and data-evaluated temperature coefficients showed good agreement with the manufacturers' MPP power temperature coefficients. The thermal losses were calculated for each system over the four-year evaluation period, using, firstly, the manufacturers' MPP power temperature coefficients and, secondly, the temperature coefficients evaluated using an outdoor technique. The highest thermal losses on the annual DC energy yield were recorded for the mono and multi-c-Si technologies, while thin-film technologies exhibited lower thermal losses, due to their lower temperature coefficients.

Finally, it was shown that thermal annealing is a significant factor in the seasonal behaviour of a-Si technologies, which exhibited an increase in power from early spring until early autumn. After constructing DC MPP power data-sets, by filtering and correcting to irradiance and temperature, it was found that the increase in power attributed to thermal annealing resulted in a power increase of up to 8.4 % in some cases.

The next chapter investigates another important loss factor, the degradation or performance loss rate, to demonstrate how this factor affects performance (especially for the new thin-film technologies).

Chapter 7

Performance loss rates

7.1 Introduction

As the penetration of PV increases and new technologies appear on the market, important questions regarding the lifetime power output and degradation of the different technologies arise. These factors are crucial for investment decisions, in an attempt to minimise the associated risk. Unfortunately, the estimation of degradation is a very difficult task, as it is required to wait until the end of life of the modules to establish credible results. PV degradation is usually the result of packaging materials degradation, loss of adhesion, degradation of cell/module interconnects, degradation caused by moisture intrusion and degradation of the semiconductor device [79].

Most manufacturers usually provide performance warranties of 20 years, with maximum loss of no more than 20 % of the rated power. As previous studies have demonstrated that both the technology and location have varied influence on the determined degradation rates [97], the performance warranties provided by manufacturers may not always be valid, especially for new PV technologies. For this reason, it is necessary to continue carrying out outdoor studies, to obtain degradation information for the typical operating environment of each PV technology.

What constitutes common practice is the extrapolation of the degradation rates from outdoor data. One method usually employed on different PV technologies installed outdoors is time series analysis on constructed monthly data-sets, of either the PR or the

maximum power normalised to PVUSA Test Conditions. For this purpose, techniques such as linear regression and CSD are commonly applied to the constructed time series to obtain the trend and, hence, the degradation rate [41], [76], [94], [96].

Trying to estimate degradation is even more difficult and complex in the case of grid-connected systems, as other factors apart from degradation might result in reduced power output over the years; such as seasonal performance variations, soiling, shading, mismatch and faults of modules. For this particular reason, it is more appropriate to define the obtained results as the performance loss rates. Other factors also affect the results, including the statistical analysis and the assumption made about the performance loss rate behaviour (usually assumed linear). The duration of the data used is also an important factor. In fact, it is depicted that the longer the monitoring period, the more credible the estimations will be, and that the results will converge to their long-term values.

With the above issues in mind, long-term monitoring of different PV technologies was undertaken, in an attempt to study the performance loss rates over the years and eventually to try to estimate, within reasonable accuracy, the performance loss rates of these technologies. It is also worth noting that having a number of systems side-by-side adds value to the results as although the absolute values of the performance loss rates might not be as accurate, the comparison between the different technologies under the same conditions yields valuable results.

More specifically, the annual performance loss rates of different PV grid-connected systems were evaluated, using the statistical techniques of linear regression and CSD, applied on the constructed monthly average DC PR time series over a five-year period. By examining the constructed series, it was first observed that the installed technologies exhibited seasonal behaviour, while a gradual performance loss tendency was evident as well.

For most technologies, with the exception of the a-Si systems, the annual performance loss rates, obtained by applying linear regression to the five-year time series, were found to be lower, compared to the CSD evaluated results. In particular, the application of linear regression resulted in average annual performance loss rates of -0.64 and -0.62 %/year for the mono-c-Si and multi-c-Si systems, respectively, over this period. The

average annual performance loss rate of the thin-film systems was -1.78 %/year. The results obtained by applying CSD were slightly higher, with the mono-c-Si and multi-c-Si systems exhibiting average annual performance losses of -1.04 and -1.10 %/year, respectively, while the corresponding value was -1.81 %/year for the thin-film systems. The results clearly show that deviations in the performance loss rates arise because of the selection of the applied technique.

Furthermore, the strength of the CSD technique in providing an adequate decomposition of the time series with no remaining pattern was verified, by investigating whether the remaining irregularities were white noise. This was determined from the plots of the autocorrelation function (ACF), partial autocorrelation function (PACF) and the 95 % confidence interval limits.

Finally, the annual performance loss rates were re-evaluated at shorter measurement time periods, using the same statistical techniques, in order to determine whether the performance loss rates can be evaluated in shorter time periods. The three- and four-year period annual performance loss rates were compared to the longer-term performance loss rates of the five-year investigation with the obtained results demonstrating that although the choice of analysis technique affects the results, the performance loss trends exhibited the same pattern for most technologies. The performance loss rates of the c-Si technologies showed convergence to a steady state value after five years, whereas more time is required to reach steady state for thin-film technologies.

7.2 Methodology

The first step in this performance loss rate analysis was to construct a time series based on a reference condition parameter, such as the DC PR, PR_{DC}, which was evaluated from the fifteen-minute average outdoor measured data, acquired from the installed infrastructure. A five-year time series of the monthly average DC PR, comprised of 60 variables, was therefore prepared. The plots in Figure 7.1 depict the constructed monthly average DC PR time series of all the PV technologies. It is evident from the plots that all technologies exhibit seasonal behaviour, with peaks according to the seasons, while a gradual performance loss tendency is more evident in some technologies than others.

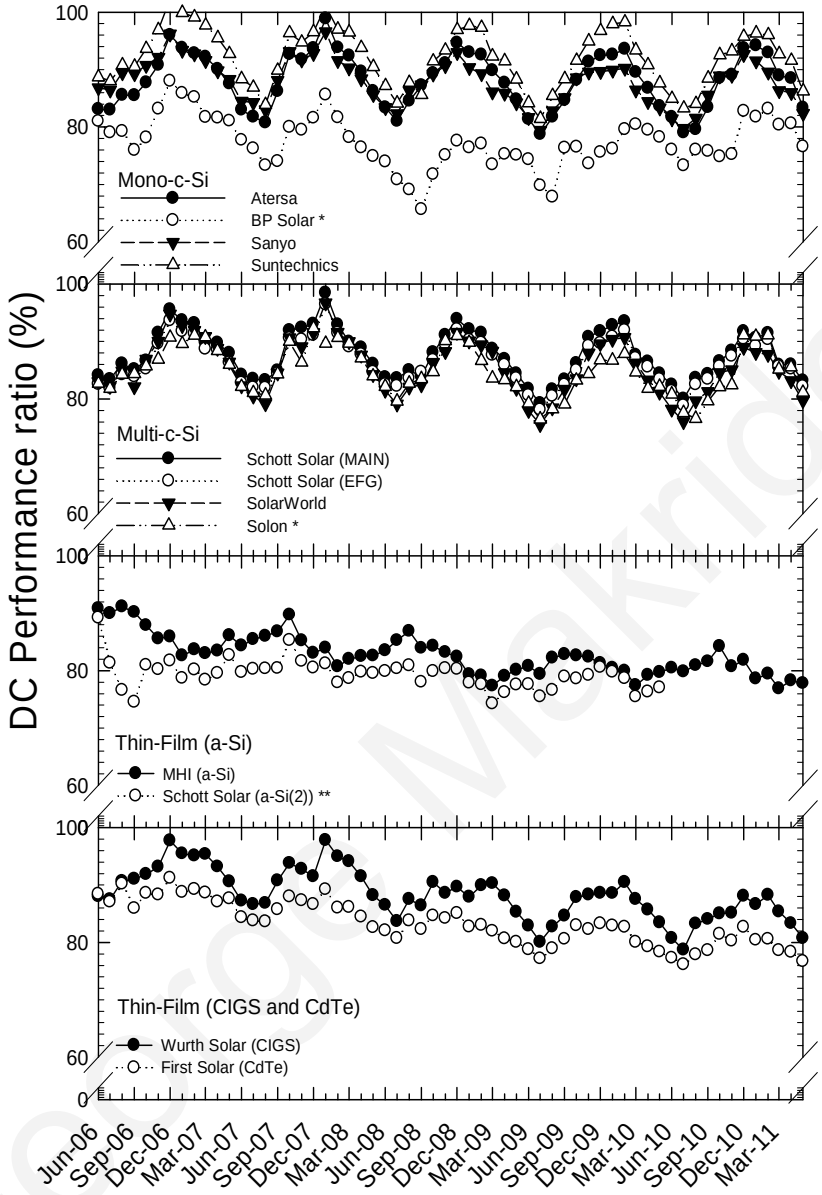

Figure 7.1. Monthly average DC PR of installed PV systems over the period June 2006 - June 2011 in Nicosia, Cyprus.

* Partial shading had been affecting the performance of the BP Solar mono-c-Si and Solon multi-c-Si systems, specifically during the second, third and fourth year.

** The Schott Solar a-Si system, which had a broken module since October 2006, was monitored only for four years.

All constructed time series were then analysed, employing statistical techniques that extract and characterise the trend from each time series, providing in this way a value for the performance loss rate of each PV system.

More specifically, the performance loss rates were initially obtained by applying linear regression to each series, while the gradient of the fit was used to calculate the annual performance loss rate.

The performance loss rates were also evaluated by employing CSD, which was used to decompose the time series by extracting the trend and seasonality for each technology. In this work, CSD was selected because it is one of the most commonly used decomposition procedures to extract the trend, seasonality and remaining irregularity from the input signal, with minimal effort and computational simplicity, while it also forms the basis for most of the modern decomposition methods [119], [124], [125]. The trend was obtained from each time series by using a 12-month centred moving average (MA). For the PV performance data, it was more appropriate to use a centred 12 month moving average, so as to include all the seasonal variations that occur over a period of a year. With an even number of data (12 months), the trend was extracted through a two-step centred moving average, by first taking the average of twelve monthly values, ranging from 6 months before, to 6 months after, for each data-point (centred MA). After the trend was extracted for each technology, linear regression was again applied, to calculate the performance loss rate.

The final step in the application of the CSD technique was to verify that the irregularities were indeed white noise, and to ascertain that the technique provided an adequate decomposition of the time series with no remaining pattern. A key statistical tool to investigate the properties of a time series is the autocorrelation function (ACF), defined as the correlation of the time series with itself at different time periods apart [125]. The autocorrelation coefficient at lag, l, is denoted as r_l and is given by [124]:

$$r_l = \frac{\sum_{t=l+1}^{N}(X_t - \bar{X})(X_{t-l} - \bar{X})}{\sum_{t=1}^{N}(X_t - \bar{X})^2} \tag{7.1}$$

where X_t is the observation at time t, l is the lag and $\bar{X}$ is the mean of X. The ACF plot of the irregularities is used as a verification tool of the CSD technique, providing statistical evidence that the decomposition of the seasonality and trend were successful and not influenced from random variations. A common approach to determine whether the irregularities are white noise is to plot the autocorrelation coefficients and the critical

values, which are boundary lines that represent limits. If the ACF coefficients fall within the critical bounds, then it can be deduced that the irregularities are white noise. For example, $\pm 1.96/\sqrt{n}$, where n is the number of observations in the series, provides the confidence interval limits within which 95 % of the sample autocorrelation coefficients must lie [124]. If this is not the case, it is assumed that the investigated series (irregularity in this case) is not white noise.

In the same manner, the partial autocorrelation function (PACF) is also used to verify that the irregularities are white noise. In general, PACF analysis is applied in autoregressive model identification. The PACF represents the degree of association between x_t and x_{t-l}, with the effects of other intervening time lags 1,2,3,…,l-1 not considered [124]. As in the case of the ACF, 95 % of the partial autocorrelations are also expected to lie within the critical value boundaries of $\pm 1.96/\sqrt{n}$ for a white noise series.

As an example, Figure 7.2a and Figure 7.2b show the ACF and PACF of the CSD extracted irregularities for the Atersa mono-c-Si, over the period June 2006 - June 2010 respectively. From both figures, as most of the autocorrelation and partial autocorrelation coefficients (19 out of the 20 lags) of the irregularities lie within the confidence intervals of ±0.3266 ($\pm 1.96/\sqrt{n}$ for n=36 observations), there is statistical evidence that the irregularities are white noise. From both plots of Figure 7.2, a strong dependence at lag 12, which lies outside the confidence bound, was observed. The ACF at lag 12, which is higher than the confidence bounds, is shown in Figure 7.2a, revealing similarity and periodicity on a 12 period basis.

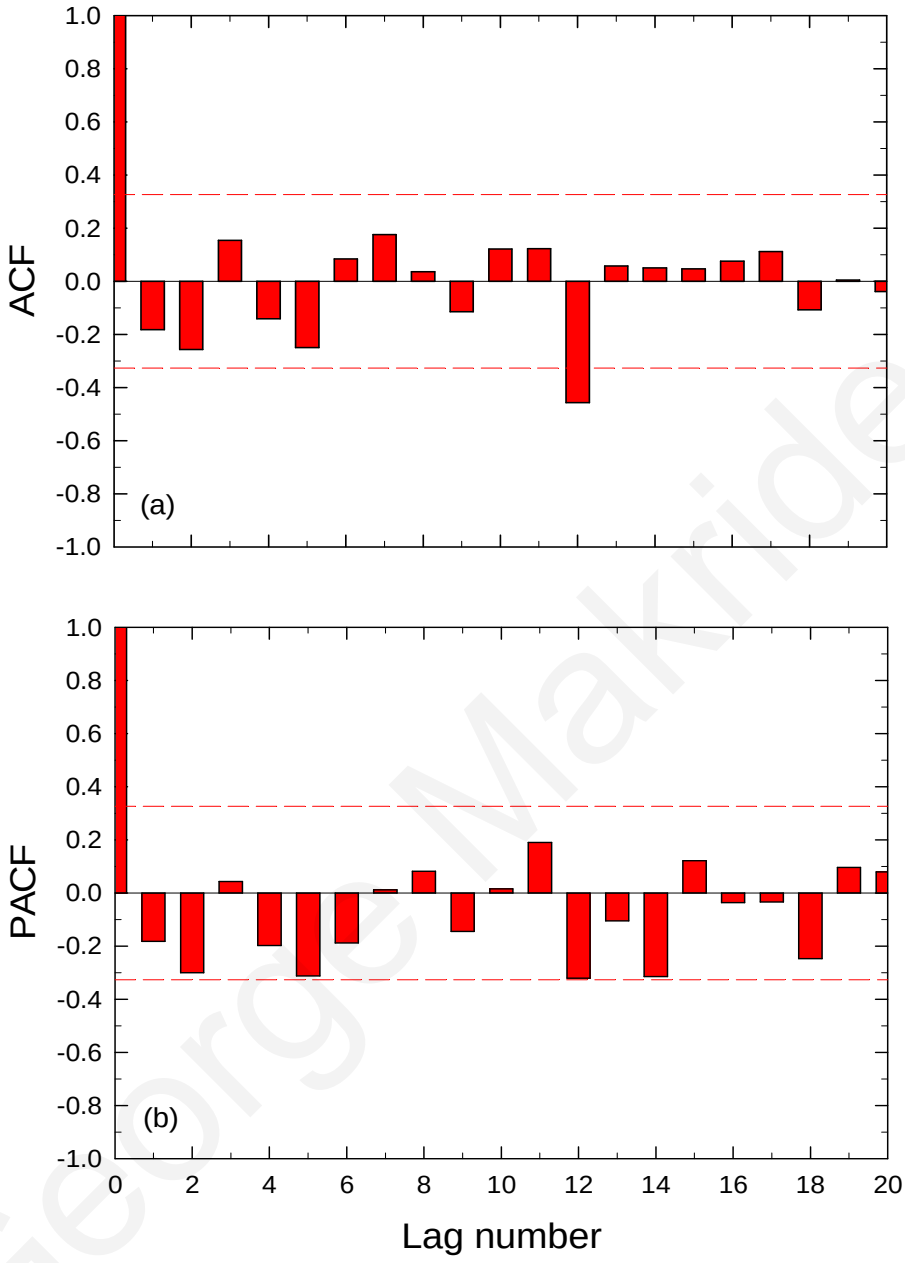

Figure 7.2. (a) ACF and (b) PACF of the CSD extracted irregularities of the monthly average DC PR time series of the Atersa mono-c-Si system over the period June 2006 - June 2010.

7.3 Results

The annual performance loss rates, evaluated using linear regression and CSD, over the five-year period for each technology are presented in this section. Additionally, the performance loss rate trends exhibited for the different time periods (three, four and five years) are also compared and analysed for each technology.

7.3.1 Annual performance loss rate using linear regression over the five-year period

Figure 7.3 shows the average monthly DC PR and the applied linear fit for each PV technology over the five-year period, June 2006 - June 2011.

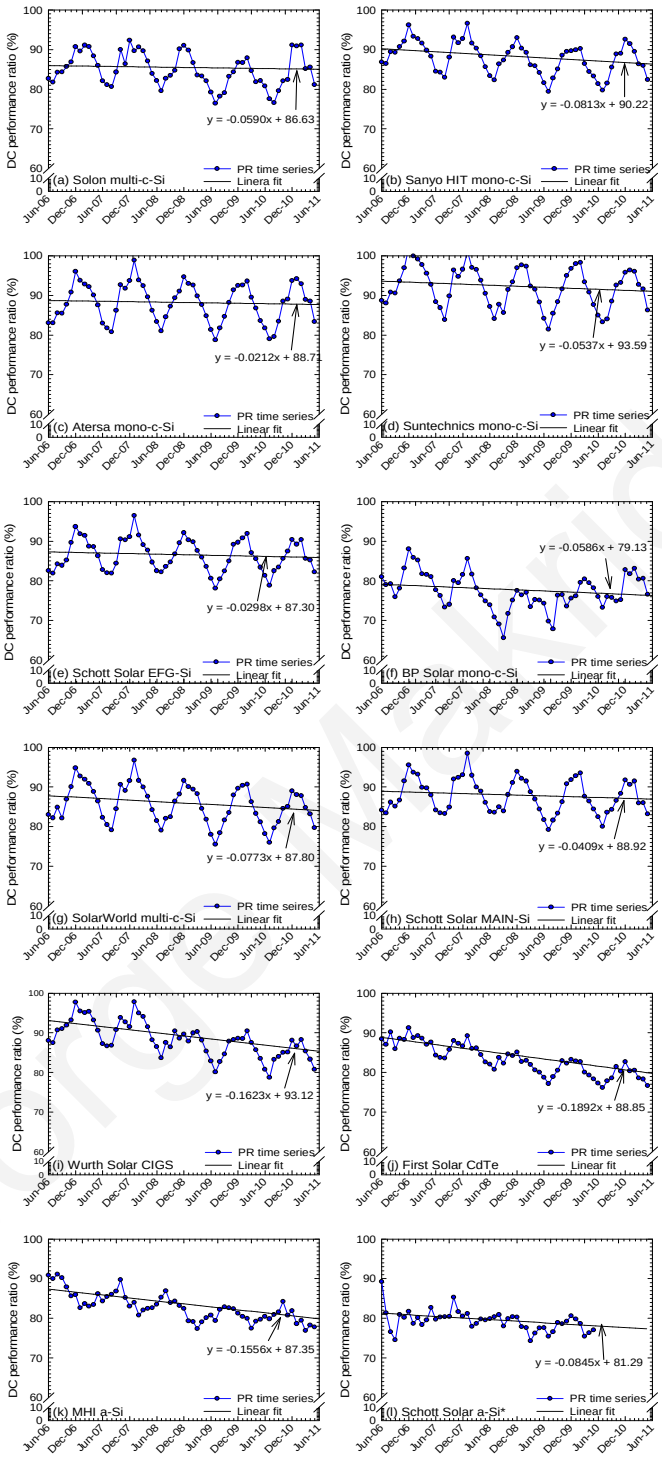

Figure 7.3. Monthly average DC PR and performance loss rates using linear regression over the period June 2006 - June 2011. (a) Solon multi-c-Si. (b) Sanyo HIT mono-c-Si. (c) Atersa mono-c-Si. (d) Suntechnics mono-c-Si. (e) Schott Solar EFG-Si. (f) BP Solar mono-c-Si. (g) SolarWorld multi-c-Si. (h) Schott Solar MAIN-Si. (i) Würth Solar CIGS. (j) First Solar CdTe. (k) MHI a-Si. (l) Schott Solar a-Si.
* The Schott Solar a-Si system was monitored only for four years.

The annual DC performance loss rates of the PV technologies, obtained by applying linear regression over this period, are summarised in Table 7.1. The annual performance loss rates were in the range of -0.25 to -0.98 %/year for the mono-c-Si systems, while all multi-c-Si systems exhibited annual performance loss rates lower than -1 %/year. In contrast, most thin-film technologies showed higher annual performance loss rates compared to the c-Si systems, in the range of -1.87 to -2.27 %/year, over the same period. The Schott Solar a-Si system, monitored for four years, demonstrated an annual performance loss rate of -1.01 %/year.

Table 7.1. Annual DC performance loss rates of PV technologies, evaluated by applying linear regression on the monthly average DC PR time series over the five-year period (with the exception of the Schott Solar a-Si system, which was monitored over a four-year period).

System	Annual DC performance loss rate (%/year)
Atersa mono-c-SI	-0.25
BP Solar mono-c-Si	-0.70
Sanyo HIT-Si	-0.98
Suntechnics mono-c-Si	-0.64
Mono-c-Si average	-0.64
Schott Solar MAIN-Si	-0.49
Schott Solar EFG-Si	-0.36
SolarWorld multi-c-Si	-0.93
Solon multi-c-Si	-0.71
Multi-c-Si average	-0.62
Würth Solar CIGS	-1.95
First Solar CdTe	-2.27
MHI a-Si	-1.87
Schott Solar a-Si	-1.01 (four-year period)
Thin-film average	-1.78

7.3.2 Annual performance loss rate using CSD over the five-year period

The plots in Figure 7.4 show the annual DC performance loss rates, evaluated using the CSD extracted trend and then by applying linear regression. The R^2 value was also obtained, to demonstrate the extent the trend was described by the fit.

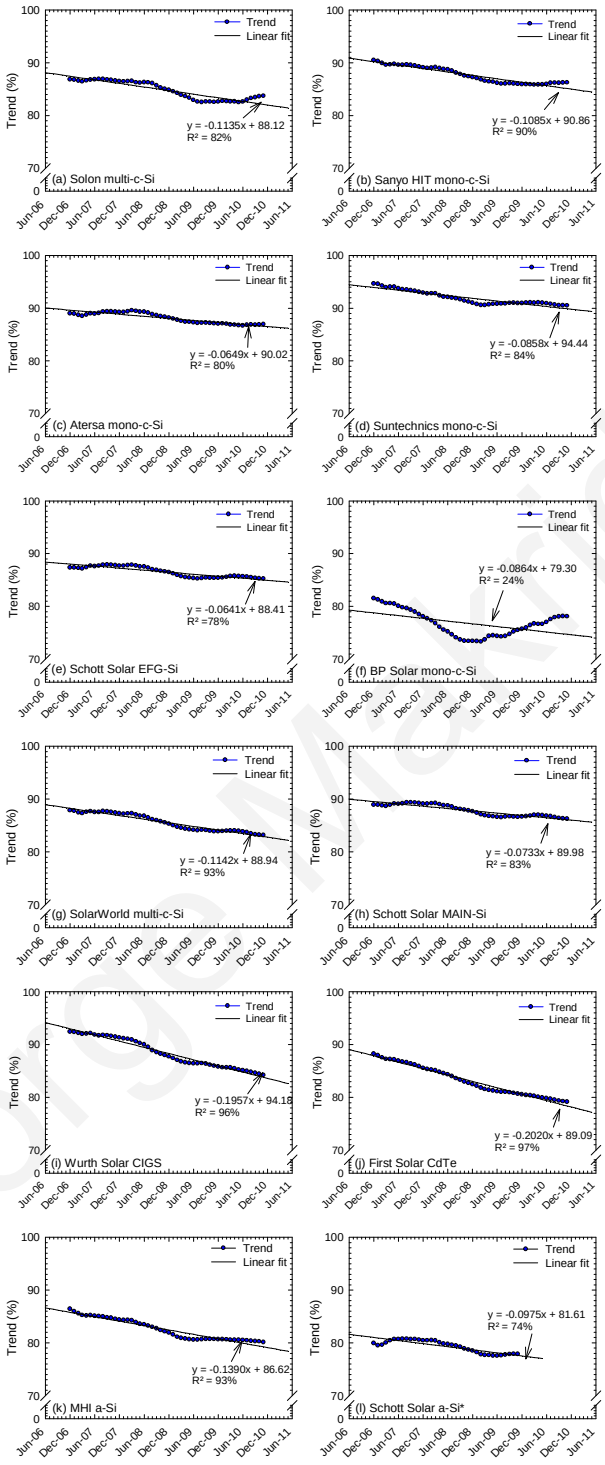

Figure 7.4. Performance loss rate applying linear regression on CSD extracted trend over the period June 2006 - June 2011. (a) Solon multi-c-Si. (b) Sanyo HIT mono-c-Si. (c) Atersa mono-c-Si. (d) Suntechnics mono-c-Si. (e) Schott Solar EFG-Si. (f) BP Solar mono-c-Si. (g) SolarWorld multi-c-Si. (h) Schott Solar MAIN-Si. (i) Würth Solar CIGS. (j) First Solar CdTe. (k) MHI a-Si. (l) Schott Solar a-Si.
* The Schott Solar a-Si system was monitored only for four years.

The general upward or downward deviation of the extracted trend, compared to the fitted lines of each technology, arises due to seasonal irregularities, either performance increases that affect the moving average of the period December 2007 - June 2008 compared to other periods, shown in Figure 7.4a-h for all c-Si technologies (possibly due to lower ambient temperature and lower seasonal loss factors). Other effects, such as shading, are responsible for the decrease in performance in the case of the BP Solar mono-c-Si during the period December 2007 - June 2009 which affects the trend of the period June 2008 - December 2008 and shown in Figure 7.4f. In addition, it is also possible that the performance loss rates are not linear for some technologies, which may also affect the linearity of the extracted trend. Such deviations affect the linearity of the trend and, therefore, the accuracy of the linear fit, represented by a decrease in the R^2 value.

Table 7.2 lists the annual DC performance loss rates for all the installed technologies, ranging between -0.77 and -1.37 %/year for the c-Si systems over this period. On the other hand, the thin-film technologies of CIGS and CdTe showed annual performance loss rates of, -2.35 and -2.42 %/year with this technique, respectively.

Table 7.2. Annual DC performance loss rates of PV technologies, evaluated by applying CSD on the monthly average DC PR time series over the five-year period (with the exception of the Schott Solar a-Si system, which was monitored over a four-year period).

Technology	**Annual DC performance loss rate (%/year)**
Atersa mono-c-SI	-0.78
BP Solar mono-c-Si	-1.04
Sanyo HIT-Si	-1.30
Suntechnics mono-c-Si	-1.03
Mono-c-Si average	-1.04
Schott Solar MAIN-Si	-0.88
Schott Solar EFG-Si	-0.77
SolarWorld multi-c-Si	-1.37
Solon multi-c-Si	-1.36
Multi-c-Si average	-1.10
Würth Solar CIGS	-2.35
First Solar CdTe	-2.42
MHI a-Si	-1.67
Schott Solar a-Si	-0.78 (four-year period)
Thin-film average	-1.81

7.3.3 Comparison of the performance loss rate with different analysis techniques

The annual DC performance loss rates, evaluated using linear regression and CSD, over the five-year period, are shown in Figure 7.5. For most technologies, apart from the a-Si systems, the annual performance loss rates obtained by applying linear regression to the time series, were lower compared to the CSD evaluated results. This clearly shows that there is an effect on the performance loss rate results on account of the selected technique analysis. The difference between the linear regression and CSD obtained results were in the range -0.20 – 0.65 %/year, while the average difference for all technologies was 0.38 %/year. The thin-film technologies of First Solar CdTe and MHI a-Si demonstrated differences lower than 0.20 %/year. The selection of the analysis technique is, therefore, significant when undertaking such studies under field conditions, as deviations in the results occur because of the technique. The fact that with CSD the annual performance loss rates were evaluated from de-seasonalised time series seems to be the reason why the annual performance loss rates are higher compared to linear regression. The presence of seasonality, in the linear regression analysis, seems to yield lower performance loss rates. This may also explain why there is better agreement between the linear regression and CSD obtained results for the thin-film systems, which exhibit lower seasonal variations compared to c-Si systems.

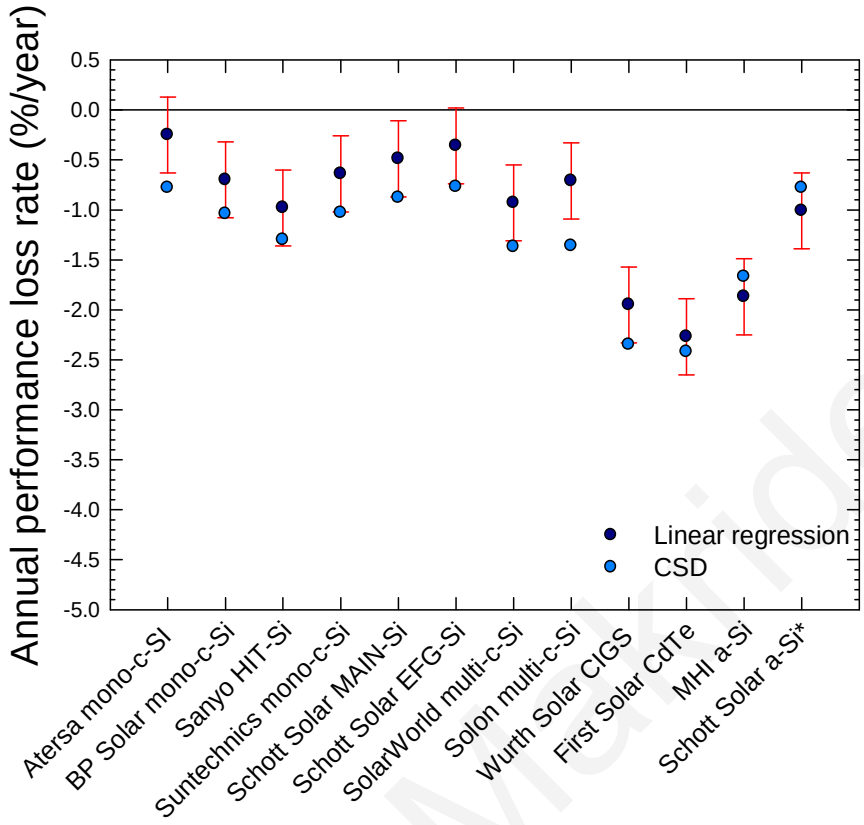

Figure 7.5. Annual performance loss rate comparison for all installed PV technologies, evaluated using linear regression and CSD applied on five-year monthly average DC PR time series. The average difference between the linear regression and CSD obtained results for all technologies, 0.38 %/year, is also shown as a guideline superimposed on the linear regression result of each technology.
* The Schott Solar a-Si system was monitored only for four years.

Figure 7.6 shows the resulting annual performance loss rates over a three-, four- and five-year period, for each technology, and for each statistical method. Both techniques showed different annual performance loss rates for the three evaluation periods, although the results seemed to converge over the five-year period for most technologies.

During the three- and four-year evaluation periods, the average differences for all technologies were 0.61 %/year and 0.67 %/year, respectively. The fact that the performance loss rates obtained with both techniques converge as the duration of the observation period increases, suggesting that duration is important in yielding more reliable performance loss rate results.

In the case of the c-Si technologies (with the exception of the Suntechnics and BP Solar mono-c-Si technologies), the performance loss rates evaluated from both

techniques exhibited the same pattern, with a clear gradual convergence to a steady state value after the five-year period, as shown in Figure 7.6a-c, e and g-h. The Suntechnics mono-c-Si system did not exhibit the same performance loss pattern as the other c-Si technologies, depicted in Figure 7.6d, because in December 2008 the drain resistance was replaced, resulting in the improved performance of this technology. Similarly, as shown in Figure 7.6f, the BP Solar mono-c-Si system did not exhibit the same pattern as the rest of the c-Si technologies over the five-year evaluation, because it was affected by shading during the second, third and fourth year.

For both the First Solar CdTe and MHI a-Si thin-film technologies systems, a high performance loss rate was initially observed, over the three-year evaluation period, which gradually reduced to a smaller performance loss rate, over the five-year period. However, no steady state has been reached, even after a period of five years. For the a-Si system, the high performance loss rate initially observed over the three-year evaluation period is attributed to the high initial degradation period, due to the Staebler-Wronski effect [80].

The results clearly demonstrate that the choice of the analysis technique affects the results but not the performance loss trend exhibited over the evaluation period for most technologies.

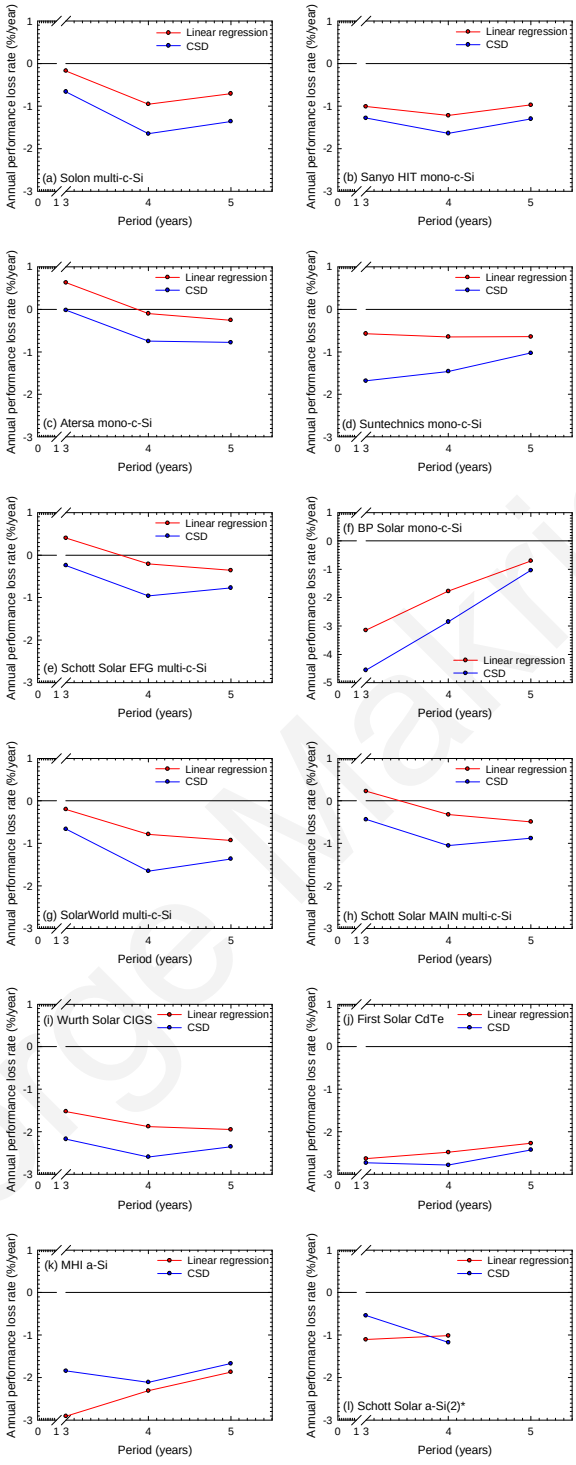

Figure 7.6. Annual performance loss rate comparison, using linear regression and CSD, applied on five-, four- and three-year DC PR time series. (a) Solon multi-c-Si. (b) Sanyo HIT mono-c-Si. (c) Atersa mono-c-Si. (d) Suntechnics mono-c-Si. (e) Schott Solar EFG-Si. (f) BP Solar mono-c-Si. (g) SolarWorld multi-c-Si. (h) Schott Solar MAIN-Si. (i) Würth Solar CIGS. (j) First Solar CdTe. (k) MHI a-Si. (l) Schott Solar a-Si.
* The Schott Solar a-Si system was monitored only for four years.

Figure 7.7 is a summary of the performance loss rate trends exhibited by a mono-c-Si, multi-c-Si, CIGS, CdTe and a-Si system. The pattern exhibited over the five-year period by the c-Si and CIGS technologies demonstrates that the performance loss rates converge gradually to a steady state value. For these technologies, the performance loss rates are approaching their steady state value after about five years.

On the other hand, no steady state has been reached for the CdTe and a-Si, even after a period of five years. For these thin-film technologies, it is clear that more time is required before the performance loss rate reaches its steady state value.

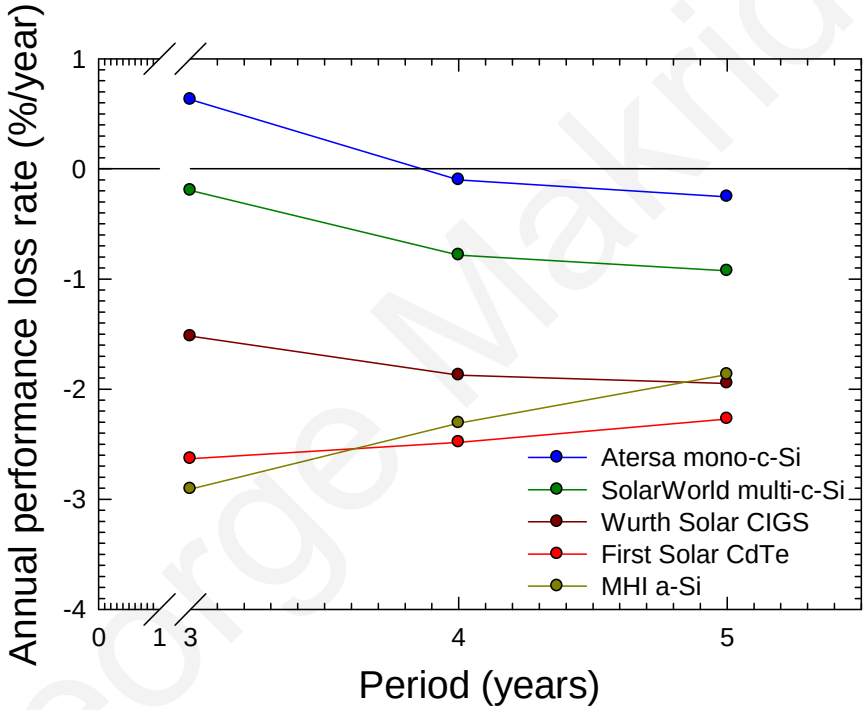

Figure 7.7. Annual performance loss rate for mono-c-Si, multi-c-Si, CIGS, CdTe and a-Si technologies, using linear regression on five, four and three-year monthly average DC PR time series.

7.3.4 Annual performance loss rate CSD verification

For the three-year time series CSD evaluation, the extracted trend and linear fit of each PV technology are shown in Figure 7.8. The annual DC performance loss rates of each technology were evaluated from the gradient of the linear fit, while the R^2 value was obtained as an accuracy indicator of how well the trend was described by the fit. Agreement between the extracted trend and linear fit with R^2 values over 90 % was exhibited by the Sanyo HIT and Suntechnics mono-c-Si technologies, presented in Figure 7.8a, and by the BP Solar mono-c-Si presented in Figure 7.8b. In addition, all the multi-c-Si technologies demonstrated lower R^2 values compared to the previously mentioned mono-c-Si technologies, in the range of 14 % - 77 %.

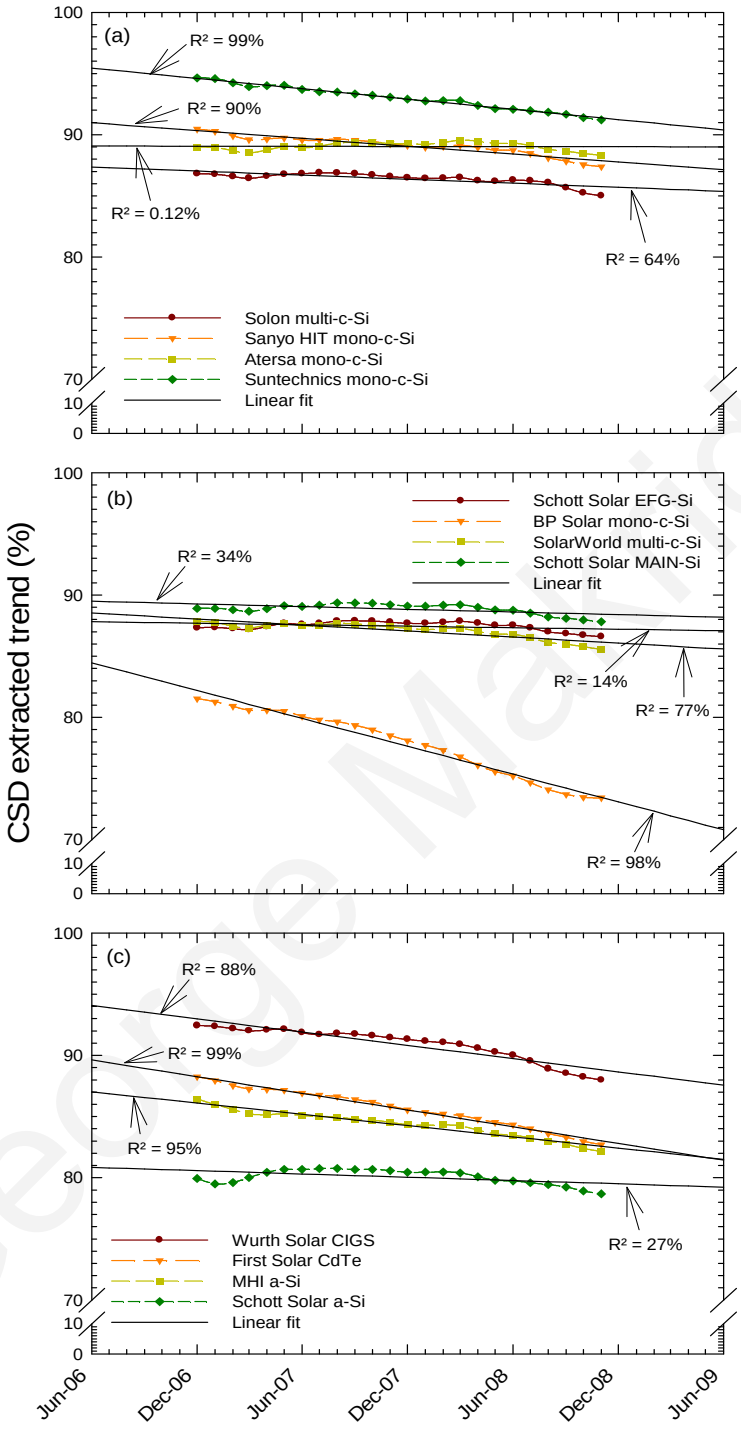

Figure 7.8. CSD extracted trend and linear least square fit over the period June 2006 - June 2009 (three-year time series) for the installed PV technologies. (a) Solon multi-c-Si, Sanyo HIT mono-c-Si, Atersa mono-c-Si and Suntechnics mono-c-Si. (b) Schott Solar EFG-Si, BP Solar mono-c-Si, SolarWorld multi-c-Si and Schott Solar MAIN-Si. (c) Würth Solar CIGS, First Solar CdTe, MHI a-Si and Schott Solar a-Si. The R^2 values of the linear fit are also shown.

The ability of the CSD technique to extract the seasonality and trend over a three-year period was evaluated, based on the ACF and PACF analysis of the irregularities. The ACF plots of the c-Si technologies shown in Figure 7.9a-h, provide evidence that the remaining irregularities of the three-year time series are not white noise, because 2 or more out of the 20 autocorrelation coefficients displayed in the ACF plots exceed the ±0.4 confidence bounds (without, of course considering the coefficient at lag 0, which is always unity). The ±0.4 confidence bounds are the levels denoting the 95 % confidence intervals of the 24 irregularity samples. On the other hand, it was obvious that all the autocorrelation coefficients of the thin-film technologies (apart from the coefficient of lag 0) lay within the confidence intervals of ±0.4, depicted in Figure 7.9i-l.

The PACF analysis of the CSD irregularities of each PV technology over the three-year period is depicted in Figure 7.10. In this analysis, the partial autocorrelation coefficients of only the Sanyo mono-c-Si and Schott Solar EFG multi-c-Si systems showed that the irregularities were not white noise, given that less than 95 % of the sample partial autocorrelation coefficients were within the confidence bounds as shown in Figure 7.10b and Figure 7.10e, respectively.

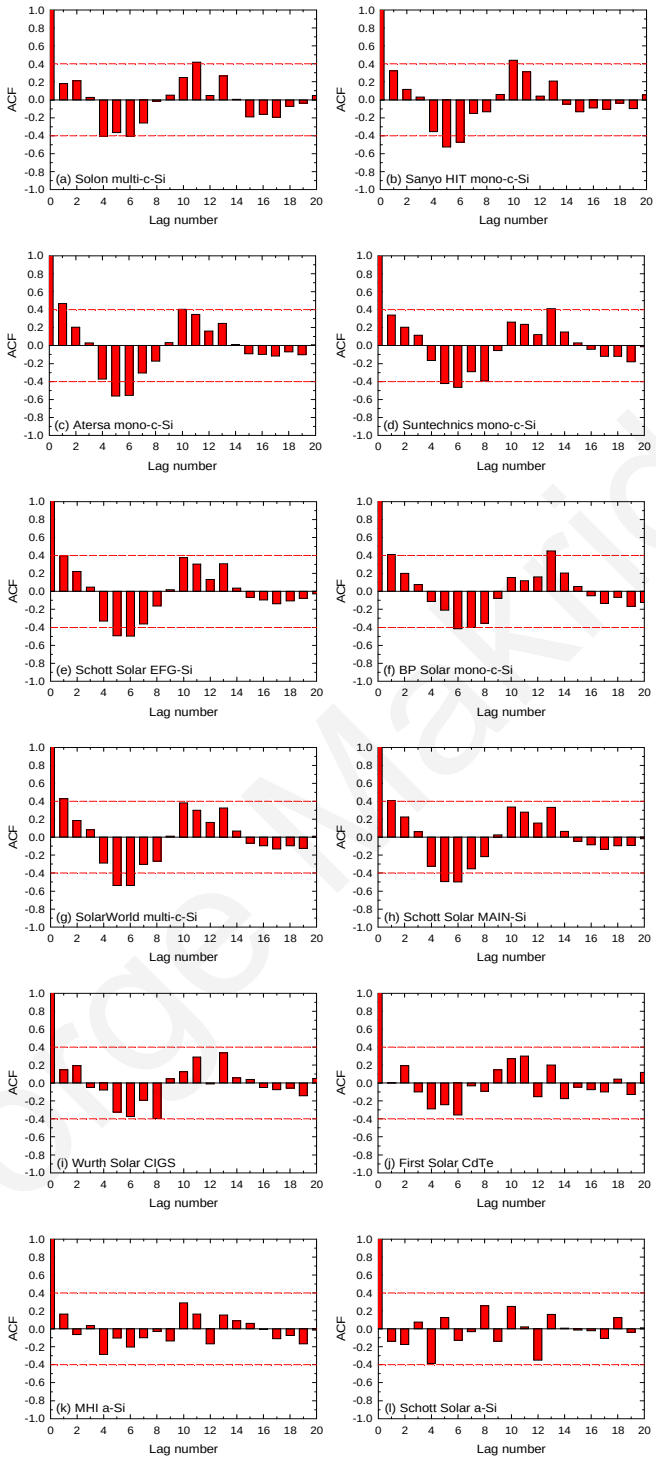

Figure 7.9. ACF of the irregularities of the PV technologies on three-year time series. (a) Solon multi-c-Si. (b) Sanyo HIT mono-c-Si. (c) Atersa mono-c-Si. (d) Suntechnics mono-c-Si. (e) Schott Solar EFG-Si. (f) BP Solar mono-c-Si. (g) SolarWorld multi-c-Si. (h) Schott Solar MAIN-Si. (i) Würth Solar CIGS. (j) First Solar CdTe. (k) MHI a-Si. (l) Schott Solar a-Si.

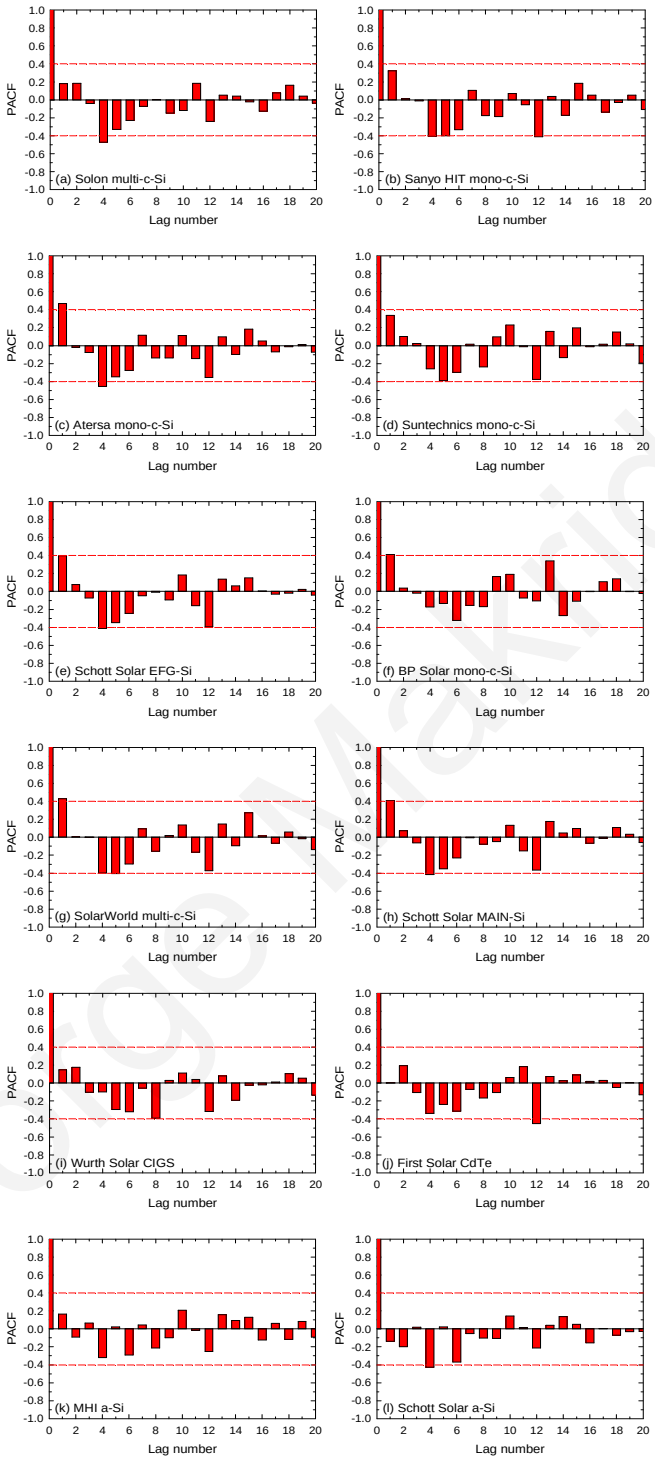

Figure 7.10. PACF of the irregularities of the PV technologies on three-year time series. (a) Solon multi-c-Si. (b) Sanyo HIT mono-c-Si. (c) Atersa mono-c-Si. (d) Suntechnics mono-c-Si. (e) Schott Solar EFG-Si. (f) BP Solar mono-c-Si. (g) SolarWorld multi-c-Si. (h) Schott Solar MAIN-Si. (i) Würth Solar CIGS. (j) First Solar CdTe. (k) MHI a-Si. (l) Schott Solar a-Si.

After CSD was performed on the three-year monthly average DC PR time series of the PV technologies, the same evaluation was applied on the four-year time series of each technology. The plots in Figure 7.11 show the extracted trend and linear fit of each technology over the four-year period. The Sanyo HIT and Suntechnics mono-c-Si technologies exhibited the best agreement between the extracted trend and linear fit, with R^2 values of 96 % and 94 %, respectively and shown in Figure 7.11a. The same applied for the SolarWorld multi-c-Si technology as the R^2 value was 91 % and demonstrated in Figure 7.11b. Finally, agreement was also obtained from the plots of the Würth Solar CIGS and First Solar CdTe (shown in Figure 7.11c), the latter exhibiting the best fit, with an R^2 value of 99 %. The general upward or downward deviation of the extracted trend, compared to the fitted lines of each technology, arises due to seasonal irregularities, either performance increases that affect the moving average of the period December 2007 - June 2008 compared to other periods, shown in Figure 7.11a and Figure 7.11b for all c-Si technologies (possibly due to lower ambient temperature and lower seasonal loss factors); or decreases due to, for example, shading in the case of the BP Solar mono-c-Si during the period December 2007 - June 2009, which affects the trend of the period June 2008 - December 2008.

The regression of the Solon multi-c-Si, Suntechnics mono-c-Si and the Würth Solar CIGS technologies also appears to be bi-linear. This may occur due to changes in the degradation rates over time, because of the long-term weathering of the module package and the different failure mechanisms from corrosion, electrolytic electromigration, diffusion, cracking and delamination [126].

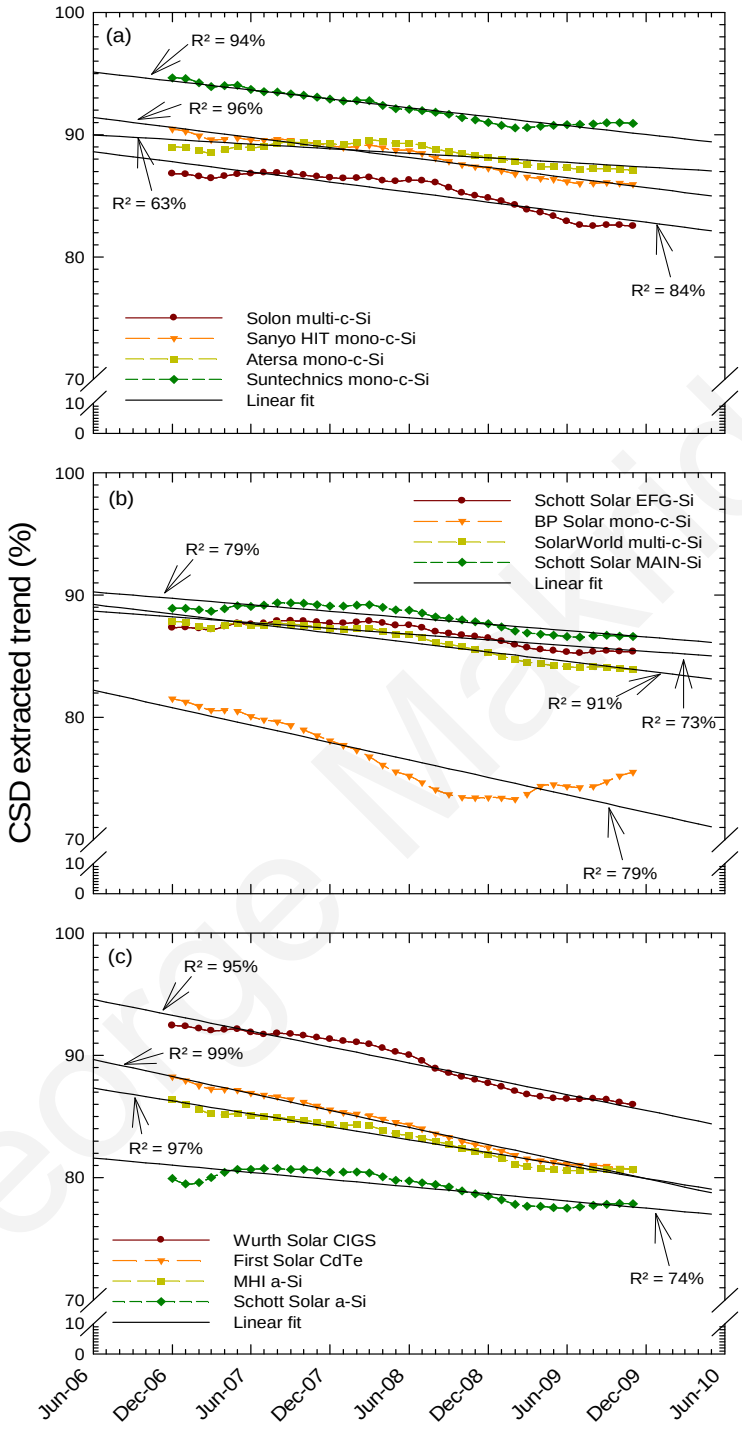

Figure 7.11. CSD extracted trend and linear least square fit over the period June 2006 - June 2010 (four-year time series) for the installed PV technologies. (a) Solon multi-c-Si, Sanyo HIT mono-c-Si, Atersa mono-c-Si and Suntechnics mono-c-Si. (b) Schott Solar EFG-Si, BP Solar mono-c-Si, SolarWorld multi-c-Si and Schott Solar MAIN-Si. (c) Würth Solar CIGS, First Solar CdTe, MHI a-Si and Schott Solar a-Si. The R^2 values of the linear fit are also shown.

From the ACF plots shown in Figure 7.12, it was obvious that, for most technologies, the autocorrelation coefficients of the four-year period irregularities fall within the confidence intervals of ±0.3266 (95 % confidence intervals). More specifically, most PV technologies showed a significant autocorrelation coefficient at lag 12, which was outside the confidence bound, with the exception of the Solon multi-c-Si shown in Figure 7.12a. For the SolarWorld multi-c-Si and Würth Solar CIGS shown in Figure 7.12g and Figure 7.12i respectively, at least two ACF coefficients lie outside the limit range of the confidence bounds signifying that the irregularities are not white noise. For all remaining technologies, 95 % of the autocorrelation coefficients of the irregularities fall within the specified range of the confidence bounds.

In addition, the PACF analysis of the four-year period irregularities of each PV technology is depicted in Figure 7.13. For almost all PV technologies, the PACF at lag 12 exceeds the confidence bounds as shown in Figure 7.13a, b and d-l indicating that a strong correlation yet exists at a 12 lag period. For the Sanyo HIT mono-c-Si, SolarWorld multi-c-Si, Schott Solar MAIN multi-c-Si and Schott Solar a-Si shown in Figure 7.13b, g, h and l, respectively, at least two PACF coefficients lie outside the limit range of the confidence bounds, signifying that the irregularities are not white noise.

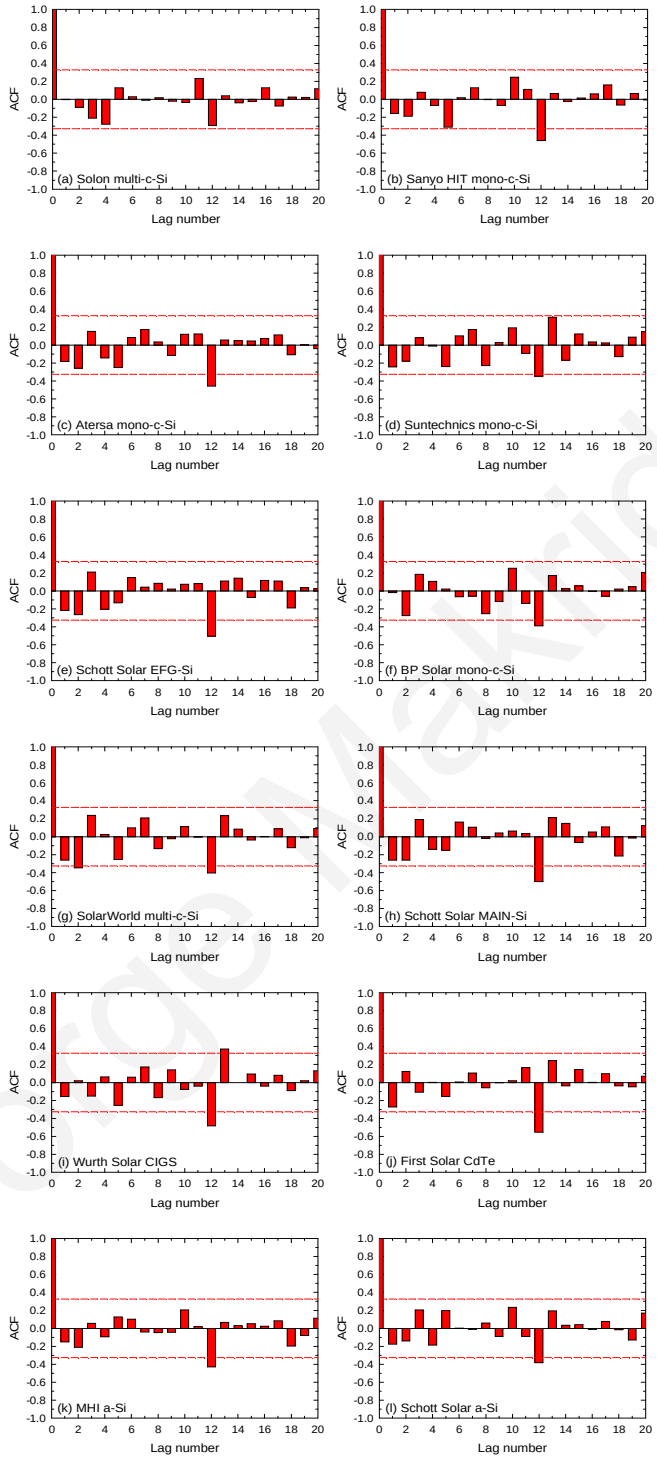

Figure 7.12. ACF of the irregularities of the PV technologies on four-year time series. (a) Solon multi-c-Si. (b) Sanyo HIT mono-c-Si. (c) Atersa mono-c-Si. (d) Suntechnics mono-c-Si. (e) Schott Solar EFG-Si. (f) BP Solar mono-c-Si. (g) SolarWorld multi-c-Si. (h) Schott Solar MAIN-Si. (i) Würth Solar CIGS. (j) First Solar CdTe. (k) MHI a-Si. (l) Schott Solar a-Si.

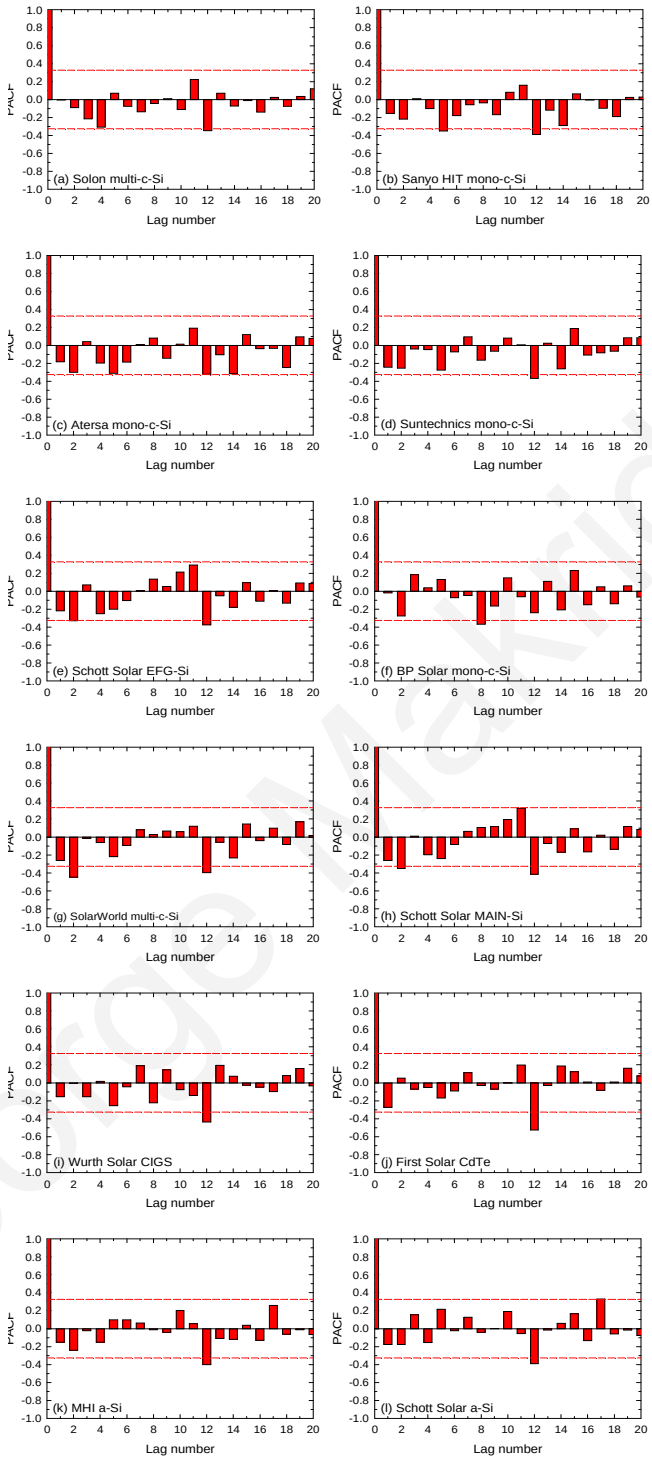

Figure 7.13. PACF of the irregularities of the PV technologies on four-year time series. (a) Solon multi-c-Si. (b) Sanyo HIT mono-c-Si. (c) Atersa mono-c-Si. (d) Suntechnics mono-c-Si. (e) Schott Solar EFG-Si. (f) BP Solar mono-c-Si. (g) SolarWorld multi-c-Si. (h) Schott Solar MAIN-Si. (i) Würth Solar CIGS. (j) First Solar CdTe. (k) MHI a-Si. (l) Schott Solar a-Si.

Figure 7.14 shows the ACF plots of the five-year period irregularities. For most technologies, the ACF coefficients fall within the confidence intervals of ±0.2829 (95 % confidence intervals); apart from the Sanyo HIT mono-c-Si, Atersa mono-c-Si, SolarWorld mulit-c-Si and Würth Solar CIGS, where at least two ACF coefficients lie outside the limit range of the confidence bounds, signifying that the irregularities are not white noise. For all remaining technologies, 95 % of the autocorrelation coefficients of the irregularities fall within the specified range of the confidence bounds.

Similarly, the PACF analysis of the five-year period irregularities of each PV technology is depicted in Figure 7.15. In this case, the systems with at least two PACF coefficients outside the limit range of the confidence bounds were the Sanyo HIT mono-c-Si, BP Solar mono-c-Si, Schott Solar EFG multi-c-Si, SolarWorld multi-c-Si, Schott Solar MAIN multi-c-Si and Würth Solar CIGS, signifying that the irregularities are not white noise.

Based on the statistical analysis of the irregularities, which identified that more systems demonstrated reliable results for both the four- and five-year time series, compared to the three-year investigation, it can be assumed that increasing the duration of the time series may yield better convergence to the longer term trend. However, it is important to stress that as the real degradation rates of each technology are unknown (these can only be obtained over the life-time of each system), it cannot be ascertained that the obtained performance loss rates of either the three- or four-year period, represent the real degradation rates over the life-time of each technology.

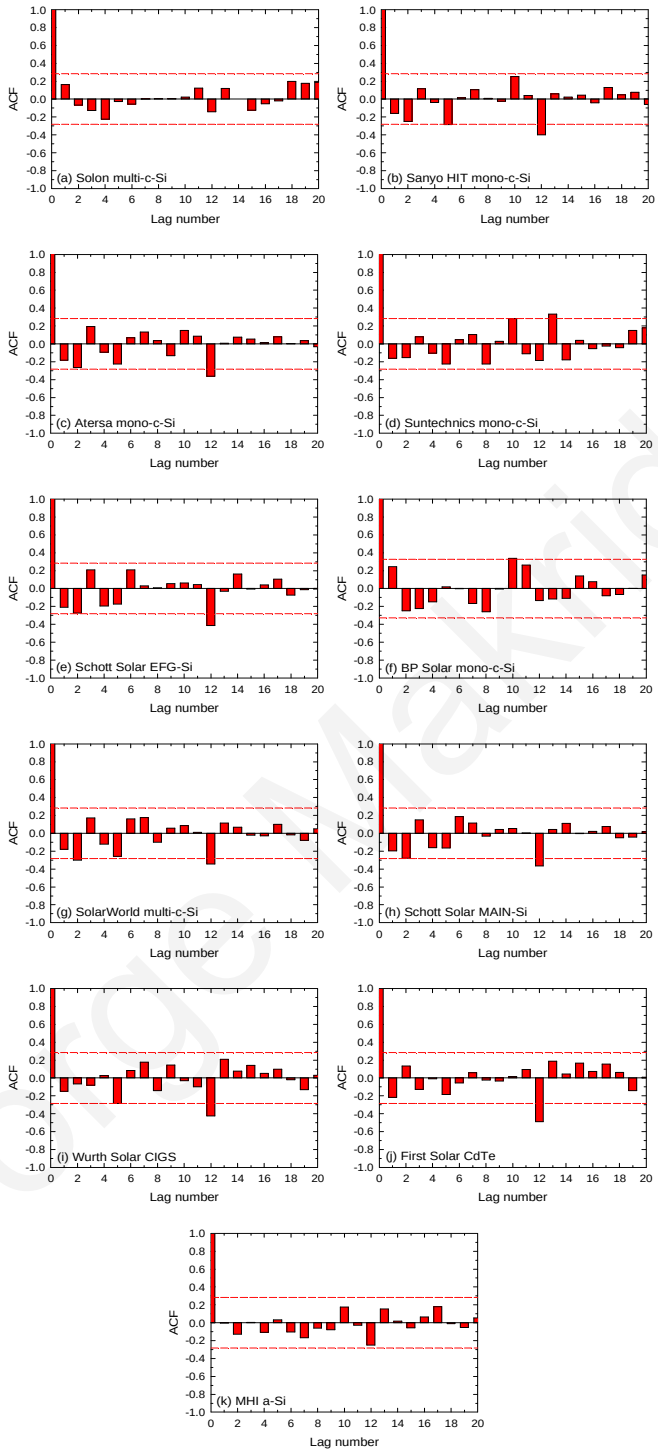

Figure 7.14. ACF of the irregularities of the PV technologies on five-year time series. (a) Solon multi-c-Si. (b) Sanyo HIT mono-c-Si. (c) Atersa mono-c-Si. (d) Suntechnics mono-c-Si. (e) Schott Solar EFG-Si. (f) BP Solar mono-c-Si. (g) SolarWorld multi-c-Si. (h) Schott Solar MAIN-Si. (i) Würth Solar CIGS. (j) First Solar CdTe. (k) MHI a-Si.

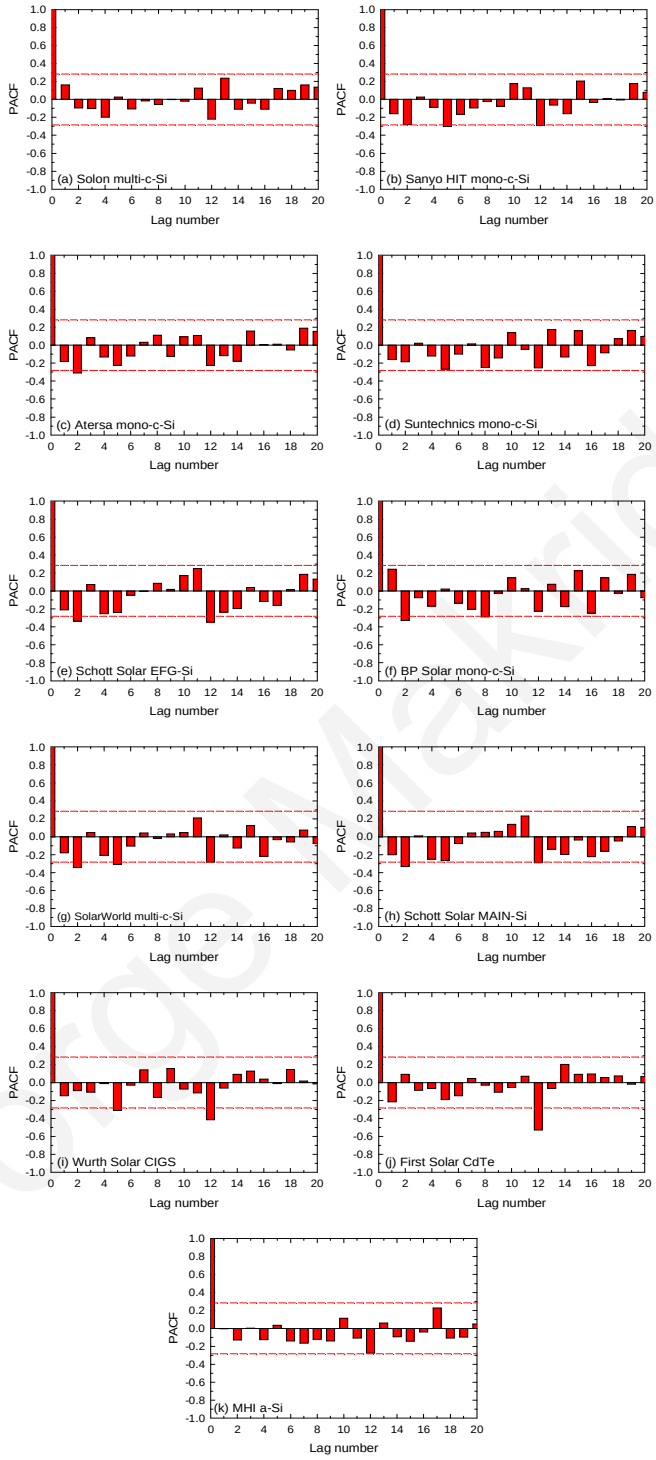

Figure 7.15. PACF of the irregularities of the PV technologies on five-year time series. (a) Solon multi-c-Si. (b) Sanyo HIT mono-c-Si. (c) Atersa mono-c-Si. (d) Suntechnics mono-c-Si. (e) Schott Solar EFG-Si. (f) BP Solar mono-c-Si. (g) SolarWorld multi-c-Si. (h) Schott Solar MAIN-Si. (i) Würth Solar CIGS. (j) First Solar CdTe. (k) MHI a-Si.

An important consideration in relation to thin-film degradation rate investigations was found to be the date of installation of the modules, as it appeared that, in the case of CdTe and CIGS, modules manufactured after 2000 seem to exhibit improved stability relative to older designs [97]. The CdTe and CIGS modules installed in Cyprus in 2006 have a rated MPP power of 60 W and 75 W, respectively, while First Solar and Würth Solar have improved the production line since then, as current produced modules have higher efficiencies and rated power.

Finally, the performance loss rates obtained might be affected by the actual batch of modules used for this study. The evaluation of the performance loss rate of PV technologies, particularly for thin-film technologies is not a straight-forward procedure, and there is not yet a technique to guarantee accurate results based on outdoor measurements. In particular, due to the initial degradation and stabilisation phase for a-Si technologies, which is attributed to the SWE [80], a non-linear performance pattern is demonstrated; which may not be appropriately characterised using linear techniques. Specifically, for some a-Si technologies, the stabilisation phase was shown to be up to two years [105].

Chapter 8

Conclusion and future work

8.1 Conclusion

Outdoor PV performance evaluations are essential because manufacturer data-sheet information is not sufficient to accurately estimate PV operation under different climatic conditions. The research outlined in this thesis was an attempt to assess the performance of different grid-connected PV technologies installed side-by-side and to provide useful information, by looking into the various factors affecting their performance.

For the purpose of this research, an advanced infrastructure was set up, comprising the different grid-connected PV systems, outdoor PV operational and meteorological sensors and a data-acquisition system. The data acquired and stored were subsequently used in the analysis of various performance aspects and investigations that were described in this work.

In particular, the annual DC energy yield produced by each PV system was compared to the estimated energy yield of four different modelling approaches: the single-point efficiency, the single-point efficiency with temperature correction, the PVUSA and the one-diode model. The results indicated that the different models estimated the energy yield of different PV technologies, with varying degree of accuracy. Specifically, the application of temperature correction, using manufacturer provided temperature coefficients, assisted to improve the single-point efficiency model for all technologies, especially mono-c-Si and multi-c-Si. On the other hand, the one-diode model provided

the best agreement between the modelled results and outdoor data for mono-c-Si and multi-c-Si technologies and the CIGS, whereas, thin-film technologies of a-Si and CdTe were more accurately estimated with the PVUSA model. In addition, corrections and modifications to the equivalent one-diode model already exist, particularly for a-Si and CdTe technologies, which improve the estimation accuracy.

Upon performing the energy yield modelling investigation, the next step was to look into the performance patterns exhibited by each technology, in order to identify the main factors affecting their performance and the reasons behind the modelling estimation deviations from the real outdoor measurements. It was obvious from the monthly evaluated performance parameters of energy yield and PR, as well as from the CSD extracted seasonality of the monthly average DC PR time series, that even though all technologies showed the highest energy production during the summer season, all the c-Si, CIGS and CdTe technologies showed the highest PR peaks during the winter seasons and the lowest PR values during the warm summer seasons. Different seasonal PR behaviour to that of c-Si was exhibited by thin-film technologies of a-Si, with high PR peaks during the summer and autumn months. All c-Si PV technologies showed higher peak-to-peak PR variations, when compared to thin-film technologies, with the exception of the Schott Solar a-Si during the first year (which was 15 % due to the high PR the technology exhibited during its initial stabilisation phase). Amongst the mono-c-Si technologies, the Sanyo HIT showed the lowest peak-to-peak PR variation at 9.75 %, while the Atersa system showed the highest at 18.08 %. For all installed technologies, the lowest seasonal peak-to-peak PR was exhibited by the thin-film technologies and, particularly, the First Solar CdTe and Schott Solar a-Si technologies, with values 5.05 % and 5.12 %, respectively.

Another important outcome from the seasonal behaviour analysis was that all technologies exhibited a performance pattern that was closely correlated to the prevailing environmental temperature conditions. The effects of temperature on the performance of the PV systems were thus further analysed, with the results showing that this is an important performance factor, especially in warm climates. The thermal losses were calculated for each system over the four-year evaluation period, using firstly, the manufacturer MPP power temperature coefficients and, secondly, the temperature

coefficients evaluated using an outdoor technique. When using the manufacturer temperature coefficient, the results showed that the highest average thermal losses in annual DC energy yield were 8 % for mono-c-Si and 9 % for multi-c-Si technologies, while, for thin-film technologies, the average losses were 5 %. Similar losses were found when using the outdoor evaluated temperature coefficients. In addition, it was shown that thermal annealing is a significant factor in the seasonal behaviour of a-Si technologies, which exhibited an increase in power from early spring until early autumn (of up to 8.4 % in some cases).

The annual DC performance loss rates of different grid-connected PV technologies were obtained by applying the statistical techniques of linear regression and CSD over a five-year period. The application of linear regression resulted in average annual performance loss rates of -0.64 and -0.62 %/year for the mono-c-Si and multi-c-Si systems, respectively, over this period. On the other hand, the average annual performance loss rate of the thin-film systems was -1.78 %/year. The results obtained by applying CSD were slightly higher, as the mono-c-Si, multi-c-Si and thin-film systems exhibited average annual performance losses of -1.04, -1.10 and -1.81 %/year, respectively. This clearly shows that the selection of the analysis technique affects the results and is important for these studies under field conditions.

Finally, the three and four-year period annual performance loss rates were compared to the longer-term performance loss rates of the five-year investigation and the obtained results demonstrated that although the choice of the analysis technique affects the results, the performance loss trends exhibited the same pattern for most technologies. In particular, for the c-Si technologies the results showed that the performance loss rate converges to a steady state value after five years, whereas more time is required to reach steady state for thin-film technologies.

8.2 Future work

As a future step, the systems in both Cyprus and Germany will remain grid-connected for some more years and data will continue to be collected. The greater number of years of measured data will further assist to re-evaluate the performance loss rates of each technology and accurately judge whether the resulting performance loss rate from a longer time series is more precise than shorter periods.

The performance loss rates will also be evaluated using indoor methodologies. More specifically, the modules will be mounted in an indoor flash tunnel and a large-area AAA-class solar simulator will be used to provide an illumination intensity of 1000 W/m^2 in the plane of the panels, whilst they are held at a constant temperature of 25 °C. The output of the module is measured by an electronic load that measures the *I-V* characteristic of the module, giving the power at STC other electrical characteristics. The obtained MPP power at STC can be compared to the manufacturer provided respective power value, in order to provide an estimate of the degradation rate at successive time periods.

Additionally, the performance loss rates of the systems in Stuttgart will also be determined and compared to the ones obtained for the systems in Cyprus. The comparison can provide useful insight of how environmental conditions may affect the degradation of each technology. Environmental conditions impose significant stress over the lifetime of a PV device. As a result, detailed understanding of the relation between external factors, stability issues and module degradation is necessary.

The annual performance loss rates of the installed PV systems will be further evaluated using other time series modelling techniques, such as the autoregressive integrated moving average (ARIMA). ARIMA modelling is used to describe the time series as linear functions of past and current values of the series. In an ARIMA model, the current value in a time series is estimated based on the past values (the autoregressive (AR) part of the model) and the past random variables (the moving average (MA) part of the model). In contrast to CSD, ARIMA model identification requires several diagnostic tests in order to construct the model. Once the model is constructed, a final analysis based

on the ACF and PACF of the irregularities is performed, to determine whether the model is a good fit.

Furthermore, the energy yield estimation of the mathematical models used can be improved with the addition of more parameters, in an attempt to fully model PV performance and account for factors such as spectrum, angle of incidence, low-light, mismatches as well as others. The accuracy of the one-diode model can also be improved by adding a second diode to account for recombination in the space-charge region. The estimation and modelling can be further addressed using signal processing tools to account for time-variations and correlations as a function time.

Another field that can be investigated is the spectral performance, given that PV technologies are affected by the change and variation of the solar spectrum. The effect of spectrum is a technology-dependent parameter, as some technologies are affected more by spectral variations than others. The spectral response of PV technologies is usually known, however, as the spectral irradiance at different installation locations is unknown, the spectral losses can be difficult to evaluate. The spectral behaviour of the installed PV technologies can be evaluated by acquiring measurements of the short circuit current or *I-V* curves in conjunction with measurements acquired using a pyranometer and a spectroradiometer. The effect of the spectrum can be presented therefore, by calculating the fraction of the solar irradiation that is usable by each PV technology.

Finally, as the implemented infrastructure is scalable, it can also be used as a platform for testing the latest PV technologies, at the cell, module and system level.

Bibliography

[1] C. P. Cameron, W. E. Boyson, and D. M. Riley, "Comparison of PV system performance-model predictions with measured PV system performance," in *33rd IEEE Photovoltaic Specialists Conference*, 2008, pp. 1-6.

[2] D. L. Evans, "Simplified method for predicting photovoltaic array output," *Solar Energy*, vol. 27, no. 6, pp. 555-560, Jan. 1981.

[3] G. Becker et al., "Energy yields of PV systems - Comparison of simulation and reality," in *23rd European Photovoltaic Solar Energy Conference*, 2008, pp. 3184-3186.

[4] D. L. King, J. K. Dudley, and W. E. Boyson, "PVSIM/sub C/: a simulation program for photovoltaic cells, modules, and arrays," in *Conference Record of the 25th IEEE Photovoltaic Specialists Conference*, 1996, pp. 1295-1297.

[5] H. Matsukawa, P. S. Pimentel, T. Izawa, S. Ike, H. Koizumi, and K. Kurokawa, "An integrated design software for photovoltaic systems," in *Proceedings of 3rd World Conference on Photovoltaic Energy Conversion*, 2003, pp. 1930-1933.

[6] D. Thevenard, G. Leng, and S. Martel, "The RETScreen model for assessing potential PV projects," in *Conference Record of the 28th IEEE Photovoltaic Specialists Conference*, 2000, pp. 1626-1629.

[7] A. Mermoud and T. Lejeune, "Performance assessment of a simulation model for PV modules of any available technology," in *25th European Photovoltaic Solar Energy Conference*, 2010, no. September, pp. 4786-4791.

[8] U. Eicke, D. Pietruschka, J. Schumacher, J. Fernandes, T. Feldmann, and E. Bollin, "Improving the energy yield of PV power plants through internet based simulation, monitoring and visualisation," in *20th European Photovoltaic Solar Energy Conference*, 2005, pp. 2670-2673.

[9] A. Mellit, M. Benghanem, and S. A. Kalogirou, "Modeling and simulation of a stand-alone photovoltaic system using an adaptive artificial neural network: Proposition for a new sizing procedure," *Renewable Energy*, vol. 32, no. 2, pp. 285-313, Feb. 2007.

[10] S. J. Ransome, J. H. Wohlgemuth, S. Poropat, and E. Aguilar, "Advanced analysis of PV system performance using normalised measurement data," in *Conference Record of the 31st IEEE Photovoltaic Specialists Conference*, 2005, pp. 1698-1701.

[11] S. Ransome, "Comparing PV simulation models and methods with outdoor measurements," in *35th IEEE Photovoltaic Specialists Conference*, 2010, pp. 2306-2311.

[12] M. D. Siegel, S. A. Klein, and W. A. Beckman, "A simplified method for estimating the monthly-average performance of photovoltaic systems," *Solar Energy*, vol. 26, no. 5, pp. 413-418, Jan. 1981.

[13] Y. Sukamongkol, S. Chungpaibulpatana, and W. Ongsakul, "A simulation model for predicting the performance of a solar photovoltaic system with alternating current loads," *Renewable Energy*, vol. 27, no. 2, pp. 237-258, Oct. 2002.

[14] W. Zhou, H. Yang, and Z. Fang, "A novel model for photovoltaic array performance prediction," *Applied Energy*, vol. 84, no. 12, pp. 1187-1198, Dec. 2007.
[15] M. Akbaba and M. A. A. Alattawi, "A new model for I–V characteristic of solar cell generators and its applications," *Solar Energy Materials and Solar Cells*, vol. 37, no. 2, pp. 123-132, May 1995.
[16] F. Almonacid, C. Rus, P. Pérez-Higueras, and L. Hontoria, "Calculation of the energy provided by a PV generator. Comparative study: Conventional methods vs. artificial neural networks," *Energy*, vol. 36, no. 1, pp. 375-384, Jan. 2011.
[17] W. De Soto, S. A. Klein, and W. A. Beckman, "Improvement and validation of a model for photovoltaic array performance," *Solar Energy*, vol. 80, no. 1, pp. 78-88, Jan. 2006.
[18] W. Xiao, W. G. Dunford, and A. Capel, "A novel modeling method for photovoltaic cells," in *35th IEEE Annual Power Electronics Specialists Conference*, 2004, pp. 1950-1956.
[19] S. Elies, M. Hermle, and B. Burger, "Improved two-diode model for more detailed simulation of I-U-curves for solar cells and modules," in *24th European Photovoltaic Solar Energy Conference*, 2009, pp. 3737-3740.
[20] S. Singer, B. Rozenshtein, and S. Surazi, "Characterization of PV array output using a small number of measured parameters," *Solar Energy*, vol. 32, no. 5, pp. 603-607, Jan. 1984.
[21] N. Blair, M. Mehos, and C. Christensen, "Modeling photovoltaic and concentrating solar power trough performance, cost and financing with Solar Advisor Model," in *Solar 2008, American Solar*, 2008, pp. 1-7.
[22] S. R. Williams, T. R. Betts, P. Vorasayan, R. Gottschalg, and D. G. Infield, "Actual PV module performance including spectral losses in the UK," in *Conference Record of the 31st IEEE Photovoltaic Specialists Conference*, 2005, pp. 1607-1610.
[23] S. J. Ransome and J. H. Wohlgemuth, "Predicting kWh/kWp performance for amorphous silicon thin film modules," in *Conference Record of the 28th IEEE Photovoltaic Specialists Conference*, 2000, pp. 1505-1508.
[24] T. Nordmann and L. Clavadetscher, "Understanding temperature effects on PV system performance," in *Proceedings of 3rd World Conference on Photovoltaic Energy Conversion*, 2003, pp. 2243-2246.
[25] D. L. King, J. A. Kratochvil, and W. E. Boyson, "Temperature coefficients for PV modules and arrays: measurement methods, difficulties, and results," in *Conference Record of the 26th IEEE Photovoltaic Specialists Conference*, 1997, pp. 1183-1186.
[26] T. Kozak, W. Maranda, A. Napieralski, G. De Mey, and A. De Vos, "Influence of ambient temperature on the amount of electric energy produced by solar modules," in *Mixed Design of Integrated Circuits & Systems International Conference*, 2009, pp. 351-354.
[27] S. R. Wenham, M. A. Green, and M. E. Watt, *Applied Photovoltaics*. Earthscan, 2007, p. 323.

[28] Y. T. Tan, D. S. Kirschen, and N. Jenkins, "A Model of PV Generation Suitable for Stability Analysis," *IEEE Transactions on Energy Conversion*, vol. 19, no. 4, pp. 748-755, Dec. 2004.
[29] R. Chenni, M. Makhlouf, T. Kerbache, and A. Bouzid, "A detailed modeling method for photovoltaic cells," *Energy*, vol. 32, no. 9, pp. 1724-1730, Sep. 2007.
[30] K. Ishaque, Z. Salam, and H. Taheri, "Simple, fast and accurate two-diode model for photovoltaic modules," *Solar Energy Materials and Solar Cells*, vol. 95, no. 2, pp. 586-594, Feb. 2011.
[31] M. G. Villalva, J. R. Gazoli, and E. R. Filho, "Comprehensive Approach to Modeling and Simulation of Photovoltaic Arrays," in *IEEE Transactions on Power Electronics*, 2009, vol. 24, no. 5, pp. 1198-1208.
[32] J. Schumacher, U. Eicker, D. Piedrushcka, and A. Catani, "Exact analytical calculation of the one diode model parameters from PV module data sheet information," in *22nd European Photovoltaic Solar Energy Conference*, 2007, pp. 3212-3217.
[33] S. Hegedus, "Current–voltage analysis of a-Si and a-SiGe solar cells including voltage-dependent photocurrent collection," *Progress in Photovoltaics: Research and Applications*, vol. 5, no. 3, pp. 151-168, May 1997.
[34] J. Merten, J. M. Asensi, C. Voz, A. V. Shah, R. Platz, and J. Andreu, "Improved equivalent circuit and analytical model for amorphous silicon solar cells and modules," *IEEE Transactions on Electron Devices*, vol. 45, no. 2, pp. 423-429, 1998.
[35] K. Bucher, "Do we need site-dependent and climate-dependent module rating?," in *Conference Record of the 23rd IEEE Photovoltaic Specialists Conference*, 1993, pp. 1056-1062.
[36] B. Kroposki, W. Marion, D. L. King, W. E. Boyson, and J. A. Kratochvil, "Comparison of module performance characterization methods," in *Conference Record of the 28th IEEE Photovoltaic Specialists Conference*, 2000, pp. 1407-1411.
[37] D. Petreus, I. Ciocan, and C. Farcas, "An improvement on empirical modelling of photovoltaic cells," in *31st International Spring Seminar on Electronics Technology*, 2008, pp. 598-603.
[38] S. Smith, T. Townsend, C. Whitaker, and S. Hester, "Photovoltaics for utility-scale applications: project overview and data analysis," *Solar Cells*, vol. 27, no. 1-4, pp. 259-266, Oct. 1989.
[39] M. Fuentes, G. Nofuentes, J. Aguilera, D. L. Talavera, and M. Castro, "Application and validation of algebraic methods to predict the behaviour of crystalline silicon PV modules in Mediterranean climates," *Solar Energy*, vol. 81, no. 11, pp. 1396-1408, Nov. 2007.
[40] C. M. Whitaker et al., "Application and validation of a new PV performance characterization method," in *Conference Record of the 26th IEEE Photovoltaic Specialists Conference*, 1997, pp. 1253-1256.
[41] J. Adelstein and B. Sekulic, "Performance and reliability of a 1-kW amorphous silicon photovoltaic roofing system," in *Conference Record of the 31st IEEE Photovoltaic Specialists Conference*, 2005, pp. 1627-1630.

[42] N. Aste, C. Del Pero, and R. S. Adhikari, "Performance analysis of ground-mounted PV plants," in *International Conference on Clean Electrical Power*, 2009, pp. 165-170.
[43] J. A. del Cueto, "Comparison of energy production and performance from flat-plate photovoltaic module technologies deployed at fixed tilt," in *Conference Record of the Twenty-Ninth IEEE Photovoltaic Specialists Conference, 2002.*, 2002, pp. 1523-1526.
[44] R. Gottschalg, T. R. Betts, D. G. Infield, and M. J. Kearney, "Experimental investigation of spectral effects on amorphous silicon solar cells in outdoor operation," in *Conference Record of the 29th IEEE Photovoltaic Specialists Conference*, 2002, pp. 1138-1141.
[45] C. Jennings and C. Whitaker, "PV module performance outdoors at PG&E," in *IEEE Conference on Photovoltaic Specialists*, 1990, pp. 1023-1029.
[46] G. Makrides, B. Zinsser, G. E. Georghiou, M. Schubert, and J. H. Werner, "Outdoor efficiency of different photovoltaic systems installed in Cyprus and Germany," in *33rd IEEE Photovoltaic Specialists Conference*, 2008, pp. 1-6.
[47] B. Marion and G. Atmaran, "Seasonal performance of three grid-connected PV systems," in *IEEE Conference on Photovoltaic Specialists*, 1990, pp. 1030-1037.
[48] J. D. Mondol, Y. G. Yohanis, and B. Norton, "Comparison of measured and predicted long term performance of grid a connected photovoltaic system," *Energy Conversion and Management*, vol. 48, no. 4, pp. 1065-1080, Apr. 2007.
[49] A. Carr and T. Pryor, "A comparison of the performance of different PV module types in temperate climates," *Solar Energy*, vol. 76, no. 1-3, pp. 285-294, Jan. 2004.
[50] T. A. Huld, M. Suri, R. P. Kenny, and E. D. Dunlop, "Estimating PV performance over large geographical regions," in *Conference Record of the 31st IEEE Photovoltaic Specialists Conference*, 2005, pp. 1679-1682.
[51] M. Itoh, H. Takahashi, T. Fujii, H. Takakura, Y. Hamakawa, and Y. Matsumoto, "Evaluation of electric energy performance by democratic module PV system field test," *Solar Energy Materials and Solar Cells*, vol. 67, no. 1-4, pp. 435-440, Mar. 2001.
[52] T. Huld, R. Gottschalg, H. G. Beyer, and M. Topič, "Mapping the performance of PV modules, effects of module type and data averaging," *Solar Energy*, vol. 84, no. 2, pp. 324-338, Feb. 2010.
[53] D. L. King, J. A. Kratochvil, and W. E. Boyson, "Stabilization and performance characteristics of commercial amorphous-silicon PV modules," in *Conference Record of the 28th IEEE Photovoltaic Specialists Conference*, 2000, pp. 1446-1449.
[54] B. Kroposki and R. Hansen, "Technical evaluation of four amorphous silicon systems at NREL," in *Conference Record of the 26th IEEE Photovoltaic Specialists Conference*, 1997, pp. 1357-1360.
[55] T. Strand, L. Mrig, R. Hansen, and K. Emery, "Technical evaluation of a dual junction same-band-gap amorphous silicon photovoltaic system," *Solar Energy Materials and Solar Cells*, vol. 41-42, pp. 617-628, Jun. 1996.
[56] R. Gottschalg, J. del Cueto, T. R. Betts, S. R. Williams, and D. G. Infield, "Investigating the seasonal performance of amorphous silicon single- and multi-

junction modules," in *Proceedings of 3rd World Conference on Photovoltaic Energy Conversion*, 2003, pp. 2078-2081.

[57] A. Abete, F. Scapino, F. Spertino, and R. Tommasini, "Ageing effect on the performance of a-Si photovoltaic modules in a grid connected system: experimental data and simulation results," in *Conference Record of the Twenty-Eighth IEEE Photovoltaic Specialists Conference - 2000 (Cat. No.00CH37036)*, 2000, pp. 1587-1590.

[58] K. Bücher, "Site dependence of the energy collection of PV modules," *Solar Energy Materials and Solar Cells*, vol. 47, no. 1-4, pp. 85-94, 1997.

[59] S. Nann and K. Emery, "Spectral effects on PV-device rating," *Solar Energy Materials and Solar Cells*, vol. 27, no. 3, pp. 189-216, Aug. 1992.

[60] B. Zinsser, G. Makrides, M. Schubert, G. E. Georghiou, and J. H. Werner, "Temperature and intensity dependence of twelve photovoltaic technologies," in *23rd European Photovoltaic Solar Energy Conference and Exhibition*, 2008, pp. 3249-3252.

[61] G. Makrides, B. Zinsser, G. E. Georghiou, M. Schubert, and J. H. Werner, "Temperature behaviour of different photovoltaic systems installed in Cyprus and Germany," *Solar Energy Materials and Solar Cells*, vol. 93, no. 6-7, pp. 1095-1099, Jun. 2009.

[62] C. R. Osterwald, T. Glatfelter, and J. Burdick, "Comparison of the temperature coefficients of the basic I-V parameters for various types of solar cells," in *19th IEEE Photovoltaic Specialists Conference*, 1987, pp. 188-193.

[63] J. Sandstrom, "A method for predicting solar cell current- voltage curve characteristics as a function of incident solar intensity and cell temperature," 1967.

[64] M. Nikolaeva-Dimitrova, R. P. Kenny, E. D. Dunlop, and M. Pravettoni, "Seasonal variations on energy yield of a-Si, hybrid, and crystalline Si PV modules," *Progress in Photovoltaics: Research and Applications*, vol. 18, no. 5, pp. 311-320, May 2010.

[65] G. Kleiss, A. Raicu, and K. Bucher, "Temperature-dependent influence of a-Si:H cell degradation on the energy delivered under realistic reporting conditions," in *Conference Record of the 23rd IEEE Photovoltaic Specialists Conference*, 1993, pp. 896-900.

[66] J. A. del Cueto and B. von Roedern, "Temperature-induced changes in the performance of amorphous silicon multi-junction modules in controlled light-soaking," *Progress in Photovoltaics: Research and Applications*, vol. 7, no. 2, pp. 101-112, Mar. 1999.

[67] K. Jansen, S. Kadam, and J. Groelinger, "The Advantages of Amorphous Silicon Photovoltaic Modules in Grid-Tied Systems," in *IEEE 4th World Conference on Photovoltaic Energy Conference*, 2006, pp. 2363-2366.

[68] K. Akhmad, A. Kitamura, F. Yamamoto, H. Okamoto, H. Takakura, and Y. Hamakawa, "Outdoor performance of amorphous silicon and polycrystalline silicon PV modules," *Solar Energy Materials and Solar Cells*, vol. 46, no. 3, pp. 209-218, Jun. 1997.

[69] J. Sutterlueti et al., "Detailed outdoor performance test of thin film and crystalline silicon based reference PV power plants in Switzerland," in *3rd International Conference Thin-Film Photovoltaics*, 2011, vol. 3, no. June, pp. 111-119.

[70] A. Virtuani, H. Müllejans, and E. D. Dunlop, "Comparison of indoor and outdoor performance measurements of recent commercially available solar modules," *Progress in Photovoltaics: Research and Applications*, vol. 19, no. 1, pp. 11-20, Jan. 2011.
[71] S. Dittmann, W. Durisch, J. Mayor, G. Friesen, and D. Chianese, "Comparison of outdoor and indoor characterisation of a CdTe PV module," in *25th European Photovoltaic Solar Energy Conference*, 2010, pp. 3508 - 3512.
[72] S. Hegedus, "Thin film solar modules: the low cost, high throughput and versatile alternative to Si wafers," *Progress in Photovoltaics: Research and Applications*, vol. 14, no. 5, pp. 393-411, Aug. 2006.
[73] D. E. Carlson, G. Lin, and G. Ganguly, "Temperature dependence of amorphous silicon solar cell PV parameters," in *Conference Record of the 28th IEEE Photovoltaic Specialists Conference*, 2000, pp. 707-712.
[74] N. Cereghetti, E. Bura, D. Chianese, G. Friesen, A. Realini, and S. Rezzonico, "Power and energy production of PV modules statistical considerations of 10 years activity," in *Proceedings of 3rd World Conference on Photovoltaic Energy Conversion*, 2003, pp. 1919-1922.
[75] E. D. Dunlop and D. Halton, "The performance of crystalline silicon photovoltaic solar modules after 22 years of continuous outdoor exposure," *Progress in Photovoltaics: Research and Applications*, vol. 14, no. 1, pp. 53-64, Jan. 2006.
[76] C. R. Osterwald, J. Adelstein, J. A. Cueto, B. Kroposki, D. Trudell, and T. Moriarty, "Comparison of Degradation Rates of Individual Modules Held at Maximum Power," in *4th World Conference on Photovoltaic Energy Conference*, 2006, pp. 2085-2088.
[77] P. Sánchez-Friera, M. Piliougine, J. Peláez, J. Carretero, and M. Sidrach de Cardona, "Analysis of degradation mechanisms of crystalline silicon PV modules after 12 years of operation in Southern Europe," *Progress in Photovoltaics: Research and Applications*, vol. 19, no. 6, pp. 658-666, Sep. 2011.
[78] A. K. Som and S. M. Al-Alawi, "Evaluation of efficiency and degradation of mono- and polycrystalline PV modules under outdoor conditions," *Renewable Energy*, vol. 2, no. 1, pp. 85-91, Feb. 1992.
[79] M. A. Quintana, D. L. King, T. J. McMahon, and C. R. Osterwald, "Commonly observed degradation in field-aged photovoltaic modules," in *Conference Record of the 29th IEEE Photovoltaic Specialists Conference*, 2002, pp. 1436-1439.
[80] D. L. Staebler and C. R. Wronski, "Reversible conductivity changes in discharge-produced amorphous Si," *Applied Physics Letters*, vol. 31, no. 4, p. 292, Aug. 1977.
[81] M. Stutzmann, W. Jackson, and C. Tsai, "Light-induced metastable defects in hydrogenated amorphous silicon: A systematic study," *Physical Review B*, vol. 32, no. 1, pp. 23-47, Jul. 1985.
[82] K. D. Dobson, I. Visoly-Fisher, G. Hodes, and D. Cahen, "Stability of CdTe/CdS thin-film solar cells," *Solar Energy Materials and Solar Cells*, vol. 62, no. 3, pp. 295-325, May 2000.
[83] K. K. Chin, T. A. Gessert, and S.-H. Wei, "The roles of CU impurity states in CdTe thin film solar cells," in *35th IEEE Photovoltaic Specialists Conference*, 2010, pp. 1915-1918.

[84] R. C. Powell et al., "Stability testing of CdTe/CdS thin-film photovoltaic modules," in *Conference Record of the 25th IEEE Photovoltaic Specialists Conference*, 1996, pp. 785-788.
[85] D. L. Bätzner, A. Romeo, M. Terheggen, M. Döbeli, H. Zogg, and A. N. Tiwari, "Stability aspects in CdTe/CdS solar cells," *Thin Solid Films*, vol. 451-452, pp. 536-543, Mar. 2004.
[86] J.-F. Guillemoles, L. Kronik, D. Cahen, U. Rau, A. Jasenek, and H.-W. Schock, "Stability Issues of Cu(In,Ga)Se 2 -Based Solar Cells," *The Journal of Physical Chemistry B*, vol. 104, no. 20, pp. 4849-4862, May 2000.
[87] M. Schmidt et al., "Influence of damp heat on the electrical properties of Cu(In,Ga)Se2 solar cells," *Thin Solid Films*, vol. 361-362, pp. 283-287, 2000.
[88] M. Igalson, M. Wimbor, and J. Wennerberg, "The change of the electronic properties of CIGS devices induced by the 'damp heat' treatment," *Thin Solid Films*, vol. 403-404, pp. 320-324, Feb. 2002.
[89] J. Malmström, J. Wennerberg, and L. Stolt, "A study of the influence of the Ga content on the long-term stability of Cu(In,Ga)Se2 thin film solar cells," *Thin Solid Films*, vol. 431-432, pp. 436-442, May 2003.
[90] T. J. McMahon, "Accelerated testing and failure of thin-film PV modules," *Progress in Photovoltaics: Research and Applications*, vol. 12, no. 23, pp. 235-248, Mar. 2004.
[91] D. L. King, B. R. Hansen, J. A. Kratochvil, and M. A. Quintana, "Dark current-voltage measurements on photovoltaic modules as a diagnostic or manufacturing tool," in *Conference Record of the 26th IEEE Photovoltaic Specialists Conference*, 1997, pp. 1125-1128.
[92] F. J. Pern, A. W. Czanderna, K. A. Emery, and R. G. Dhere, "Weathering degradation of EVA encapsulant and the effect of its yellowing on solar cell efficiency," in *Conference Record of the 22nd IEEE Photovoltaic Specialists Conference*, 1991, pp. 557-561.
[93] E. L. Meyer and E. E. van Dyk, "Assessing the Reliability and Degradation of Photovoltaic Module Performance Parameters," *IEEE Transactions on Reliability*, vol. 53, no. 1, pp. 83-92, Mar. 2004.
[94] C. R. Osterwald, A. Anderberg, S. Rummel, and L. Ottoson, "Degradation analysis of weathered crystalline-silicon PV modules," in *Conference Record of the 29th IEEE Photovoltaic Specialists Conference*, 2002, pp. 1392-1395.
[95] M. Ikisawa, A. Nakano, S. Igari, and H. Terashima, "Outdoor exposure tests of photovoltaic modules in Japan and overseas," *Renewable Energy*, vol. 14, no. 1-4, pp. 95-100, May 1998.
[96] D. C. Jordan and S. R. Kurtz, "Analytical improvements in PV degradation rate determination," in *35th IEEE Photovoltaic Specialists Conference*, 2010, pp. 2688-2693.
[97] D. C. Jordan, R. M. Smith, C. R. Osterwald, E. Gelak, and S. R. Kurtz, "Outdoor PV degradation comparison," in *35th IEEE Photovoltaic Specialists Conference*, 2010, pp. 2694-2697.
[98] J. A. del Cueto, "Method for analyzing series resistance and diode quality factors from field data of photovoltaic modules," *Solar Energy Materials and Solar Cells*, vol. 55, no. 3, pp. 291-297, Aug. 1998.

[99] L. Mrig and S. Rummel, "Outdoor stability performance of CIS and CdTe photovoltaic modules at SERI," in *21st IEEE Photovoltaic Specialists Conference*, 1990, pp. 1038-1039.
[100] H. S. Ullal, K. Zwelbel, and B. Von Roedern, "Current status of polycrystalline thin-film PV technologies," in *Conference Record of the 26th IEEE Photovoltaic Specialists Conference*, 1997, pp. 301-305.
[101] T. Carlsson and A. Brinkman, "Identification of degradation mechanisms in field-tested CdTe modules," *Progress in Photovoltaics: Research and Applications*, vol. 14, no. 3, pp. 213-224, May 2006.
[102] K. H. Lam, J. Close, and W. Durisch, "Modelling and degradation study on a copper indium diselenide module," *Solar Energy*, vol. 77, no. 1, pp. 121-127, Jan. 2004.
[103] J. A. del Cueto, S. Rummel, B. Kroposki, C. Osterwald, and A. Anderberg, "Stability of CIS/CIGS modules at the outdoor test facility over two decades," in *33rd IEEE Photovoltaic Specialists Conference*, 2008, pp. 1-6.
[104] B. Marion et al., "Performance parameters for grid-connected PV systems," in *Conference Record of the 31st IEEE Photovoltaic Specialists Conference*, 2005, pp. 1601-1606.
[105] P. Lechner et al., "Long-term performance of ASI tandem junction thin film solar modules," in *25th European Photovoltaic Solar Energy Conference*, 2010, pp. 3283-3287.
[106] E. & Greenpeace, "Solar Generation 6. Solar Photovoltaic Energy Empowering the World," 2011.
[107] P. J. Cousins et al., "Generation 3: Improved performance at lower cost," in *35th IEEE Photovoltaic Specialists Conference*, 2010, pp. 275-278.
[108] EPIA, "Market Report 2011," 2011.
[109] C. A. Wolden et al., "Photovoltaic manufacturing: Present status, future prospects, and research needs," *Journal of Vacuum Science & Technology A: Vacuum, Surfaces, and Films*, vol. 29, no. 3, pp. 30801-30816, 2011.
[110] A. Shah, "Photovoltaic Technology: The Case for Thin-Film Solar Cells," *Science*, vol. 285, no. 5428, pp. 692-698, Jul. 1999.
[111] B. Zinßer, G. Makrides, W. Schmitt, G. E. Georghiou, and J. H. Werner, "Annual Energy Yield of 13 Photovoltaic Technologies in Germany and Cyprus," in *Proceedings of the 22nd European Photovoltaic Solar Energy Conference*, 2007, pp. 3114-3117.
[112] G. Makrides, B. Zinsser, M. Norton, G. E. Georghiou, M. Schubert, and J. H. Werner, "Potential of photovoltaic systems in countries with high solar irradiation," *Renewable and Sustainable Energy Reviews*, vol. 14, no. 2, pp. 754-762, Feb. 2010.
[113] H. Neuenstein, "PHOTON International The Photovoltaic Magazine," *Photon Profi*, Germany, pp. 50-55, 2009.
[114] B. Zinsser, G. Makrides, M. B. Schubert, G. E. Georghiou, and J. H. Werner, "Rating of annual energy yield more sensitive to reference power than module technology," in *35th IEEE Photovoltaic Specialists Conference*, 2010, pp. 1095-1099.

[115] B. Taylor and C. Kuyatt, "Guidelines for evaluating and expressing the uncertainty of NIST measurement results," 1994.
[116] J. a. del Cueto, "Comparison of energy production and performance from flat-plate photovoltaic module technologies deployed at fixed tilt," in *Conference Record of the 29th IEEE Photovoltaic Specialists Conference*, 2002, pp. 1523-1526.
[117] F. Macaulay, *The smoothing of time series*, 1st ed. NBER, 1931, pp. 1-172.
[118] S. Makridakis et al., "The accuracy of extrapolation (time series) methods: Results of a forecasting competition," *Journal of Forecasting*, vol. 1, no. 2, pp. 111-153, Apr. 1982.
[119] D. Miller and D. Williams, "Shrinkage estimators of time series seasonal factors and their effect on forecasting accuracy," *International Journal of Forecasting*, vol. 19, no. 4, pp. 669-684, Dec. 2003.
[120] P. Damrongkulkamjorn and P. Churueang, "Monthly energy forecasting using decomposition method with application of seasonal ARIMA," in *International Power Engineering Conference*, 2005, pp. 225-229.
[121] G. Makrides, B. Zinsser, G. E. Georghiou, M. Schubert, and J. H. Werner, "Degradation of different photovoltaic technologies under field conditions," in *35th IEEE Photovoltaic Specialists Conference*, 2010, pp. 2332-2337.
[122] G. Makrides, B. Zinsser, A. Phinikarides, M. Schubert, and G. E. Georghiou, "Temperature and thermal annealing effects on amorphous silicon PV," in *26th European Photovoltaic Solar Energy Conference*, 2011, pp. 3600-3603.
[123] P. Kenny, D. Dunlop, T. Sample, K. Reitz, and D. Anderson, "Energy rating of diverse PV module technologies through indoor outdoor characterisation," in *Proceedings of 3rd World Conference on Photovoltaic Energy Conversion*, 2003, pp. 2015-2018.
[124] S. Makridakis, S. Wheelwright, and R. Hyndman, *Forecasting: methods and applications*, 3rd ed. New York: John Wiley & Sons, 1998.
[125] C. Chatfield, *The Analysis of Time Series: An Introduction*, 5th ed. Florida: Chapman and Hall/CRC, 1996.
[126] T. J. McMahon, "Solar cell/module degradation and failure diagnostics," in *2008 IEEE International Reliability Physics Symposium*, 2008, pp. 172-177.

List of publications out of thesis

Book chapters

I. G. Makrides, B. Zinsser, M. Norton, M. Schubert, G. Georghiou "Important Performance Factors Determining the Assessment of Photovoltaic Technologies", INTECH (2012), Third Generation Photovoltaics; pp. 201-232.

Journals

I. G. Makrides, B. Zinsser, A. Phinikarides, M. Schubert, G. E. Georghiou, "Temperature and thermal annealing effects on different photovoltaic technologies," *Renewable Energy*, vol. 43, pp. 407-417, Jul. 2012.

II. G. Makrides, B. Zinsser, M. Schubert, G. E. Georghiou, "Energy yield prediction errors and uncertainties of different photovoltaic models," *Progress in Photovoltaics: Research and Applications*, 2011.

III. G. Makrides, B. Zinsser, M. Norton, G. Georghiou, M. Schubert, J. Werner, "Outdoor Performance Evaluation of Grid-Connected PV technologies in Cyprus," *Journal of Energy & Power Engineering*, vol. 4, no. 2, pp. 52 – 57, Feb. 2010.

IV. F. Mavromatakis, G. Makrides, G. E. Georghiou, A. Pothrakis, Y. Frangiadakis, E. Drakakis, E. Koudoumas "Modelling the Phototvoltaic Potential of a site," *Renewable Energy*, vol. 37, no. 7, pp. 1387-1390, Jul. 2010.

V. G. Makrides, B. Zinsser, M. Norton, G. E. Georghiou, M. Schubert, and J. H. Werner, "Potential of photovoltaic systems in countries with high solar irradiation," *Renewable and Sustainable Energy Reviews*, vol. 14, no. 2, pp. 754-762, Feb. 2010.

VI. G. Makrides, B. Zinsser, G. E. Georghiou, M. Schubert, and J. H. Werner, "Temperature behaviour of different photovoltaic systems installed in Cyprus and Germany," *Solar Energy Materials and Solar Cells*, vol. 93, no. 6-7, pp. 1095-1099, Jun. 2009.

Conferences

I. G. Makrides, B. Zinsser, A. Phinikarides, M. Schubert and G. E. Georghiou, "Temperature and thermal annealing effects on amorphous silicon PV", in *26th European Photovoltaic Solar Energy Conference*, 2011, pp. 1 - 6.

II. G. Makrides, B. Zinsser, A. Phinikarides, G. E. Georghiou and M. Schubert, "Photovoltaic model uncertainties based on field measurements," in *37th IEEE Photovoltaic Specialists Conference*, 2011, pp 1 - 6.

III. B. Zinsser, G. Makrides, M. B. Schubert, G. E. Georghiou, and J. H. Werner, "Rating of annual energy yield more sensitive to reference power than module technology," in *35th IEEE Photovoltaic Specialists Conference*, 2010, pp. 1095-1099.

IV. G. Makrides, B. Zinsser, G. E. Georghiou, M. Schubert and J. H. Werner, "Degradation of different photovoltaic technologies under field conditions," in *35th IEEE Photovoltaic Specialists Conference*, 2010, pp 1 - 6.

V. G. Makrides, B. Zinsser, M. Schubert, G. E. Georghiou and J. H. Werner, "Modelling the power output and energy yield of 13 different photovoltaic systems," in *25th European Photovoltaic Solar Energy Conference*, 2010, pp. 4682 - 4687.

VI. G. Makrides, B. Zinsser, M. Schubert, G. E. Georghiou and J. H. Werner, "Evaluation of grid-connected photovoltaic system performance losses in Cyprus," in *Medpower Conference*, 2010.

VII. G. Makrides, B. Zinsser, G. E. Georghiou, M. Schubert and J. H. Werner, "Two year performance evaluation of different grid connected photovoltaic systems," in *34th IEEE Photovoltaic Specialists Conference*, 2009, pp 1 - 6.

VIII. B. Zinßer, M. Ibrahim, G. Makrides, H. El-Sherif, E. Hamouda, G. E. Georghiou, M. Schubert, and J. H. Werner, "Mehrertrag durch Nachführung in Deutschland, Zypern und Ägypten, in *24th Symposium Photovoltaische Solarenergie*, 2009.

IX. M. Ibrahim, B. Zinßer, H. El-Sherif, E. Hamouda, G. Makrides, G. E. Georghiou, M. Schubert, and J. H. Werner, "Advanced photovoltaic test park in Egypt for investigating the performance of different module and cell technologies," in *24th Symposium Photovoltaische Solarenergie*, 2009, pp. 318-323.

X. A. Petousis, S. Petousis, X. Zhang, G. E. Georghiou, M. Patsalides, G. Makrides and K. Godfrey, "Electricity market modelling with photovoltaic active and reactive power generation," in *PP&PSC, Conference*, 2009

XI. G. Makrides, B. Zinsser, G. E. Georghiou, M. Schubert and J. Werner, "Outdoor efficiency of different photovoltaic systems installed in Cyprus and Germany," in *33rd IEEE Photovoltaic Specialists Conference*, 2008, pp 1 - 6.

XII. M. Strobbel, G. Makrides, B. Zinsser, M. Norton, M. Schubert, G. E. Georghiou and R. Gottschalg, "Energy yield forecasting for high-efficiency PV systems in three locations using artificial neural networks," in *23rd European Photovoltaic Solar Energy Conference*, 2008, pp. 3409 - 3412.

XIII. M. Patsalides, G. Makrides, V. Efthimiou, A. Stavrou, G. E. Georghiou, "Power quality issues in light of the future uptake of photovoltaic (PV) technology," in *Transmission and Distribution Europe Conference*, 2008.

XIV. B. Zinsser, G. Makrides, M. Schubert, G. E. Georghiou and J. Werner, "Temperature and intensity dependence of twelve Photovoltaic technologies," in *23rd European Photovoltaic Solar Energy Conference*, 2008, pp. 3249 - 3252.

XV. G. Makrides, B. Zinsser, Matthew Norton, G. E. Georghiou and J. H. Werner, "Energy yield of different photovoltaic systems installed in Cyprus," in *PVSAT-4 Conference*, 2008, pp. 199-203.

XVI. G. Makrides, B. Zinsser, M. Schubert, G. E. Georghiou and J. H. Werner, "Error sources in outdoor performance evaluation of photovoltaic systems," in *23rd European Photovoltaic Solar Energy Conference*, 2008, pp. 3904-3909.

XVII. B. Zinsser, G. Makrides, Markus Schubert, G. E. Georghiou and J. H. Werner, "Jahresenergieertrag von 13 verschiedenen photovoltaik-technologien in Deutschland und Zypern," in *23rd Symposium Photvoltaische Solarenergie Conference*, 2008, pp. 294-299.

XVIII. G. Makrides, B. Zinsser, G. E. Georghiou, M. Schubert and J. H. Werner, "Potential of Photovoltaic Systems in countries of high solar irradiation," in *DEMSEE08 International Workshop on Deregulated Electricity Market Issues in South-Eastern Europe*, 2008.

XIX. G. Makrides, B. Zinsser, G. E. Georghiou and J. H. Werner, "Performance assessment of different photovoltaic systems under identical field conditions of high irradiation," in *PV RES Conference*, 2007, pp. 4-12.

XX. G. Makrides, B. Zinsser, G. E. Georghiou and J. H. Werner, "Temperature behaviour of different photovoltaic systems installed in Cyprus and Germany," in *17th Photovoltaic Solar Energy Conference*, 2007, pp. 385-386.

XXI. B. Zinsser, G. Makrides, G. E. Georghiou and J. H. Werner, "First operation year of 13 photovoltaic technologies in Germany and Cyprus," in *22nd European Photovoltaic Solar Energy Conference*, 2007, pp. 3114-3117.

XXII. B. Zinsser, G. Makrides, W. Schmitt, G.E. Georghiou, and J. H. Werner, "Annual energy yield of 13 photovoltaic technlologies in Germany and in Cyprus," in *4th Workshop Photovoltaik-Modultechnik*, 2007.